Copyright

by

Blake Robert Copple

2014

**The Thesis Committee for Blake Robert Copple**
**Certifies that this is the approved version of the following thesis:**

# Development of a Fully Automated Rapid Irradiated Sample Transport System for Neutron Activation Analysis

**APPROVED BY**
**SUPERVISING COMMITTEE:**

**Supervisor:** _____
Steven Biegalski

**Co-Supervisor:** _____
Sheldon Landsberger

# Development of a Fully Automated Rapid Irradiated Sample Transport System for Neutron Activation Analysis

**by**

**Blake Robert Copple, B.S.M.E.**

**Thesis**

Presented to the Faculty of the Graduate School of

The University of Texas at Austin

in Partial Fulfillment

of the Requirements

for the Degree of

**MASTER OF SCIENCE IN ENGINEERING**

**The University of Texas at Austin**

**December 2014**

# Dedication

To the Teams, my loving Wife, and Pancake II the Cat. Without y'all I would be truly lost.

Tater…still trying to keep up with you bud, miss you every day – Quis Custodiet Ipsos Custodes.

And to Steve, Sheldon, and my parents. Thanks for never giving up on me.

# Acknowledgements

First and foremost, I would like to thank Dr. Steve Biegalski for his constant insight, support, and patience which made the completion of this project possible. Without Dr. Biegalski's encouragement to return to The University of Texas at Austin after six years in the military, the awarding of my M.S.M.E would not have been possible. Steve limitless knowledge base was tapped constantly and proved critical to the completion of the FARIST system and my M.S. degree.

Secondly, I would like to thank Dr. Landsberger for his constant support throughout the duration of the project. The constant influx of information and experience was an absolute asset to the successful completion of not only the FARIST system project, but to my own education.

Thirdly, I would like to thank Donald Stokes whose wisdom, guidance, and example constantly reminds me of what it is to be a great Team guy. Mr. Stokes has imparted onto me that even though our job/position/rank may change, our dedication to the Team, the craft, and the people we work with must never waiver, otherwise we lose the edge.

Lastly, I would like to give a sincere thank you to the entire staff of NETL, especially Larry Welch and Mike Krause for being there to support the completion of the project. Their technical expertise and experience proved invaluable over the course of the project.

# Abstract

## Development of a Fully Automated Rapid Irradiated Sample Transport System for Neutron Activation Analysis

Blake Robert Copple, M.S.E

The University of Texas at Austin, 2014

Supervisors: Steven Biegalski and Sheldon Landsberger

The need for trace, minor and main element analysis becomes more prevalent each year with an every expanding variety of applications. Neutron Activation Analysis (NAA) is an attractive non-destructive analysis tool that can be utilized on small samples regardless of what physical state the material is in. The analysis process however, typically requires researchers to physically handle a radioactive sample in order to transport the sample to detection systems for data gathering.

The purpose of this project was to design a Fully Automated Rapid Irradiated Sample Transit (FARIST) system that could deliver samples into a reactor core and then transfer them to a detector for analysis with zero human interaction. The system would be designed to hold up to 30 samples prior to analysis with the irradiation, decay, and counting times programmed in initially so that once analysis was initiated, no user interaction was required for the next 29 samples. The last requirement of the system was that it supports cyclic NAA. This work discusses the science and history behind NAA as well as the design, construction, installation, and testing of the new FARIST system.

# Table of Contents

# List of Tables

# List of Figures

# Chapter 1: Introduction

In the past 60 years, trace, minor and major element analysis has become an integral component in the fields of science and industry. Applications can be extended from the analysis of a water sample near an old chemical factory for an EPA lawsuit, to multi-billion dollar oil corporations looking for oil indicative *tell-tall* elements in a core sample drilled from miles below the earth surface. With the global economy doubling in the past 40 years, the presence of such elemental analysis tools has afforded significant advances on the commercial industry [1]. The primary benefactors of these advances have been the industrial, oil, mining and pharmaceutical industries; significant cornerstones of both the U.S. and world economy. With an ever expanding world economy, the need for a powerful quantitative elemental analysis tool in the world is imperative.

One of the most reliable methods for trace and main element analysis is a method known as Neutron Activation Analysis (NAA). Beyond being reliable, it is also one of the most accurate and quantitative multi-element analysis methods available today. The NAA process has several advantages over other methods that exist. The most significant advantages being that the process is non-destructive and can be conducted on any material regardless of physical state [2]. Coupled with the fact that NAA can simultaneously analyze multiple elements with high accuracy and sensitivity, while also only requiring a minimal amount of material for a sample, makes the NAA process very attractive for research purposes. NAA's primary use is to determine elemental

concentrations within a sample. Additionally, isotopes contained within a sample can be detected and measured separate from the base elements allowing the researcher to determine what percent of the sample is comprised of certain isotopes [3].

NAA is employed at several Universities and many research centers around the globe. Research reactors serve universities, industrial, and government needs. The University of Texas maintains such a type of reactor. What makes these small reactors ideal is their ability to conduct NAA in a moderate neutron flux environment where the primary task of the reactor is research and training.

### 1.1 THE UNIVERSITY OF TEXAS NUCLEAR LABORATORY

The University of Texas owns and operates a 1.1 MW TRIGA MKII (Training Research and Isotope General Atomics) reactor developed by General Atomics. The Texas TRIGA reactor provides a high degree of flexibility for the researcher. This is done primarily through its five beam ports located around the reactor core and its multiple pneumatic loading tubes located inside the reactor core.

The five beam ports located around the reactor provide the researcher an abundant array of different experimental setups. Beam Port (BP-1) is utilized as a positron source for the Texas Intense Positron Source (TIPS) facility. BP-2 and BP-3 are utilized for Neutron Depth Profiling (NDP) and Prompt Gamma Activation Analysis (PGAA) respectively. PGAA is a subcategory of the NAA process and is explained in greater detail in the following chapter. The last port, BP-5 is utilized for neutron radiography.

Currently BP-4 is not in use. Shown below in Figure 1.1 is the scale representation of the TRIGA Reactor beam ports.

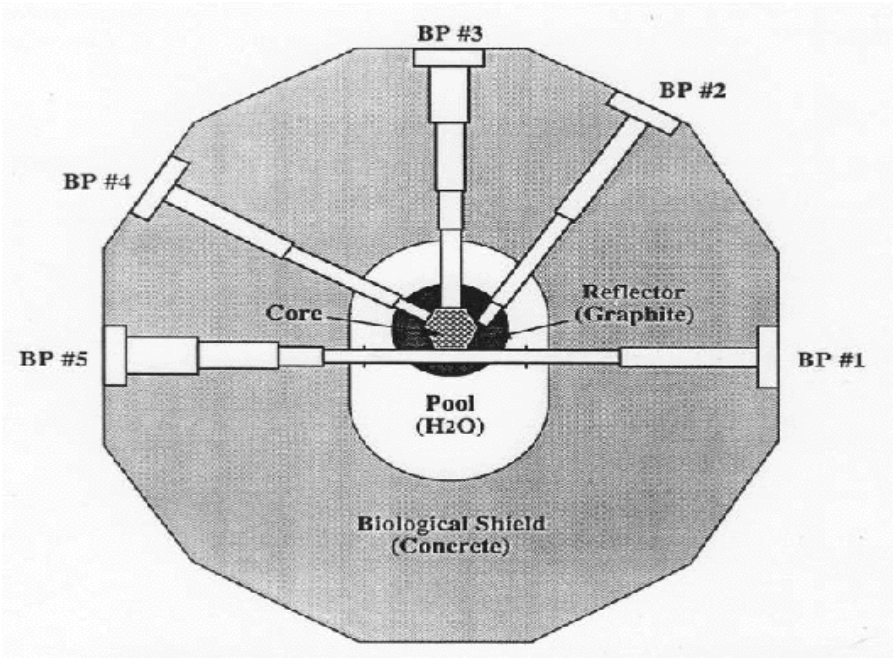


Figure 1.1: TRIGA Reactor Beam Port Geometry.

Along with the five beam ports are two pneumatic loading tubes, one located inside the reactor core while the other is located on the outer ring of the core as shown in Figure 1.2. Inside of the reactor core these tubes can expect to have a neutron flux incident up them on the order of 4 x $10^{12}$ $\frac{neutrons}{\frac{cm^2}{sec}}$; ideal for NAA research. Additionally this pneumatic system allows the user to vary irradiation time for the samples. It is important to note that these tubes are almost exclusively used for Delayed Neutron Activation Analysis (DNAA) and Cyclic Neutron Activation Analysis (CNAA).

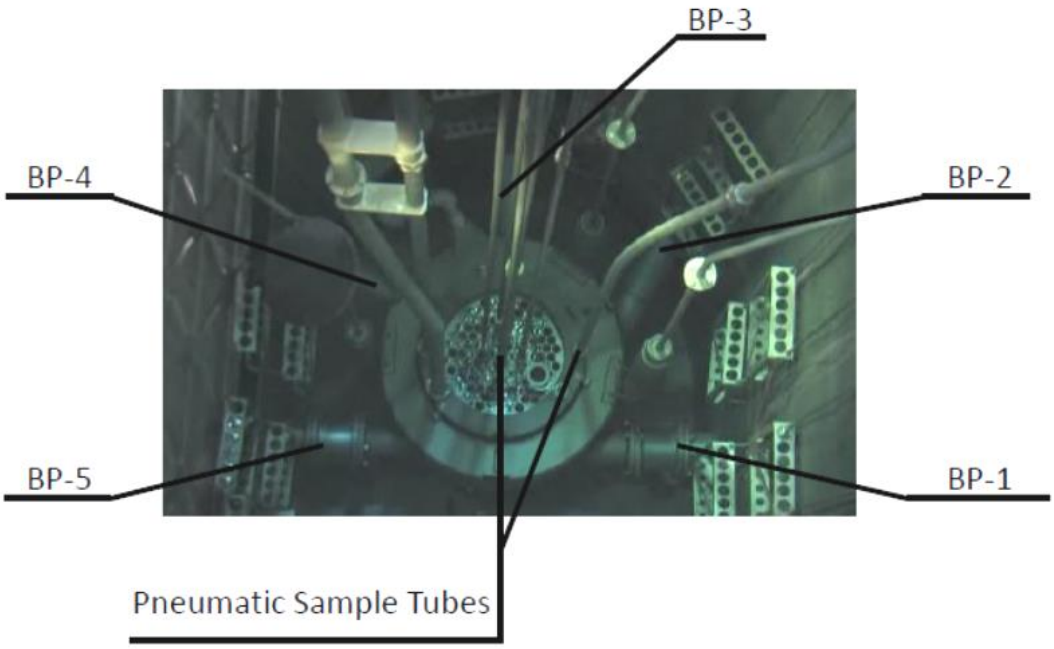


Figure 1.2: TRIGA Reactor Photo Taken From Top of Reactor Pool.

With the tubes unique placement inside of the reactor, the samples have the ability to be bombarded with neutrons of all energies (thermal to fast). The pneumatic tubes primary purpose is to transport un-irradiated samples to the core and irradiated samples to a location outside of the reactor bay for analysis. This is done in order to minimize ambient radiation sources from the reactor. From that separate location (shielded as best as possible from ambient radiation) the samples can be safely analyzed using specialized gamma ray detectors that can quantitatively measure the energies being emitted from the sample. This paper aims to provide a background on the science of NAA as well as the improvements that were made to the pre-existing pneumatic NAA system. This new system would be called the Fully Automated Rapid Irradiated Sample Transport System, or FARIST.

## 1.2 PROBLEM STATEMENT

The existing NAA facility located at the University of Texas was a non-ergonomic, user intensive, and limited capability system. The need for constant human interaction requires researchers to expose themselves to activated samples in order to physically relocate the sample to a detector for analysis. With modern day advances, the technology is present to rectify all the issues and downfalls with the current system. This paper discusses the process that was taken to create an entirely new fully automated system capable of NAA and cyclic NAA.

## 1.3 PROJECT GOALS

The primary purpose of this project was to make a safer, more effective NAA system. To accomplish this objective, several project goals were established to act as cornerstones for the design. The design consisted of three primary goals. The first was to create a system that minimized the need for researcher interaction during operation through the use of automation. The second primary goal was to devise a system that would afford rapid sample transit times from the reactor to the detector in order to analyze short lived radionuclides. The third was to create a system capable of both single-shot NAA and cyclic NAA; a setup previously not offered at the research facility.

The project had two secondary goals as well. The first included system to store and analyze up to 30 samples. This goal would require that a sample storage system be

devised as well as the creation of additional programming to account for the number of samples. The other secondary goal of the project was to minimize changes to the existing laboratory infrastructure. The final goal for the project, which remained flexible in nature, was that the system's total costs remain under $10,000. Due to the flexible nature of the amount, this was deemed as a tertiary goal for the project.

## 1.4 OVERVIEW

Chapter TWO of this thesis will provide a brief review on the concepts that are important to the NAA process. In addition the different applications of NAA will be discussed as well as a background on the detectors utilized in these systems. This chapter will conclude with a discussion on the different analysis software programs and calculation methods that exist to support the user.

Chapter THREE will discuss topics more specific to the DGNAA process. Single iteration, pseudo-cyclic and cyclic NAA will be presented with corresponding data highlighting the advantages and disadvantages of each method. A brief history of these methods will be introduced and the chapter will conclude with an overview of typical system setups.

Current facilities and DGNAA/cyclic experimental setups will be presented and discussed in Chapter FOUR. A comprehensive look at each system will be discussed focusing on the different facilities capabilities and limitations. The chapter will conclude

with a look at how the FARIST system will aim to make up for current facilities shortfalls.

Chapter FIVE will be focused primarily on the research and design of this project. Project goals will be presented. Every aspect of the design of the mechanical system will be discussed along with justification for decisions made in the design. Every component from the bolts that hold the valves together, to the type of tubing that was used is presented and discussed.

Chapter SIX is solely reserved for an in depth look at the construction and installation of the FARIST System. In this chapter the manufacturing of all the different components will be discussed. In addition, the installation procedures of each component will be discussed and accompanied with figures and supporting graphics. By the end of this section, the reader will possess a comprehensive knowledge as to of the placement of all the FARIST system components.

Chapter SEVEN will delve into how the system has been utilized with the results of several experiments displaying the increased safety, capability and accuracy of the NAA system. Specific metrics will be introduced and compared to previous NAA systems to characterize overall system improvement. The chapter will wrap up with a summary of the all the different metrics and how the FARIST system is a significant improvement over previously designed DGNAA cyclic systems.

The conclusion of this thesis will provide a broad overview of what the FARIST system offers to the user that is unique to any other system in existence. The end of this

chapter provides a conclusion to the paper and summarizes some of the significant achievements that were made possible by this project.

# Chapter 2: Delayed Neutron Activation Analysis

Hevesy and Levi first discovered NAA in 1936, when it was observed that when a geological sample was irradiated with neutrons, certain rare earth elements would become radioactive [4]. This observation led to the idea that induced radioactivity could be used to identify elements using their corresponding isotopes. From that point on this discovery would provide researchers an alternative means of determining the elemental composition of not just rare-earth elements, but many other elements and their corresponding isotopes. Later on, with the development of high performance detectors, simultaneous multi-element analysis was made possible allowing researchers to extract more raw data from laboratory results. This added data allowed researchers to determine the relative concentration of each element and isotope in the activated material, allowing for a more comprehensive analysis.

In order to fully understand the constraints behind the FARIST system, a qualitative understanding of NAA is required. In the following sections, a detailed look at the science behind NAA is provided with accompanying graphs and data that attest to the efficiency and effectiveness of NAA. Topics covered throughout this chapter begin with an overview of neutron capture and gamma ray emission concepts followed by a discussion on delayed gamma ray energies, neutron cross sections and nuclear half-life's. This chapter continues with tutelage on gamma detection systems that are applicable to the NAA process, specifically a look at High-Purity Germanium Detectors (HPGe)

detectors. Chapter TWO concludes with a look at the NAA software utilized and a how relative elemental concentrations are determined using that software.

## 2.1 NEUTRON EMISSION

Radiation may primarily be observed through the decay of unstable atoms into their smaller daughter atoms. This process is more commonly known as radioactive decay, and is commonly induced by fission neutrons. Fission occurs when an incident neutron is captured by the nucleus of uranium in conventional reactors. The resulting reaction causes the heavy atom to normally split into two smaller atoms known as fission fragments, or daughter nuclei, while releasing heat, gamma rays, and neutrons. It is important to note however that neutrons can also be emitted through series of other reactions such as (α,n), (p,n), and (γ, n) in other nuclear accelerators.

In Figure 2.1, a graphic is shown of a typical fission reaction resulting in the release of neutrons of all energies. This reaction is what drives modern commercial reactors and research reactors like the one at the University of Texas. The fast neutrons that are released from the fission process, slowed down by water (and the hydrogen in the TRIGA reactor fuel) to thermal and epithermal energies, are what sustain the reactor's criticality. In a TRIGA Reactor, the core design utilizes that neutron flux to its advantage for NAA research by specially designed locations in the core for sample placement.

In order for the DGNAA system to work efficiently, samples need to be in the immediate vicinity of a reactor core. For the purposes of the FARIST System, samples will be irradiated in the reactor core through the use of pre-existing pneumatic tubes. It is

important to note that for NAA analysis however, the experimenter is mainly concerned with thermal neutrons (0.025eV), and epithermal neutrons (>0.4eV, as these are the two neutron reaction rates used in the relative concentration calculations.

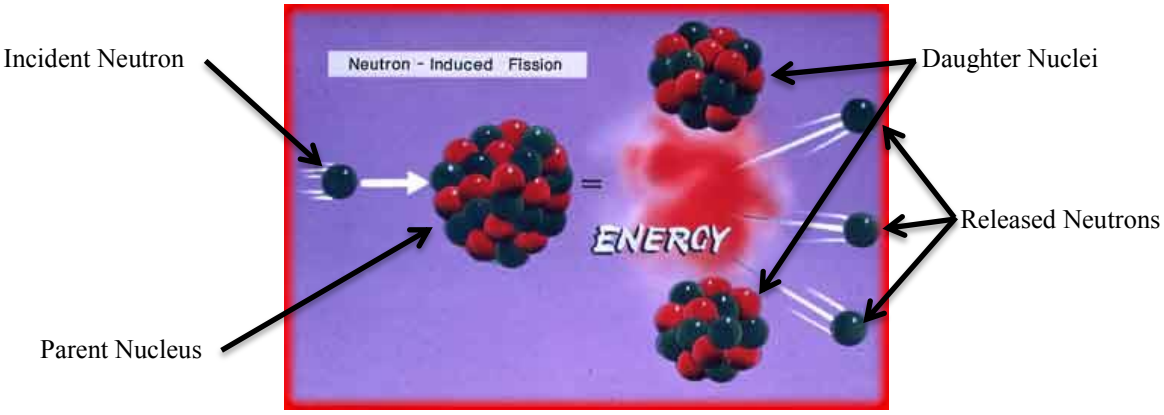


Figure 2.1: Fission Reaction [5].

## 2.2 GAMMA RAY CONCEPTS

The second type of radiation that is integral to the NAA process is gamma ray radiation (γ). Gamma radiation may typically be observed from two types of sources. The first major source of gamma rays is from the fission reaction. Referring to Figure 2.1, it is observed that fission atoms, their daughter products, neutrons, and energy are the typical by-products of a fission reaction. The energy that is released in the process primarily comes in two forms: kinetic energy and gamma rays. For the NAA process however, this prompt radiation from fission plays no significant role thus no further information on the subject is necessary.

The second major source of gamma rays is from the decay of radioactive isotopes. For NAA research, placing a material inside a reactor core and exposing it to a neutron flux induces the creation of radioactive isotopes of the original elements present. Typically these radioactive isotopes become activated and can remain unstable for either short, or long, periods of time. In order for the nuclei to regain stability from its unstable state, the isotope must shed the excess energy. This excess energy is typically released in the form of characteristic gamma rays (with the energy being proportional to the binding energy) and beta particles. This is important for the researcher because gamma photons can be readily detected and distinguished by a gamma ray detection system. The emissions of these gamma rays are the basis of how elemental analysis performed using NAA. In Figure 2.2, a graphical representation of neutron activation is shown. For the purposes of this work, only the delayed gamma energy is utilized for analysis.

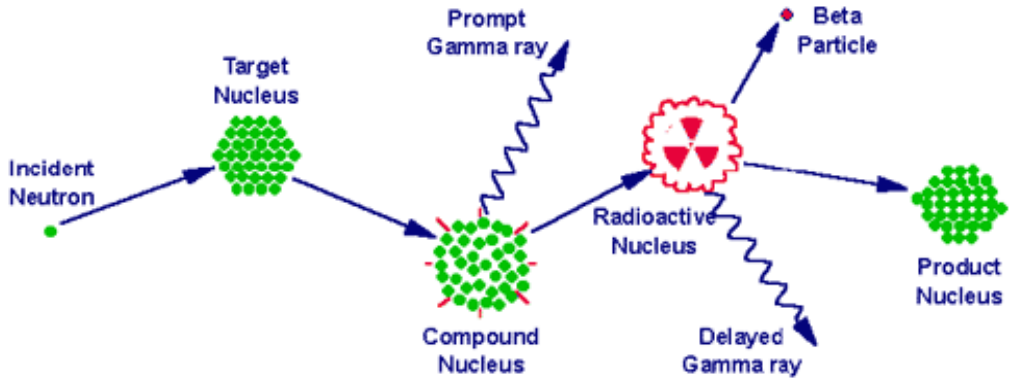


Figure 2.2: Neutron Activation Atomic Representation [6].

In Figure 2.2 there are two types of gamma rays shown: prompt and delayed. Gamma ray detection systems will register any gamma energy, regardless whether it's prompt or delayed. Researchers eliminate the prompt gamma interference by removing the sample from the neutron source. By removing the sample from the neutron flux, the researcher is then able to isolate the delayed gamma.

## 2.3 DELAYED GAMMA RAY ENERGIES

Following the discovery that radioactive elements emitted specific gamma ray energies, further research was completed to determine if more radioactive elements would emit specific gamma ray energies. It was eventually discovered, that not only is it possible to determine which elements are present, but also their corresponding isotopes. This discovery led to the conclusion that if it was possible to identify specific gamma ray energies being emitted from the radioactive source simultaneously, the elemental makeup and relative elemental concentrations of the sample source could be determined as well. This cataloging of gamma ray energies is what will allow for the proper analysis of samples in the FARIST system. In Table 2.1, a typical decay scheme is displayed for $^{137}$Cs along with the observed half-life and delayed gamma ray energies.

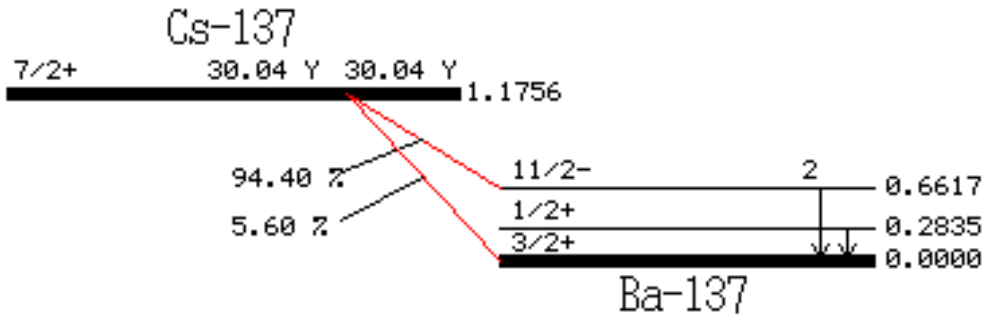


Figure 2.3: $^{137}$Cs Decay Scheme [7].

## 2.2 NUCLEAR CROSS SECTION

It is important to discuss that not every element or stable isotope will capture a neutron when placed in the locality of a neutron flux. For some, it is nearly impossible to gain an extra neutron. Instead it is better practice to say that any given element or isotope has a specific probability of absorbing an incoming neutron. The probability that any given element or isotope will absorb or capture an incoming neutron is directly proportional to an arbitrary unit of measurement called the *nuclear cross section* with a unit of measurement in $cm^{-2}$.

Every element and its stable isotope(s) possess a nuclear cross section. Nuclear cross sections can be easily referenced from several different sources and World Wide Web locations. For the purposes of our research only the *thermal* cross section will be utilized. Since the cross section of an element quantitatively describes its ability to capture neutrons, we can expect that the larger the elemental cross-section, the greater probability that an element will absorb an incoming thermal neutron and undergo gamma ray emission. It is important to note that cross section is a function of energy. To better

illustrate that relationship Figure 2.4 presents a radiative capture cross section graph for $^{137}Cs$.

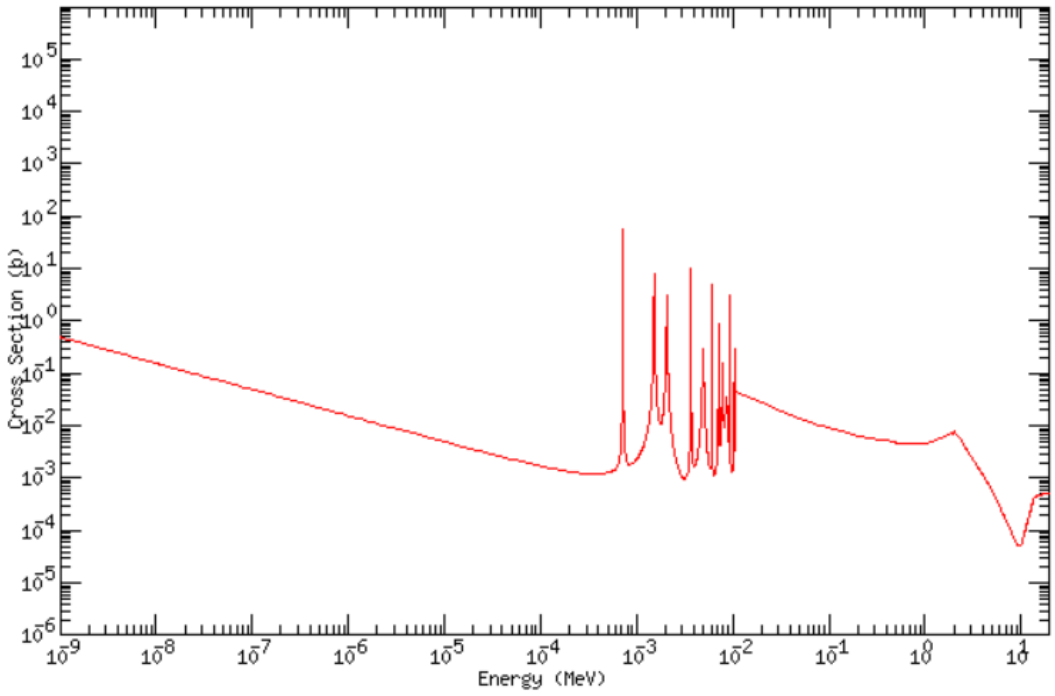


Figure 2.4: $^{137}Cs$ Radiative Capture Cross Section Graph as a Function of Energy [7].

## 2.4 NUCLEAR HALF-LIFE

One extremely important facet to understanding NAA is the concept of half-life. The half -life for an element and their corresponding unstable isotopes have been experimentally observed and cataloged. Their values can be referenced fairly easily and from several different sources however, a comprehensive list of atomic half-lives can be referenced at http://nndc.bnl.gov. Half-lives, typically measured in either seconds, hours, days or years, indicate how long it takes for half of the original activated atoms to decay

away. Half-life's can range on the order of $10^{-6}$ sec to thousands of years. In Table 2.1 the half-lives of the commonly referenced elements is provided.

Table 2.1: Half Life Values for Commonly Referenced Elements [8].

| A# | Isotope | Z # | Type | Half-life | |
|---|---|---|---|---|---|
| | | | | Text | Seconds |
| 19 | 20-F | 9 | Delayed | 11.163 S | 1.12E+01 |
| 23 | 24-Na | 11 | Delayed | 20.20 MS | 2.02E-02 |
| 37 | 38-Cl | 17 | Delayed | 37.24 M | 2.23E+03 |
| 40 | 41-K | 19 | Delayed | 1.265E+9 Y | 3.99E+16 |
| 45 | 46-Sc | 21 | Delayed | 18.75 S | 1.88E+01 |
| 51 | 52-V | 23 | Delayed | 3.75 M | 2.25E+02 |
| 55 | 56-Mn | 25 | Delayed | 2.5789 H | 9.28E+03 |
| 55 | 56-Mn | 25 | Delayed | 2.5789 H | 9.28E+03 |
| 64 | 65-Ni | 28 | Delayed | 2.51719 H | 9.06E+03 |
| 71 | 72-Ga | 31 | Delayed | 39.68 MS | 3.97E-02 |
| 103 | 104-Rh | 45 | Delayed | 4.34 M | 2.60E+02 |
| 103 | 104-Rh | 45 | Delayed | 42.3 S | 4.23E+01 |
| 115 | 116-In | 49 | Delayed | 54.41 M | 3.26E+03 |
| 115 | 116-In | 49 | Delayed | 54.41 M | 3.26E+03 |
| 115 | 116-In | 49 | Delayed | 54.41 M | 3.26E+03 |
| 115 | 116-In | 49 | Delayed | 54.41 M | 3.26E+03 |
| 133 | 134-Cs | 55 | Delayed | 2.903 H | 1.05E+04 |
| 139 | 140-La | 57 | Delayed | 1.6781 D | 1.45E+05 |
| 235 | 236-U | 92 | Delayed | 703.8E+6 Y | 2.22E+16 |

From Table 2.1, it should be fairly to clear to observe a wide range of half-life times. In the past, most DNAA facilities restrict the user from physically conducting immediate analysis of activated samples simply because the samples were too radioactive or "hot." These samples must cool for several minutes, and up to days, before they could become safe enough for an individual to handle and place near a detector. The problem with this process is short-lived radionuclides were decaying away prior to the sample ever being placed in the presence of a detector. With a large number of elements possessing half-lives on the order of seconds and minutes, the ability to detect the short-

lived gamma peaks degrades quickly which in turn diminishes the quality of the analysis. The FARIST system aims to rapidly transport the irradiated samples from inside the reactor core straight to a gamma ray detection system in under 10 seconds, thereby allowing detection of a majority of the short-lived radioisotope's gamma rays [9].

## 2.4 High Purity Germanium (HPGe) Detector Dynamics

The type of detector typically employed to register both prompt and delayed gamma rays is known as a High Purity Germanium detector (HPGe). The University of Texas utilizes HPGe detectors in multiple labs at their nuclear research facility. High purity germanium detectors are widely known as one of the best detectors available for the use of gamma ray analysis. It has several advantages over its cheaper option, the sodium iodide detector. The primary advantage of the HPGe detectors is their ability to detect a wide range of gamma ray energies with extremely high resolution. Another advantage of using the HPGe setup include favorable peak-to-Compton. With the HPGe detector typical peak-to-Compton ratios from 30 to 60 can be observed [10].

A physical HPGe detector setup is shown in Figure 2.5 and 2.6 with two pictures of the detector. In the first, Figure 2.5, the HPGe detector is shown attached to the liquid nitrogen dewar used for cooling the germanium crystal. In the Figure 2.6, the aluminum detector housing has been removed to expose the high purity germanium crystal.

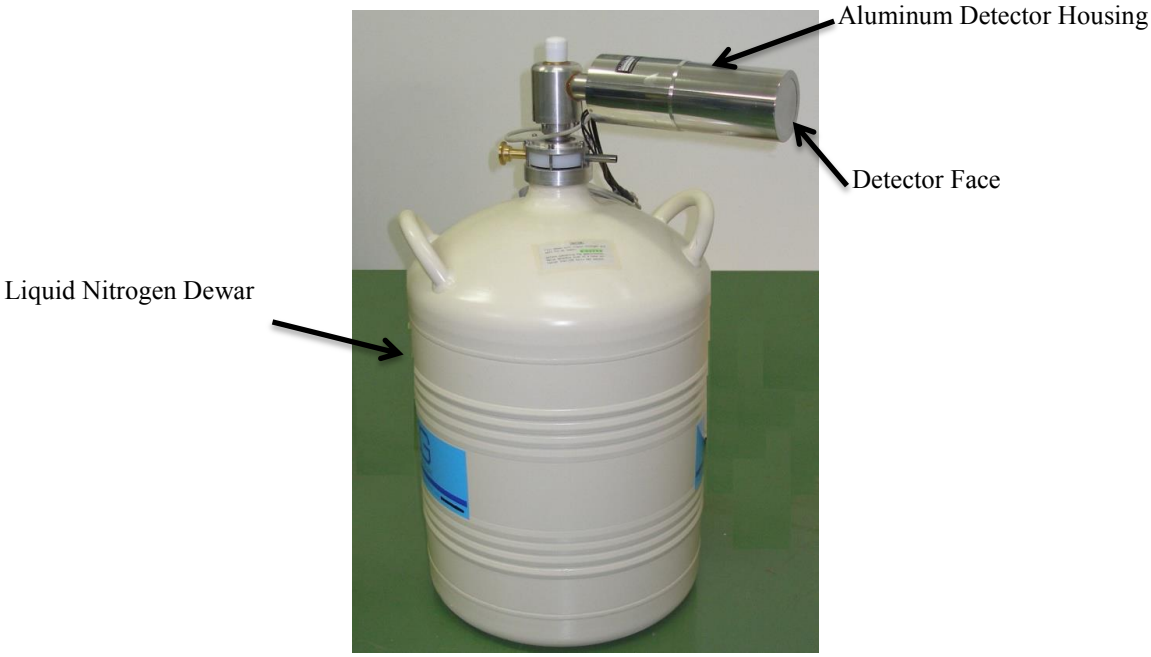


Figure 2.5: HPGe Detector Standard Setup [9].

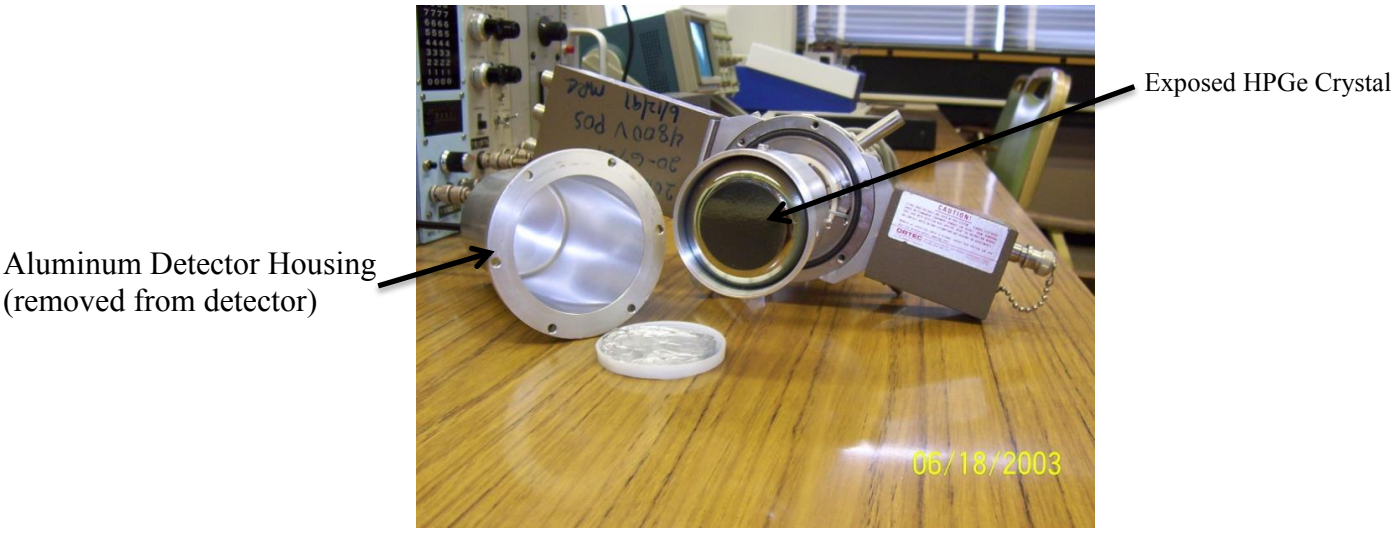


Figure 2.6: HPGe Detector with Housing Removed to Expose Ge Crystal [9].

It wasn't until 1970 that the HPGe detector was made available through advanced purification techniques. Originally germanium detectors utilized a lithium-germanium semiconductor crystal (Ge(Li)) to emit electric signals from incident gamma rays. Ultra-pure germanium detectors were then created by using bulk germanium stock earmarked for the semiconductor industry. Inherent impurities were removed by slowly heating the germanium and allowing it to pass through a melted zone from one end of the stock to the other. Numerous repetitions of this process eventually yielded impurities on the order of $10^9$ atoms/cm$^3$; acceptable for use in high resolution NAA spectroscopy. With the ultra-purified germanium stock that was leftover, germanium crystals were then slowly grown similar to any other crystalline structure [10].

The reason for selecting the ultra-purified germanium stock for the crystal lattice is due to their excellent energy resolution across the gamma ray spectroscopy spectrum. This resolution can be attributed to a combination of three factors: the inherent statistical spread in the number of charger carriers, variations in charge collection efficiency and contributions from electric noise [10].

One of the disadvantages to note is the observed "dead layer" propagated by the contacts along the surface of the detector crystal. These contacts can sometimes have an appreciable thickness which can inadvertently affect the crystal by effectively creating a zone in which incident radiation can interact with. The effect of this "dead layer" is generally negligible for $\gamma$ energies above 200 keV however, for energies below 200 keV, this setup can present attenuation problems. This issue can be overcome however through the use of thin beryllium windows on the face of the detector. The presence of x-

ray with energies below 200 keV also compounds the detector issues at low energies. In essence, below 200 keV, the spectrum gets rather congested with many photopeaks making it difficult to extract accurate and qualitative results [10]. Through different analytical techniques however, some of these effects can be mitigated. These different low energy issue mitigation techniques will be discussed later.

The HPGe detector works through a series of interactions at the atomic level. Inside of the detector incident gamma rays can be expected to interact through photoelectric absorption, Compton scattering and pair production; all of which affect detector response. These reactions then transfer energy proportional to the energy of the incident gamma ray into the germanium crystal lattice causing a vibration in the lattice structure. This vibration can then be electronically converted to raw data and sent to specialized programs for analysis and further refinement [10].

The peak-to-Compton ratio was mentioned earlier as one of the advantages of the HPGe detector system. The peak-to-Compton ratio is a metric used for to indicate overall detector performance. The peak-to-Compton ratio is found by taking the ratio of the number of counts at the maximum of a typical gamma peak and dividing it by the number of counts in the Compton continuum associated with original peak. The Compton continuum can be sampled using the flat portion to the left or right of the Compton edge on the associated peak. It should be mentioned that the 30-60 arbitrary value for peak-to-Compton ratio that was referenced earlier is quoted for a $^{60}$Co standard with a 1332keV gamma peak [10].

One readily observed characteristic with a gamma spectrum utilizing HPGe detectors is the 511 keV peak, or more commonly referred to as the "annihilation peak." The 511 keV peak is a result the photons produced from positron annihilation. At high energies pair production can result at the site of the gamma ray interaction causing the creation of an electron/positron pair which can significantly affect the detector. The positron however will annihilate and create two 511 keV photons. There is a high probability that one, or both, of these photons will escape. When one escapes and the other is absorbed, a peak can be observed at 511keV less than the full-energy peak. When both escape, a double escape peak can be observed at 1.22 MeV less than the full energy peak [10].

When qualitatively describing overall detector performance, there are three other metrics in addition to peak-to-Compton ratio worth mentioning as they will be introduced later to assign performance benchmarks for the FARIST system. The other two metrics are the efficiency, the expected FWHM values, and the % resolution curves. The efficiency can be found determining the ratio of the number of photons received by the detector divided by the total number of photons emitted from the sample. This is usually done utilizing known standards to determine efficiencies across the gamma ray spectrum. The equation for detector efficiency is shown in Equation 1. Also, shown in Figure 2.5 is a typical efficiency vs gamma energy curve that was taken using a $^{152}$Eu standard.

$$\epsilon = \frac{Number\ of\ Photons\ Measured\ Across\ the\ Spectrum}{Number\ of\ Photons\ Emitted\ from\ Sample} \quad (2.1)$$

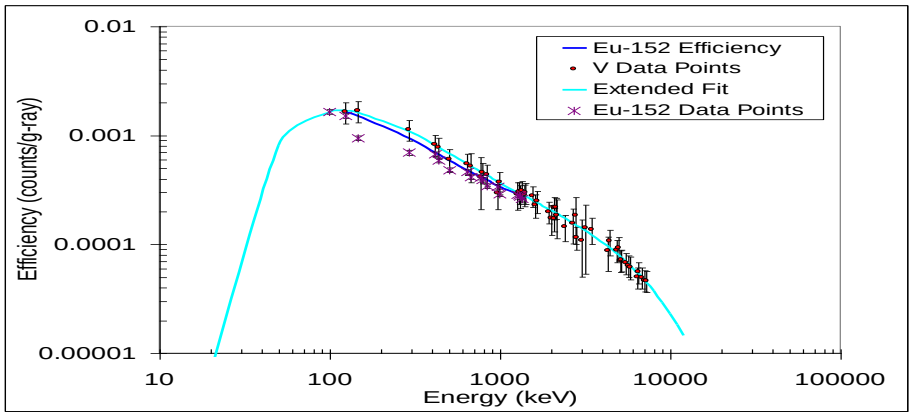


Figure 2.7: HPGe Detector Efficiency Curve Utilizing $^{152}$Eu Source [6].

In order to calculate the percent resolution, the Full Width Half the Maximum (FWHM represented in Figure 2.8) value of a photopeak must be determined. This is calculated utilizing a counting software (NETL utilizes MAESTRO) then taking that FWHM and dividing it by the energy of the photopeak. This calculation is then extrapolated across the gamma ray spectrum. Using the different peaks, a curve can be formulated showing the percent resolution of the detector across the different energies. The equation used to determine the percent resolution is shown in Equation 2.2.

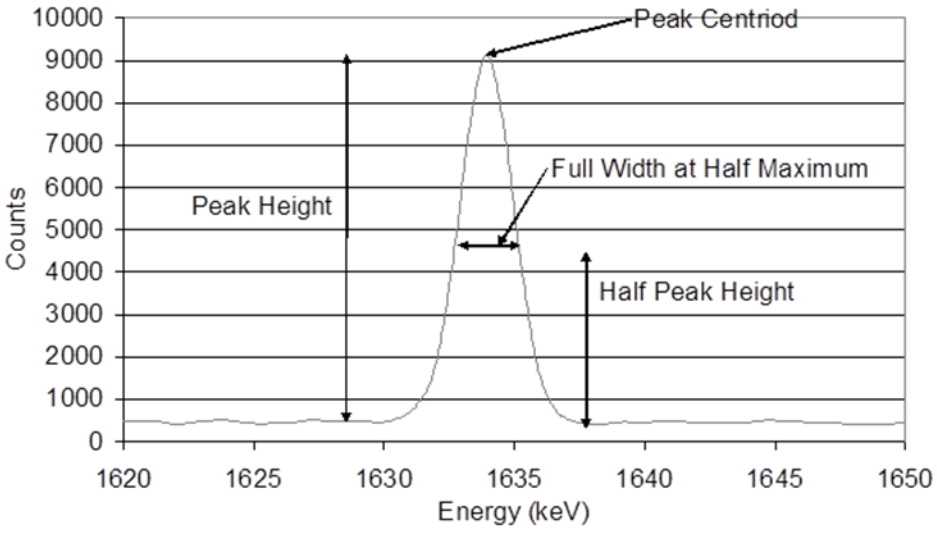


Figure 2.8: FWHM Graphical Representation [6].

$$\%\, resolution = \frac{100 \cdot FWHM}{Photopeak\ energy(in\ keV)} \tag{2.2}$$

In addition to knowing how to calculate the percent resolution of the detector, observing the FWHM vs gamma ray energy chart and the peak-to-Compton ratio will help to quantify detector performance. The equation for the ratio is by the following equation:

C.R. = # of Counts at $^{60}$Co Photopeak Center (1332 keV)/ # Counts at ($E_0$-256 keV) (2.3)

The previous pages should provide some insight on how the HPGe detector works as well as its typical setup and operational considerations. Following the installation of the FARIST system, the above equations will be utilized to analyze peak-to-Compton ratios, detector efficiencies, and % resolution. These metrics will help to quantify the overall quality of the detector portion of the FARIST system.

## 2.7 NAA ANALYSIS SOFTWARE

Once an HPGe detector has registered gamma rays, and their corresponding electronic signals have been registered, this information is then sent to a computer program for signal analysis. Examples of this type of software include programs such as Ortec's MAESTRO or Canberra's GENIE-2K. At the University of Texas NAA facilities, both programs are utilized, however, they are applied for different experimental setups. These programs work by assigning specific gamma ray energies that are registered by the HPGe detector to specific "bins". Every gamma ray detected by the detector, or "count" as it is called, gets added to the previous counts of that energy. This process is done for a large range of energies and the results are plotted on a graph of gamma ray energy vs. counts [11]. The result is several closely spaced energy bins that form a statistical peak. An example of a typical NAA acquisition spectrum is shown in Figure 2.9 with the element peaks labeled accordingly.

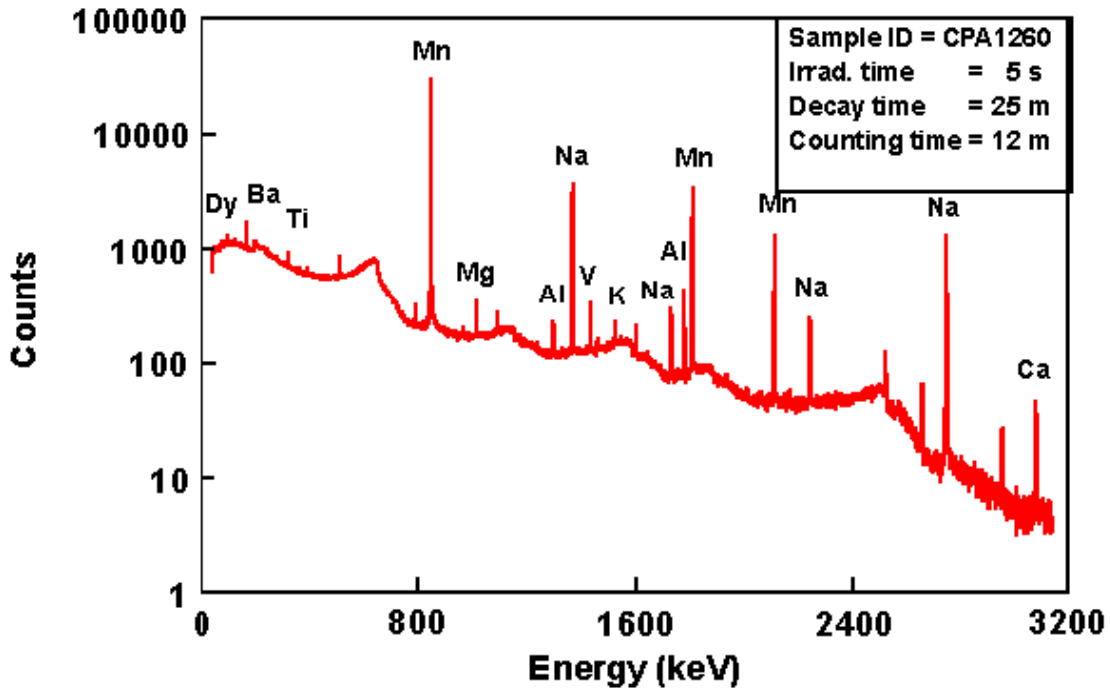


Figure 2.9: NAA Gamma Ray Acquisition Spectrum [2].

From Figure 2.9 it is readily observable that some of the registered peaks are very close, energy wise, to other peaks. The poorer the resolution, the more the peaks would blend themselves together. Further analysis of the graph can yield just how closely two different gamma ray energies can be identified.

### 2.8 NAA Concentration Calculation Methods

The NAA method also permits the researcher to identify relative elemental concentrations from an activated sample. The process, in short, is completed by taking the unknown sample's data and comparing it to that of a standard sample. In order to calculate the relative concentration of the unknown sample, both the Standard and the

unknown sample must have the same geometric configuration and be counted in front of the same detector. Equations that are applicable to the NAA concentration calculation are shown in Equation 2.4 and 2.5 [12].

$$\frac{N_u^*}{N_k^*} = \frac{N_u}{N_k} \frac{e^{-\lambda t_{du}}}{e^{-\lambda t_{dk}}} \frac{(1 - e^{-\lambda t_{cu}})}{(1 - e^{-\lambda t_{ck}})}. \quad (2.4)$$

Where: N = Number of Atoms

$\lambda$ = Decay Constant (1/sec)

$t_c$ = Counting Time

$t_d$ = Decay Time

M = Mass (grams)

C = Concentration

Subscript of *u* or *k* refers to the *unknown* or *known* sample

* in the Superscript represents an activated sample

$$C_u = C_k \frac{M_k}{M_u} \frac{N_u^*}{N_k^*} \frac{e^{-\lambda t_{dk}}}{e^{-\lambda t_{du}}} \quad (2.5)$$

**2.9 NAA SUMMARY**

With the concepts discussed in this chapter, the reader now has a basic understanding of not only how NAA works, but what it offers to the researcher. The concepts discussed in this chapter will be used continually throughout the entirety of this

project. These concepts affect everything from the material selection of certain components to how the detector will be positioned in the final assembly. While the FARIST system is a NAA system, it allows the researcher to do more. The reason for this project is to create a more capable NAA assembly meaning: attaining results with a more functionally flexible system. In order to attain "better results with a more functionally flexible system" the FARIST system will provide the user with the ability to conduct cyclic-NAA with no user interaction. This capability is a subset of NAA and few facilities in the world have the infrastructure to support such experiments. Using the concepts from Chapter TWO, Chapter THREE will provide an introduction into the types of NAA that the FARIST system will employ.

# Chapter 3: FARIST Employed Techniques

As explained in the previous chapters, NAA is simply another way to determine the elemental composition of a sample based on the corresponding energies of emitted gamma rays. Gamma ray spectroscopy, like chemical spectroscopy, has several different methods of employment with their own unique advantages, disadvantages, and experimental setups. The three primary methods for NAA are Prompt Gamma Neutron Activation Analysis (PGNAA), Delayed Neutron Activation Analysis (DNAA), and the last is cyclic (and Pseudo-Cyclic) NAA. Chapter THREE provides a general overview of the two NAA spectroscopy methods that will be used in conjunction with the FARIST system: DNAA and Cyclic NAA. Accompanied in the overview will be the experimental setups as well as the advantages, disadvantages, and theory behind each method.

## 3.1 DNAA Capabilities and Experimental Setup

### 3.1.1 DNAA Advantages and Disadvantages

DNAA is an excellent tool for radionuclide detection where half-lives on the order of minutes, hours, days, months, or years can be expected. A majority of radionuclides have half-lives longer than a few seconds making them ideal for DNAA. Additionally, with certain DNAA systems, better sensitivity and experimental accuracy can be expected due to the lack of high background counts, pulse pile ups and longer dead times associated with high activity samples and certain detection systems.

As mentioned in the previous chapter, DNAA systems traditionally place their detectors in locations separate from the neutron source in an effort to minimize background radiation. Coupled with effective detector shielding methods to help minimize ambient and environmental radiation, the resulting background counts on HPGe detectors can remain very low. Another advantage of separating the neutron source and detector is that by allowing a few seconds of sample transit time, (which doubles as decay time for the sample) the majority of short-lived (high activity) radionuclides decay away. By lowering both the sample activity and background in front of the detector, nearly all of the issues that detector systems have with dead time and pulse pile up are mitigated thus allowing for a more precise analysis.

The disadvantages of DNAA are fairly apparent in that in order to detect longer-lived radionuclides, longer counting times are required. These counting times can be as long as several hours at a time; making the process unattractive if results are required in a timely manner.

Certain DNAA systems however, do not employ a separation of the detector with the reactor, but rather a co-location of the two. Setups mirror those typically associated with a PGAA system. The only difference between the two methods being that counting begins once the neutron beam port shutter closes and the sample is no longer being irradiated. By co-locating the detector system, sample, and neutron source through means of fixed experimental setup, there is no longer any physical transfer of the sample. With this setup configuration, counting can begin within a few milliseconds from the conclusion of irradiation. Advantages of this process include the detection of short live

radionuclides that would have otherwise decayed away through extended sample transit times. Overall physical system efficiency is also improved by removal of the traditionally large sample transfer systems. Disadvantages however, include large dead times and pulse pile up issues from the highly activated samples. In the following section, graphical representations of both detector setups is presented and discussed.

### 3.1.2 DNAA System Setup

DNAA facilities are historically designed with the segregation of the neutron source and detector by means of distance and shielding. Shown in Figure 3.1 is a graphical representation of a typical DNAA facility where neutron source and sample detection take place in separate locations. Conversely Figure 3.2 is an example of a DNAA system setup where the sample undergoes no physical movement once the irradiation is complete, thus allowing for the analysis of extremely short lived radionuclide's. The setup from Figure 3.1 is what the University of Texas Nuclear Engineering Teaching Laboratory possesses and is what the FARIST system will utilize for sample activation and transport.

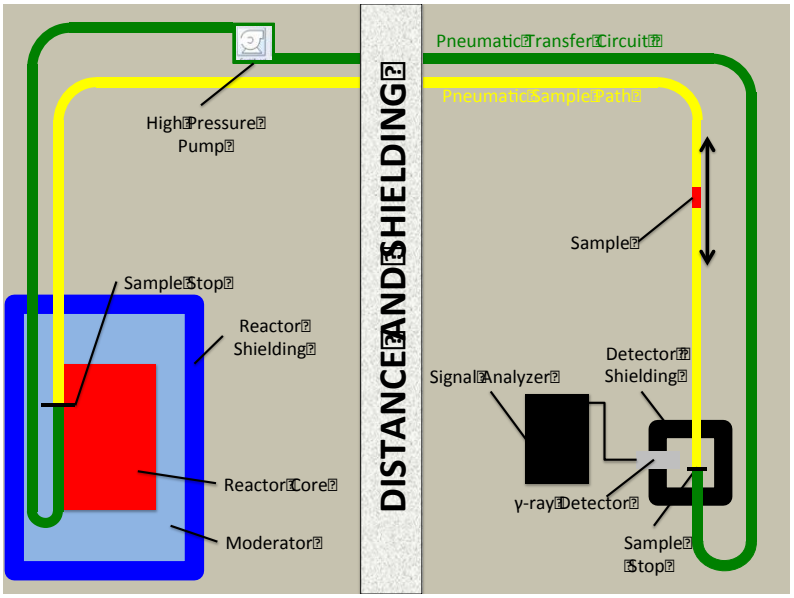


Figure 3.1: Typical DNAA Setup Where Physical Relocation of Sample Occurs.

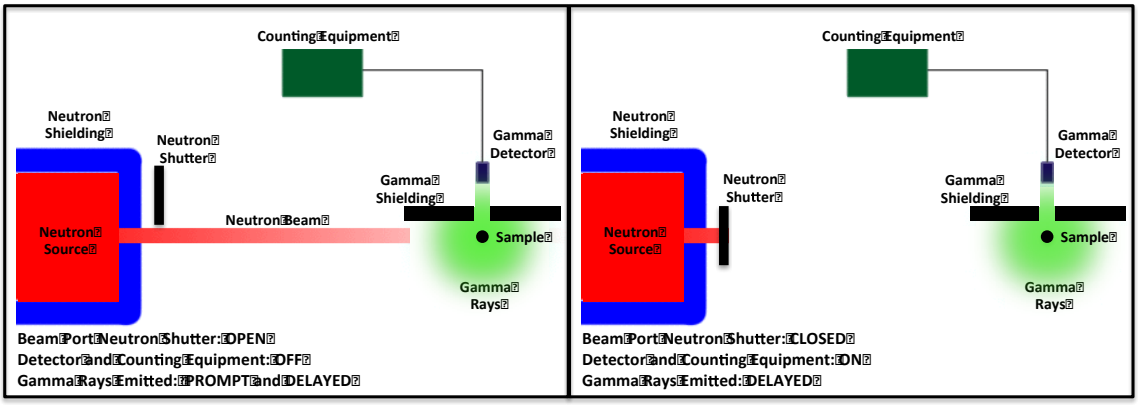


Figure 3.2: Typical DNAA Setup Where Sample Position Remains Fixed [6].

## 3.2 Cyclic and Pseudo-Cyclic Concepts and Capabilities

### 3.2.1 Cyclic NAA History and Concepts

Cyclic NAA can be first be referenced by ANDERS back in the 1960 & 1961 where samples were cycled between an irradiating source and a detector in order to

improve sensitivity, detection limits, signal-to-noise ratios, and lower the statistical uncertainty of the analysis [13]. Although not termed "cyclic," samples in these experiments were repeatedly irradiated from a Be target of a 2 MeV Van de Graaff accelerator, then counted on a NaI detector for two consecutive iterations of equal length. By subtracting the spectra obtained from each other, the resulting "difference" spectra would represent only the contribution of short-lived isotopes while simultaneously suppressing the contribution of longer-lived isotopes (essentially improving the peak to background ratio) [13]. Preliminary calculations indicated the usefulness of the technique in the determination of 18 elements: O, F, Na, Sc, Ge, Se, Br, Y, Rb, Rh, Ag, In, Er, Hf, W, Yb, Ir, Au[14]. Caldwell et al. also suggested the technique in 1966 in relation to a combination neutron experiment for remote element analysis of lunar and planetary surfaces using a pulsed neutron generator source. It was in this work that the term "cyclic" was first used [14].

The term "Cyclic Activation Analysis" (CAA) was however first used in 1968, and then again in 1970, by GIVENS et. al [14]. GIVENS was able measure $^{16}N$ and $^{24m}Na$, half-lives ≈7.14sec & ≈20msec respectively, using the technique given by ANDERS [14]. GIVENS however utilized a setup in which the sample was cycled electronically and the detector, sample, and neutron source were fixed in relation to each other; similar to the setup in Figure 3.2. TANI et al in 1969 utilized a similar experimental setup and observed photon spectra from $^{205m}Pb$ and $^{207m}Pb$, with half-lives ≈ 4msec and 800 msec respectively [14]. It was not until 1980 that SPYROU published a qualitative paper on the concepts and theory of CAA with a method to confirm the half-

life of radionuclides. An in depth look at the theory of NAA is presented in the next section providing a justification of why the new FARIST will be developed with the ability to conduct cyclic NAA.

### 3.2.2 Cyclic Neutron Activation Analysis Theory

The principles of CAA have been discussed extensively in Givens et al. and Spyrou's publications on CAA [13 14]. In their method, a sample is irradiated for a short period of time and then transported to a detector for a pre-determined counting period. Following counting, the sample is then transported back to the neutron source and the process is repeated. This process is completed for a total of *n* iterations where the irradiation, transport, and counting times remain fixed. Figure 3.3 illustrates the activity of a sample across the cyclic process.

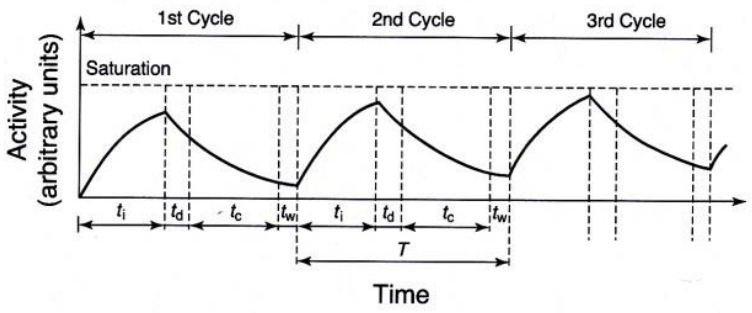


Figure 3.3: Sample Activity During Cyclic NAA Analysis [14].

Counts received by the detector for *n* iterations are then summed to obtain an overall detector response for the cumulative total time $T_t$. If the total cycle period is T, then T can be broken down into four components:

$$T = t_i + t_w + t_c + t_{w'} \tag{3.1}$$

Where:

$t_i$= Irradiation Time

$t_w$= Time from conclusion of irradiation to start of counting

$t_c$ = Counting Time

$t_{w'}$ = Time from conclusion of counting to start of irradiation

n = number of iterations

Thus cumulative total time can be expressed as:

$$T_t = nT \tag{3.2}$$

Additionally, if we assume that the system requires transit time to and from the both the neutron source and the detector we can assume that the transit times are identical, thus $t_w = t_{w'}$. Additionally detector response for the first counting period can thus be found using the following equation:

$$D_1 = \frac{I\epsilon\Phi\sigma N}{\lambda}\left(1 - e^{-\lambda t_i}\right)\left(e^{-\lambda t_w}\right)\left(1 - e^{-\lambda t_c}\right) \tag{3.3}$$

where:

$I$: Intensity of the radiation of interest (#/sec)

$\epsilon$: Detector Efficiency

$\Phi$: Neutron Flux ( neutrons/($cm^3$/sec))

$\sigma$: Cross Section of Isotope of Interest (1/$cm^2$)

N: Number of Target Nuclei

$\lambda$: Decay Constant of Isotope of Interest (1/sec)

Detector response for the second counting cycle can be determined with the following equation:

$$D_2 = D_1 + D_1 e^{-\lambda T} = D_1(1 + e^{-\lambda T}) \tag{3.4}$$

Thus for the $n^{th}$counting cycle:

$$D_n = D_1(1 + e^{-\lambda T} + e^{-2\lambda T} + e^{-3\lambda T} + \cdots e^{-(n-1)\lambda T}) \tag{3.5}$$

Utilizing mathematical methods this equation can be expressed as:

$$D_n = \frac{I\epsilon\Phi\sigma N}{\lambda}\left(1 - e^{-\lambda \mathrm{t_i}}\right)\left(e^{-\lambda t_w}\right)\left(1 - e^{-\lambda t_c}\right)\frac{\left(1-e^{-n\lambda T}\right)}{\left(1-e^{-\lambda T}\right)} \tag{3.6}$$

Now in order obtain overall detector response for all n cycles, the individual responses are added together with the following equation:

$$D_c = \sum_{i=1}^{n} D_i \tag{3.7}$$

Again using mathematical methods, Equation 3.7 can be expressed mathematically as:

$$D_c = D_1\left(\frac{n}{\left(1-e^{-\lambda T}\right)} - \frac{e^{-\lambda T}\left(1-e^{-n\lambda T}\right)}{\left(1-e^{-\lambda T}\right)}\right) \tag{3.8}$$

which when fully expanded is:

$$D_c = \frac{I\epsilon\Phi\sigma N}{\lambda}\left(1 - e^{-\lambda \mathrm{t_i}}\right)\left(e^{-\lambda t_w}\right)\left(1 - e^{-\lambda t_c}\right)\left(\frac{n}{\left(1-e^{-\lambda T}\right)} - \frac{e^{-\lambda T}\left(1-e^{-n\lambda T}\right)}{\left(1-e^{-\lambda T}\right)}\right) \tag{3.9}$$

Thus, Equation 3.9 is the cumulative detector response equation for CAA. Figure 3.4 is provided as a graphical representation of how detector response ($D_c$), as a function of the number of iterations, increases through successive iterations, leading to the obvious conclusion that CAA is an effective and relatively simple method to improve detector response.

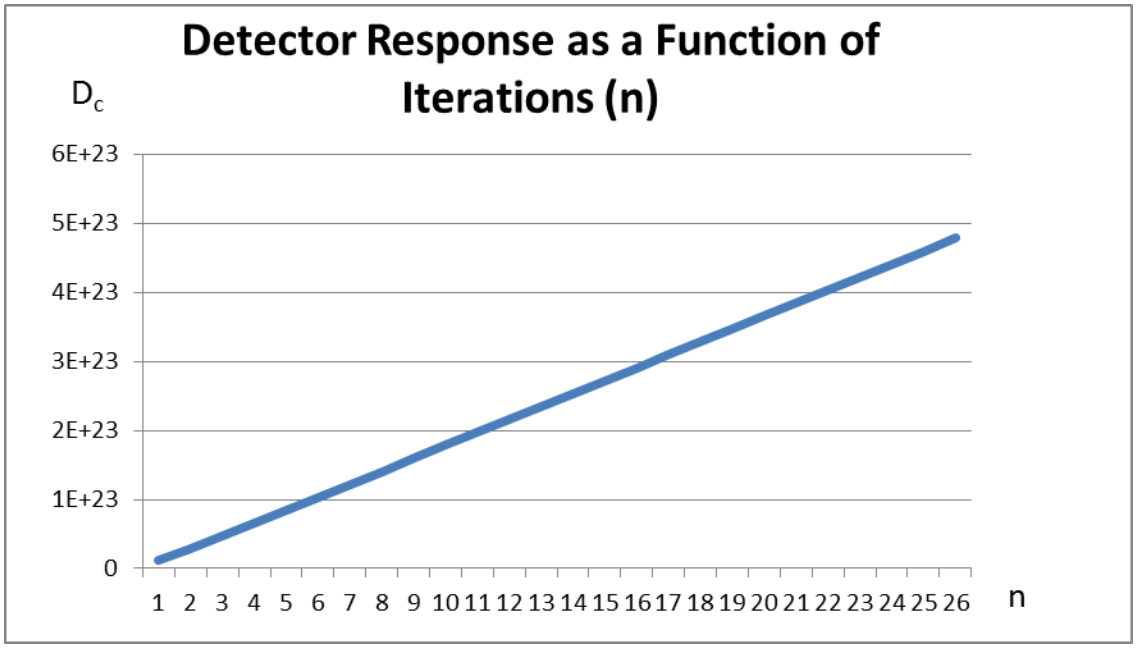

Figure 3.4: Detector Response as a Function of Cycles.

Additionally, another major advantage to using the CAA method lies in the uncertainty calculation. If Poisson or Gaussian counting statistics for uncertainty are employed, then the uncertainty, or standard deviation, is assumed to be the square root of the detector response. Thus, it is observed that uncertainty improves as a function of the square root of the number of cycles. Observing the linear relationship that detector response has with the number of iterations, it is prevalent that the ratio of the uncertainty

to the signal (uncertainty ratio) will decrease in an exponential matter. This relationship is displayed in Figure 3.5.

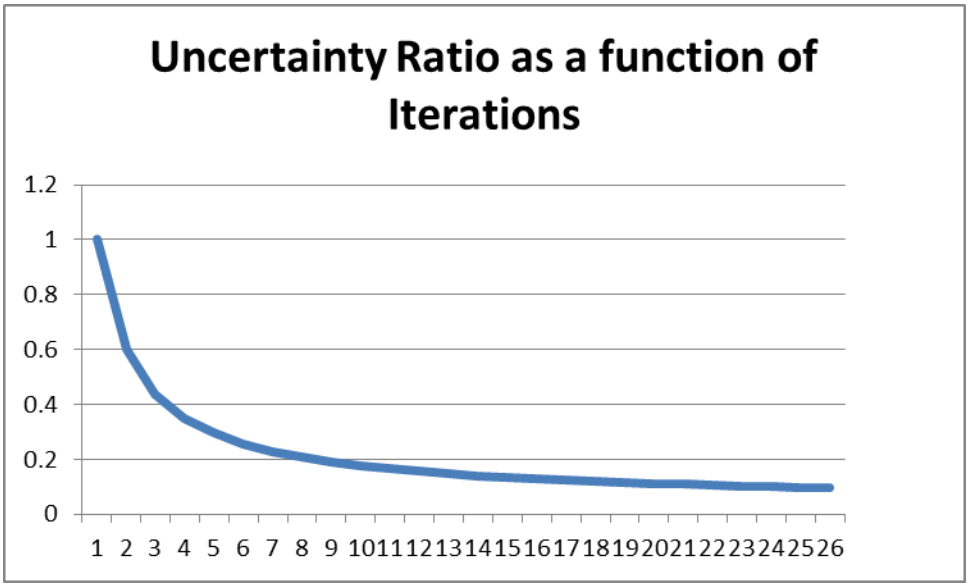


Figure 3.5: Uncertainty Ratio as a Function of Number of Iterations.

The signal-to-noise ratio (SNR) is also affected by the cyclic process. With the inclusion of the additional background signals as well as the source signals, an in depth look at SNR is necessary to optimize the system quality analysis. This in depth look at SNR is provided in the following section on how to optimize the CNAA system input parameters.

### 3.2.3 Cyclic NAA Theory Optimization Parameters

Detector response can be maximized with the selection of optimal system parameters. From a cursory look at Equation 9, the lower the transfer time ($t_w$) the better the detector response. Because of this relationship, a design goal for the FARIST system

was to minimize the sample transfer time from the irradiation source to detector, and vice versa. As discussed earlier, the FARIST system aimed to complete sample transfer in around/under 10 seconds, so for any detector response calculations following, $t_w$was set to 5 sec for data analysis.

It is important to note that detectors not only register signals from the isotope of interest, but also those from other radioisotopes present in the sample. These additional signals accumulate and represent the "background" that the detector registers. This background increases over successive iterations and plays a significant role in signal to noise ratio calculations. Spyrou used a background radiation equivalent to 100 times the half-life of the isotope of interest in his research, overall an appropriate approximation for background [13]. Using Equation 3.9 and changing the half-life to that of the background value, a summation of detector response for the background can be found. Assuming a Poisson or Gaussian counting statistic where the standard deviation is the square root of the mean background, the Signal to Noise (SNR) can be found with the following equation:

$$SNR = \frac{D_c(Isotope\ of\ Interest)}{\sqrt{D_c(Background)}} \tag{3.10}$$

It is important to note that when modeling experimental results, assigning a general background half-life of 100 times the isotope of interest will work for a *rough* evaluation [13]. If a more detailed analysis is necessary however, a detailed knowledge of the background radionuclides present will be needed. In 1981 Tout and Chatt

developed an analytical modeling program to determine the selection of optimum timing parameters for CNAA by inputting total experimental time, transfer time, mass data, and relevant nuclear data into a matrix program [14]. For this program, an advanced knowledge of the background elements was required in order input them into their program and help determine timing parameters. A more detailed explanation of the methods developed for background analysis can be found in *"The effect of Sample Matrix on Selection of Optimum Timing Parameters in Cyclic Neutron Activation Analysis"* by Tout and Chatt.

The relationship that all these variables have in relation to the calculation of SNR is obviously complex. In an effort to evaluate these relationships and help identify general trends, a suite of programs was developed in Fortran IV under the name "CYCLOPS" [13]. From these programs the most prevalent trend observed was that overall, if $t_w$remains low, the SNR will generally continue to increase through successive iterations. The trend for better experimental accuracy however must then be balanced between allotted experimental time and cost. Conversely, as $t_w$ increases, a limit can be found when additional iterations no longer continually produce an increase in the SNR. The relationship between the detector response for the sample and the background ($D_c$ and $D_B$) have with $t_w$ has also been studied extensively by Spyrou and Kerr with their results publish in *Cyclic Activation Analsyis – A Review* [13]. Shown in Figure 3.6 is the relationship that a varying $t_w$ has with the SNR. Additional SNR curves are provided in Figure 3.6 to highlight the differences between cyclic analysis and the conventional "*one shot"* irradiation. It is important to observe the significant

improvements in the SNR obtained from CNAA as opposed to the "*one-shot*" irradiation technique. Another observation deduced from Figure 3.6 is the degradation in the SNR with increasing $t_w$ times, thus the importance of minimizing the transit time is readily apparent.

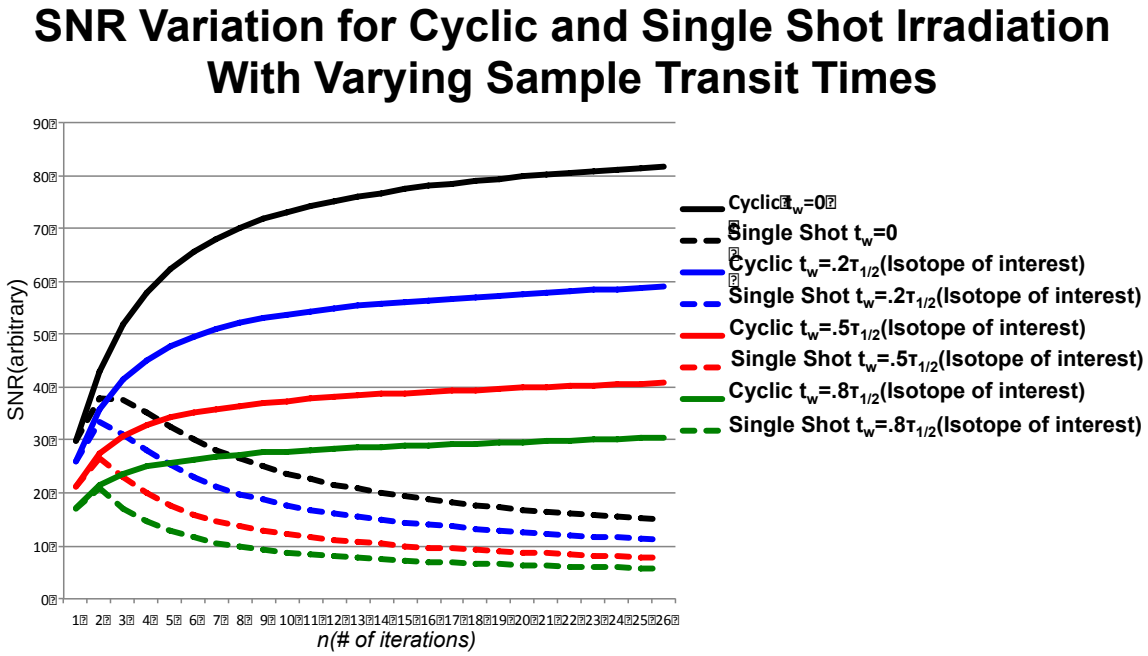


Figure 3.6: SNR Variation Between Cyclic and One-Shot Irradiation with Varying Sample Transit times.

As a result of all the different inputs to the calculations for SNR, it is obvious that there are an infinite number of combinations that affect the SNR curve in a variety of ways. An in-depth discussion on all the different variations is beyond the scope of this subject matter however several prevalent trends are identified through numerous statistical analysis iterations. The first trend is that irradiation time selection must be less than the time required for the sample to reach activity saturation, thus the irradiation time

must be less than five half-lives. If irradiation is longer than that time, all the researcher is doing is continuing to activate additional background which can severely interfere with the SNR. The second general trend is that iterative analysis is not always the better method. To determine whether cyclic activation or single shot irradiation is the preferred method researchers should consult SNR modeling programs to identify which method would be preferred. Figure 3.7 is an example where, based on the experimental inputs, single iteration irradiation is preferable to CAA. Again, these trends are the most significant and are the ones worth mentioning.

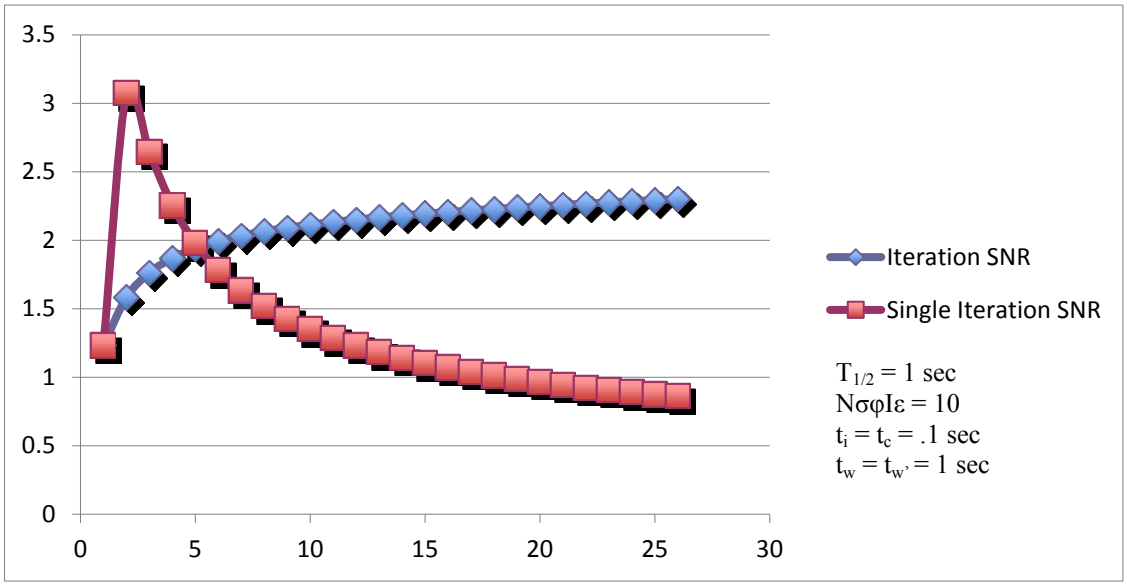


Figure 3.7: System Parameters Where Single Shot Irradiation is Preferable to Cyclic Analysis.

### 3.2.4 Detection Limit Calculation

In addition to the SNR, determining the detection limit is also another important benchmark in comparing cyclic activation to that of the standard one-shot irradiation

method. The detection limit can be found for a single iteration from Equation 3.11 [15 16]:

$$l_d = \frac{3\sqrt{B}}{(\frac{S}{m})} = \frac{3m\sqrt{B}}{S} \tag{3.11}$$

Where $\frac{S}{m}$= counts per unit mass of the isotope of interest, B is the background count, and S is the counts under the peak of interest.

Equation 3.11 however, is for a single shot irradiation. For CAA, with n cycles, the detection limit can be found using Equation 3.12. Through this equation it is fairly easy to identify the advantages of cyclic analysis as long as the system inputs and sample composition promote the use of cyclic analysis [15] [16].

$$l_d(n) = \frac{3m\sqrt{D_c(Background)}}{D_c(Isotope\ of\ interest)} \tag{3.12}$$

### 3.2.5 Half Life Confirmation Methods Utilizing CAA

The use of CAA to estimate and confirm half-life values was first suggested by Spyrou et al [13]. Spyrou observed that for large values of n from Equation 3.8, $(1 - e^{-n\lambda T})$ would move closer to a value of one. The change is reflected in Equation 3.13.

$$D_c = D_1\left[\frac{n}{(1-e^{-\lambda T})} - \frac{e^{-\lambda T}}{(1-e^{-\lambda T})^2}\right] \tag{3.13}$$

Equation 3.13 can then be re-arranged into the basic slope formula of y=ax-b:

$$D_c = \left[\frac{D_1}{(1-e^{-\lambda T})}\right] n - \frac{D_1 e^{-\lambda T}}{(1-e^{-\lambda T})^2} \tag{3.14}$$

where a:

$$a = \frac{D_1}{(1-e^{-\lambda T})} = \text{Slope of the line} \tag{3.15}$$

and where b:

$$b = \frac{D_1 e^{-\lambda T}}{(1-e^{-\lambda T})^2} = \text{Intercept} \tag{3.16}$$

The ratio between *a* and *b* can then be written as:

$$\frac{a}{b} = -\frac{(1-e^{-\lambda T})}{e^{-\lambda T}} \tag{3.17}$$

Thus the half-life of the isotope of interest can be calculated by re-arranging Equation 3.17 to make:

$$\tau_{1/2} = \frac{T \ln(2)}{\ln(1-\frac{a}{b})} \tag{3.18}$$

### 3.3 DNAA REVIEW

The topics discussed in this chapter provide a detailed understanding of the different forms of DNAA available to the researcher. The cyclic and pseudo-cyclic portions of this chapter readily identify why having a cyclic capability with the FARIST system is important. The equations used for benchmarking, and determining overall system efficiency/improvement will be re-addressed in Chapter SEVEN. Prior to understanding the design phase and what the future holds for the FARIST system, a look back at previous cyclic NAA systems is appropriate. Chapter FOUR provides a few examples of current DNAA facilities along with a brief discussion on each systems

advantages and disadvantages. Using the information gleaned from prior systems will help to provide better design input into the final product.

# Chapter 4: Current DNAA Facilities and Experimental Setups

There are generally two types of DNAA facility setups that exist for sample analysis. The difference between the two setups is based on detector proximity to the reactor core. The first setup involves DNAA facilities that utilize detection systems near or around the reactor core resulting in elevated backgrounds but extremely short transfer times. The second DNAA setup utilizes separation of the detection system and the reactor through means of additional shielding and distance resulting in lower backgrounds but elevated sample transfer times. Separation is attained through installation of long sample transit lines to ferry the sample from the reactor to locations isolated from the reactors radiation. Each setup discussed in this chapter has its own unique pros and cons. Most systems lack cyclic capability however, a few do exist and their setups are studied to provide input into the design of the FARIST system [17 18].

This chapter examines three DNAA facilities that are currently operating across the globe. The three facilities examined in this chapter are: The University of Texas "old" DNAA system, the NAA facility in Vienna Austria, and the NAA facility at the Technical Research Centre of Finland's Reactor Laboratory. A brief analysis of each facilities physical setup will be presented highlighting unique system advantages and disadvantage. By analyzing existing mechanical DNAA setups, educated decisions can be made in the design phase of the FARIST system by utilizing lessons learned from previous systems.

## 4.1 THE UNIVERSITY OF TEXAS DNAA SYSTEM

### 4.1.1 Overall Physical System Setup

Prior to the installation of the FARIST system, the University of Texas at Austin utilized a manually operated pneumatic transfer system to conduct DNAA. The system required the user to load samples into a pneumatic tube inside a fume hood located inside the NAA lab; a laboratory room separate from the reactor bay. The samples were transported into the F-ring of the reactor core via polyethylene tubing to be irradiated. Inside of the reactor, the samples were held in thin walled aluminum tubing. Irradiation time was controlled by the user through the control of a $CO_2$ pneumatic pump, or blower. When irradiation time was complete, the pneumatic flow was reversed causing the samples to exit the core and arrive back inside of the fume hood. The user would then allow the activated sample to decay to a safe level whereby the researcher could then safely physically transport the sample to a detector. The *old* DNAA setup is shown in Figure 4.1.

Several inherent problems are presented by requiring the sample to "cool" prior to transport and subsequent analysis. The first is that radionuclides with half-lives under 45 seconds decay away prior to the sample ever arriving at the detector. As a result, the quality of the experimental analysis is degraded for such radionuclides. The second, and more important problem; the researcher must expose themselves to an activated sample in order to physically transfer the sample from the fume hood to a detector. Additionally, due to the lack of repeatability among the system parameters and researcher-exposure concerns, the original DNAA facility was unable to support cyclic irradiation analysis.

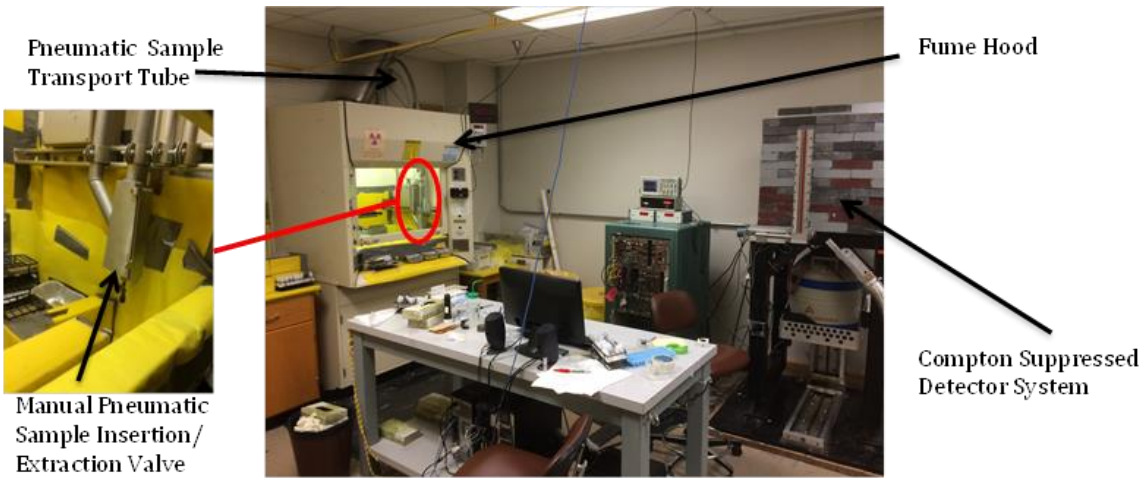


Figure 4.1: Original Texas DNAA Laboratory and Setup

### 4.1.2 Lessons Learned

The inherent problem with the original Texas DNAA facility was the necessity for constant user interaction. From manually controlling the pneumatic airflow circuit, to physically transporting the sample to the detector, the dependence on human interaction was high, inefficient, and prone to human error. The FARIST system was designed to completely negate these issues through the employment of a pneumatic circuit that rapidly transports a sample from the reactor core to the detector with no human interaction. The result is a safer, more efficient system able to detect short lived radionuclides that would have otherwise decayed away.

## 4.2 AUSTRIAN DNAA SETUP

### 4.2.1 Overall Physical System Setup

The TRIGA research reactor in Vienna, Austria is similar to the one at the University of Texas. The overall system setup however is fundamentally different in that the pneumatic circuit transfers the sample from the reactor core to a detector located **inside** of the reactor bay thereby affording the system short sample transfer times [19]. The system employs an in-core aluminum tube (the same as the Texas facility) connected to plastic tubing at the top of the reactor pool (Figure 4.2). Air is utilized in the circuit to provide the means of transport for the sample. The plastic tubing is directed using a series of guides to the detector located at core level where the tubing is attached to a sample catch/valve.

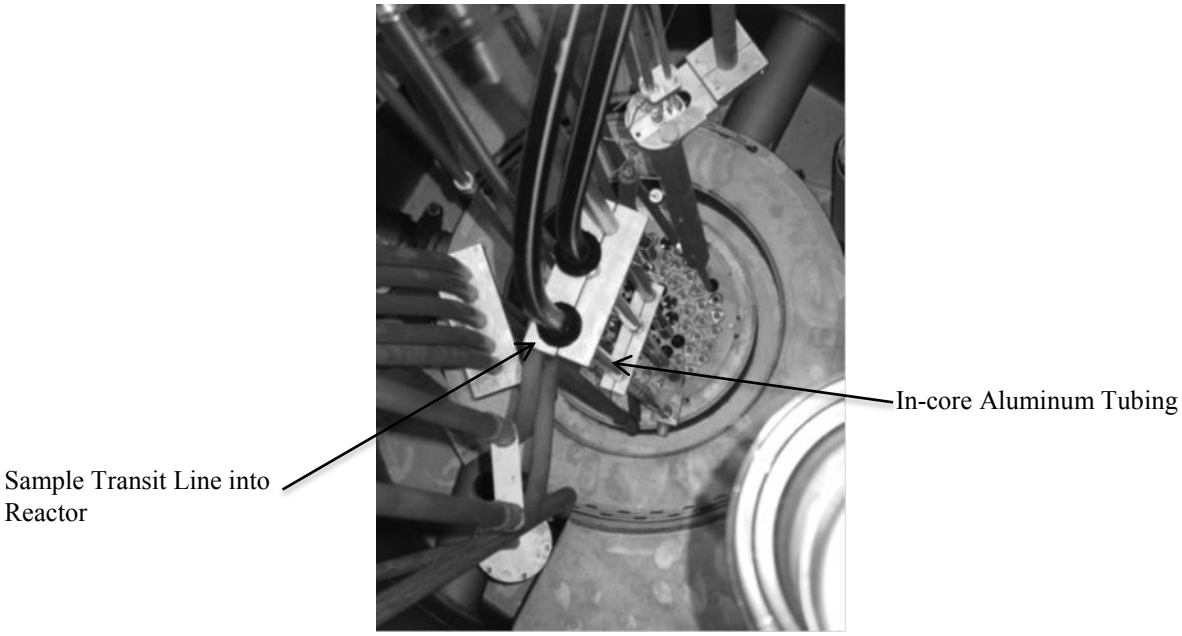


Figure 4.2: Pneumatic Tubing Placement Inside TRIGA Reactor Pool [19].

The sample catch/valve is a unique component of this NAA system combining the functionality of inserting, ejecting, and transferring samples in a DNAA pneumatic loop into a single device. Built into the valve is a sample catch near the top which acts to stop the irradiated sample in front of the detector. The system unfortunately, is controlled manually through a hand crank thus still requiring user interaction. As a result of component geometry, the system is able to support cyclic irradiation and counting operations. A graphical illustration of the valve is provided in Figure 4.3 along with an actual image of the valves placement in the reactor bay in Figure 4.4. Due to the necessity for human interaction, the system can present exposure risks to the user and therefore those risks must be managed accordingly.

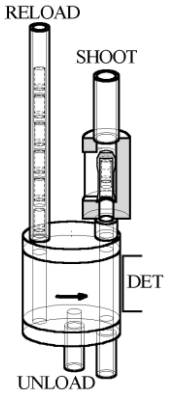


Figure 4.3: Austrian Sample Injection/Ejection Valve [19].

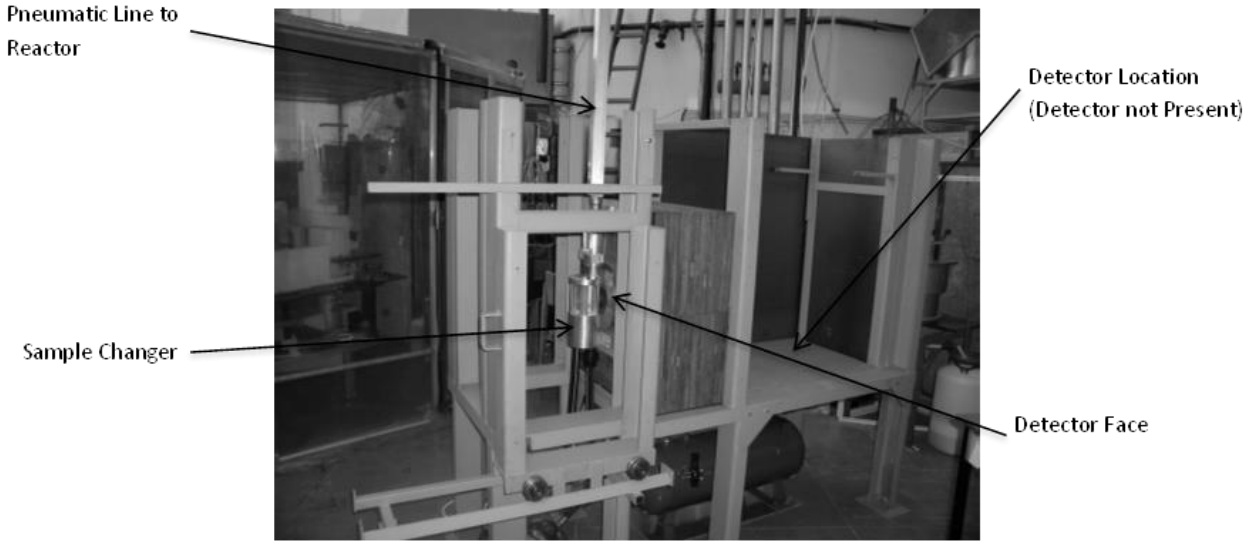


Figure 4.4: Austrian NAA Sample Receiving Station [19].

The pneumatic circuit clocks in at around 2.3 seconds from the end of sample irradiation to detection; overall a very quick transfer. Advantages include the detection of short lived radionuclides and an overall simple and physically efficient system. With co-location of the reactor and high sample activity however, issues with dead-time and pulse pile up are introduced. It should be readily evident by now that the advantages of a shortened transfer time, or $t_{w,}$ must be balanced with the limitations of the detector. The system can still be effective in detection of short lived radionuclides however, the employment of additional analytical techniques are required to mitigate the detector issues.

### 4.2.2 Lessons Learned

The creation of a sample transfer valve assembly in close proximity to the detector helped to improve overall system simplicity, efficiency and capability. By reducing the need for constant human interaction, the system is safer than its predecessors. Through an ingenious valve design the system is also ideally suited for cyclic analysis. Coupled with short irradiation to detector times, the system is also overall very appealing for short lived radionuclide analysis.

The system did have several downfalls however. The need for an individual to manually adjust the sample valve can pose exposure issues to the user. While sample transit times are expedited, issues with an elevated background due to the proximity of the reactor core are propagated by the high activity of the sample. If the receiver/detector system were located outside of the reactor bay, reactor background effects could be mitigated with minor effect to sample transit times. This setup is an excellent example of the "80% solution." With a few simple adjustments and some added automation the system could be significantly improved.

## 4.3 FINNISH DNAA SYSTEM

### 4.3.1 Overall Physical System Setup

The Finnish DNAA facility is similar to the Austrian setup through the placement of the detector in close proximity to the reactor core. The Finnish facility actually goes so far as to place the detector system at the top of the reactor pool so that the actual distance between the irradiation position and the measurement position is reduced to only a few meters. As a result of the shortened distance, transfer times on the order of 60-80

milliseconds can be observed when nitrogen is used in the pneumatic loop. That transfer time slows to around 300 milliseconds when air is used instead throughout the loop [20]. To prevent samples from fracture as a result of the high transfer speed, a pneumatic brake was installed around the detector housing to slow the sample prior to hitting the sample stop.

Once counting is complete at the detector, the sample can either fall back into the core for cyclic analysis or it can be ejected up and out of the detector using the pneumatic circuit. If the sample is ejected away from the detector it then utilizes plastic tubing to shuttle the sample to a specialized sample changing unit for either storage or disposal. Both the sample holder and waste receptacle were positioned and shielded so that previously activated samples would not affect ongoing detection analysis.

The sample storage facility was a positive addition to the system due to the fact that it could hold up to 160 samples for analysis. The necessity to test 160 samples may be a bit redundant; nonetheless the capability is nice to have. Figure 4.5 illustrates the mechanical system setup complete with detector, reactor, and sample storage location along the pneumatic loop. Additionally, Figure 4.5 also details out the electrical component of the NAA system and its employment of advanced counting hardware [20].

Another unique aspect of the Finnish system is the employment of "loss-free counting," or LFC, methods. Westphal outline the technique for LFC with his work on "Real-Time Correction of Counting Losses in Nuclear Pulse Spectroscopy" [21]. In his work he describes an internal system pulser that monitors, real-time, the system dead time multiplying each count by a weighing factor. The system analyzer then monitors

both the amplifier and ADC dead time and applies this technique so that dead time is accounted for across the entirety of the system. Using the LFC technique researchers were able to compensate for up 65% dead time with excellent NAA results [20].

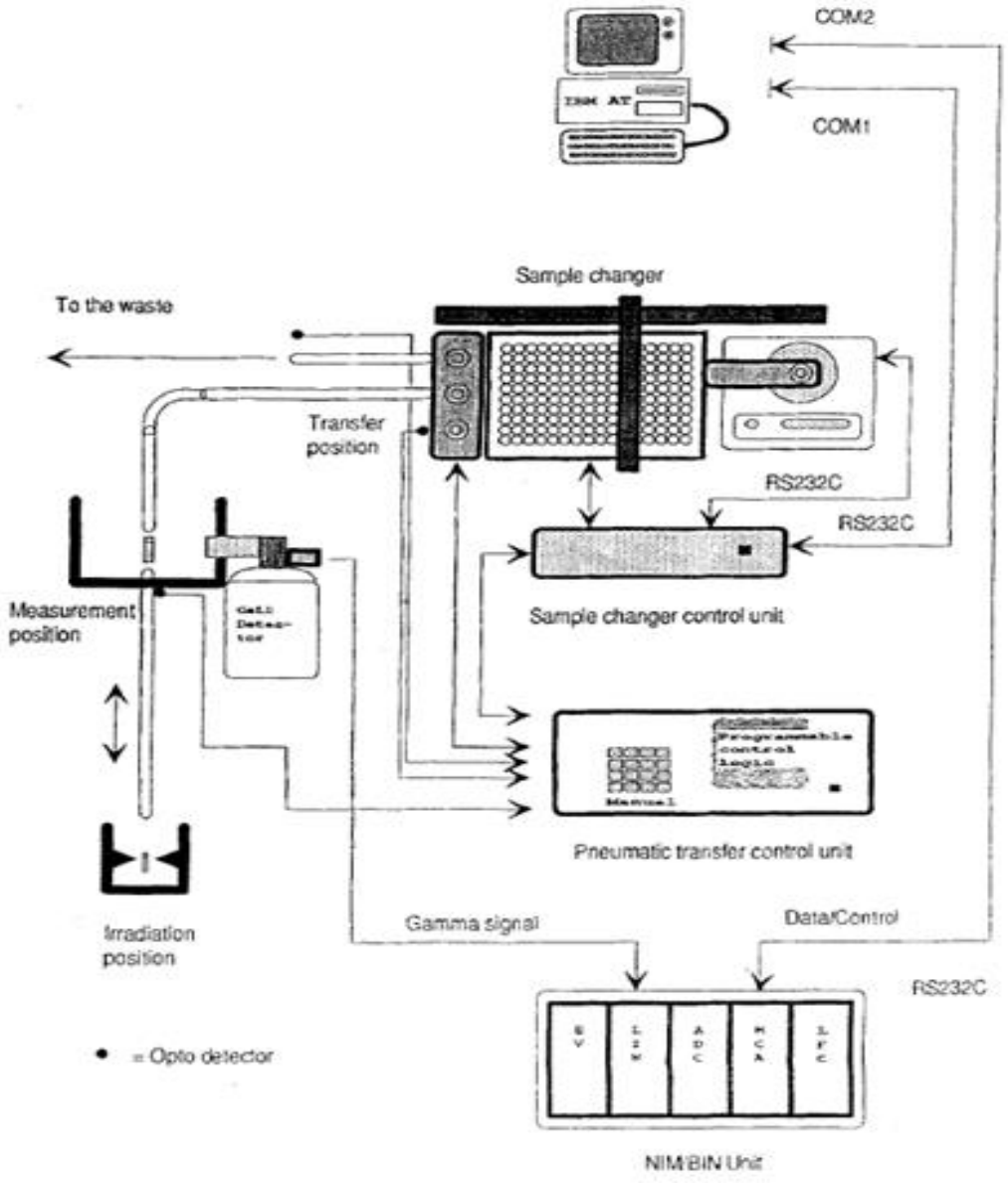


Figure 4.5: Finnish DNAA System Setup [20].

### 4.3.2 Lessons Learned

The extremely short sample transfer times from the reactor to the detector make the Finnish system unique. High sample activity and reactor proximity present the same issues as they did with the Austrian system however, their effects are mitigated either by allowing the sample to decay prior to detection or by applying loss free counting (LFC) techniques. Coupled with using electronics and automation to minimize user interaction, along with a "magazine" to store samples, the Finnish system was one of the safest and most effective DNAA systems in the world.

There are however a few points for possible improvement to the Finnish design. The sample changing storage system that holds up to 160 samples is rather large and cumbersome, requiring several large outdated servo motors to operate along the x and y axis through the use of a logic board. Technology has significantly advanced in recent years and an updated approach to the electrical components, sample storage and retrieval is warranted.

## 4.3 Overview of Current DNAA Facilities

As discussed, each of these DNAA facilities offer a wealth of knowledge whether it be on *what to do* or, *what not to do*. Each systems advantages and disadvantages were highlighted and discussed. Through this examination a more modern, effective, and robust system can be designed and installed. Setups from this chapter allotting certain benefits to the NAA process are injected into the design phase of the FARIST system to potentially be adopted into the final FARIST design. Previous system components that

ultimately degraded the quality of the NAA results are abandoned. Chapter Five provides an in depth look at the decision making process behind component design and selection utilizing the lessons learned from this chapter.

# Chapter 5: Conceptual and Advanced Component Design of the FARIST System

## 5.1 Requirements and Constraints

The requirements and constraints for this project are numerous due not only to overall system complexity, but the radioactive environment in which the system is placed. The most important requirements and constraints to the experimenter include user free operations, sealed pneumatic loops, expedited sample transit times, high repeatability, manageable cost, and overall favorable system efficiency. Specific requirements and constraints are listed in the following paragraphs to identify system specifications in order to influence component design.

The most important requirement of the system was that it remained 100% hands free after sample irradiation and counting times had been entered into the computer. This function serves to eliminate any user exposure from the activated samples as a result of ongoing analysis. With the use of a computer input system, it was required that the program utilized be both user friendly and ergonomic. Per the design requirements, the system must possess the capability store and program for up to 30 samples. Component wise, some sort of "magazine" or storage unit would have to be created that can store samples prior to analysis. Additionally an automated mechanical device would have to be created to pull the samples from the storage unit and inject them into the pneumatic loop.

Other important requirements of the system include high repeatability of the sample position next to the detector. A HPGe detector will be utilized for the detection system to provide extremely precise results. These results are affected by sample proximity to the detector. In order to mitigate any sample/detector proximity issues, the samples position from analysis to analysis was allotted a fluctuation tolerance of no more than 0.09 inches. Additionally, both the material and corresponding thickness of the sample stop must be designed to minimize gamma ray attenuation due to material attenuation concerns. The time required to transit from the reactor core to the detector house is also a design requirement. For the purposes of DNAA at the University of Texas, having a sample transit time shorter than 10 seconds is required. These requirements are organized onto a specification sheet shown in Table 5.1.

Table 5.1: Requirements Specification Sheet.

| Demand/Wish | **Requirement** |
|---|---|
| Demand | No User Interaction Required After Input of System Parameters |
| Demand | 30 Sample Capacity |
| Demand | Sample Position Repeatable (.09") |
| Demand | $T_w$ Under 10sec |
| Wish | System Utilizes a Graphical User Interface |
| Demand | Material between Sample and Detector Minimized |

There are a multitude of constraints involved with creation of the system. A few of the most important constraints are that the new system must work to minimize changes to the already existing testing facilities. Also, as a result of using $CO_2$ as the transport

gas medium, the pneumatic loop must be hermetically sealed to prevent possible user asphyxiation in the analysis room if $CO_2$ were to flood the room. Other constraints include programming compatibility between the detector and the operating software used to control the FARIST system. Additionally, as a result of the radioactive environment and potentially high activity samples, non-reactive materials must be utilized throughout the system. Another significant constraint included the available space to physically place the FARIST system. The two candidates for system location included either at the top of the reactor pool, or along a wall in the existing NAA laboratory. The last constraint of the project was total cost. As with any project, overall system effectiveness and speed would have to be balanced with cost, so for the FARIST system, a flexible budget of $10,000 was established.

Table 5.2: Constraints Specification Sheet.

| Demand/Wish | **Constraint** |
|---|---|
| Demand | System Must be Hermetically Sealed |
| Demand | Coding Must Interface with Canberra Software |
| Demand | Material Must Not be Affected by Radioactive Environment |
| Demand | Available Space |
| Wish | Minimize Changes to Existing Infrastructure. |
| Wish | Cost under $10,000 |

## 5.2 SYSTEM CONCEPT SELECTION/DESIGN METHODOLOGY

The FARIST system can essentially be broken up into five separate components for design purposes. The first component is the pneumatic loop. This subsystem not only acts as the propulsion mechanism for the sample, but also dictates the FARIST's systems overall physical setup. The pneumatic loop passes through every component of the FARIST system and presents challenges in maintaining the $CO_2$ on the system while concurrently promoting a smooth and uninterrupted path for the sample to transit along. The second component of the system is the device utilized to transfer the sample in and out of the pneumatic circuit. In order to combine functionality and simplify the system, that device was designed to direct the sample into and out of the circuit and additionally direct the sample to the detector. The third component concerns the detector and its housing. Everything from shielding setup to the sample stop design is grouped into this FARIST sub-system. The fourth component of the system concerned sample sensor selection and emplacement across the FARIST system to maintain situational awareness on sample location and dictate system operation. The last component of the FARIST system is the electrical and programming portion employed to ensure seamless system operation.

To assist in the decision making process a common engineering decision making metric, the Peugh chart (Table 5.4), was employed with a unique weighting system to help identify which options available best suited the constraints and requirements of the system.

The first decision to be made regarding the FARIST system concerned the physical placement of the detector system. As discussed earlier, having the detector located near the reactor afforded rapid sample transfer times however; issues with detector performance were introduced. As a result of these reasons, it was decided that the detector/sample changer system should be located outside of the reactor bay inside of the existing NAA laboratory.

## 5.3 PNEUMATIC CIRCUIT/OVERALL SYSTEM SETUP

The existing NAA lab was utilized as the location to place the detector for the FARIST system. With the design specification to minimize irradiation to counting time, it was obvious the sample circuit should remain as smooth and curve free as possible to reduce overall resistance to the sample. With these constraints, and some additional considerations, the overall design of the pneumatic circuit could begin.

### 5.3.1 Pneumatic Airflow Considerations

There are several considerations that needed to be taken into account in the design of the pneumatic circuit. The first concern was the $CO_2$ utilized throughout the circuit and its potential to leak. As a result, the tubing, fittings, and valves had to provide a seal to prevent leakage of the $CO_2$. The NAA lab constitutes as a confined space and if filled with $CO_2$ would pose as a toxic environment to the researcher. The second major concern of the system involves the activity of the irradiated samples. The activity can pose potential problems to rubber and other components that deteriorate rapidly in a radioactive environment. As a result, system components were designed and selected

based on their low attenuation to incident radiation. An additional consideration was the speed at which the sample would strike the sample stop in front of the detector. If the sample is travelling too quickly when it strikes the sample stop the potential for the sample case to fracture, resulting in contamination of the loop, can be significant. To mitigate the possibility of this situation occurring, it was decided that a pneumatic brake, or buffer, would be implemented near the sample stop to slow the sample. The last major airflow concern was the drag created through the circuit. In order to reduce drag throughout the loop, the setup had to minimize points throughout the system that constituted airflow resistance to the circuit. With the loop powered by a 20 watt blower, the importance of minimizing drag directly effects system sample transfer performance.

The last major consideration to affect the pneumatic loop setup was the requirement that while a sample is being counted, the airflow must be shut off to prevent potential vial vibration during analysis. This coupled with the requirement for the airflow to be "on" when a sample is in the core meant that an advanced circuit design would be required to satisfy both requirements simultaneously.

### 5.3.2 Pneumatic Circuit Design/Diagram/Control

To promote a straight path from the reactor to the detector, it was decided a sample injection/ejection valve be placed midway through the pneumatic system with the ability to allow the sample to transfer through uninterrupted. The sample would then transit to the detector housing where a fixed sample stop design would be implemented to arrest the sample in front of the detector. As discussed earlier, if the sample was

travelling too rapidly, the researcher runs the risk of fracturing the sample when it strikes the stopper. To mitigate the chances of fracture, the use of pneumatic breaking was employed to slow the sample prior to arrival at the stop. This was completed by adjusting the airflow circuit to cut the pneumatic propulsion of the sample just prior to arrival at the detector. By cutting the propulsion and isolating the $CO_2$ to the detector housing, the ambient $CO_2$ slowed the in-motion sample as result of the tight tolerance between the sample (0.66" O.D) and the circuits polyethylene tubing inside diameter(0.75" I.D.). The result was a cushioned landing on the sample stop thereby mitigating sample fracture concerns.

By placing the sample injection/ejection valve in the middle of the pneumatic loop, simultaneous irradiation and counting of two separate samples was possible. This was done placing pneumatic control valves at key positions on the circuit to create component bypass loops. The purpose of the bypass loops was to allow for an isolation of the detector system while still maintaining the functionality to inject and eject a sample from the reactor core. Additionally the bypass loops were created so that during ongoing sample irradiation a cooling flow could be provided to the in-core sample while simultaneously ejecting the sample from the detector housing, and transferring the sample to waste. This dual functionality would allow researchers to save time by overlapping counting time with irradiation time.

Through successive planning iterations a final design was formulated capable of satisfying the design and safety requirements and considerations. This final circuit design is shown in Figure 5.1 along with an outline of the planned valve positions during each

phase of operation shown in Table 5.3. It should be noted that the two pneumatic circuit lines that are departing the system connect to the blower not shown in the Figure 5.1. The blower is located in adjacent facility and can be programmed to reverse the flow of the circuit. This ability allows for selectable system flow direction based on the programmers input.

With a cursory look at the system it is easy to identify three pneumatic valves the sample is required to transit through between the reactor and the detector. Extra care had to be given to these valves to ensure the sample did not catch on any "lip" or gap between the tubing and the valve system. This would be done through a combination of smoothing the insides of the valves and maintaining tight tolerances between the pneumatic tubing and the valve. It is also fairly apparent that through the proposed setup of the valve system, each component of the pneumatic circuit can be bypassed. This is done deliberately for two reasons. The first being in the event if there was a sample jam or leak in the circuit, the malfunctioning or clogged section could be isolated to allow for repair. The second reason for the additional component bypass loops was due to additional safeguards required in the event of an emergency situation. These safeguards dictated that during any phase of sample irradiation, counting, or transport, the vials could be immediately ejected from the core and transferred to a safe waste receptacle in the event of an emergency. Following the evacuation of the samples from the loop, the system would shut down the circuit to prevent possible spread of contamination.

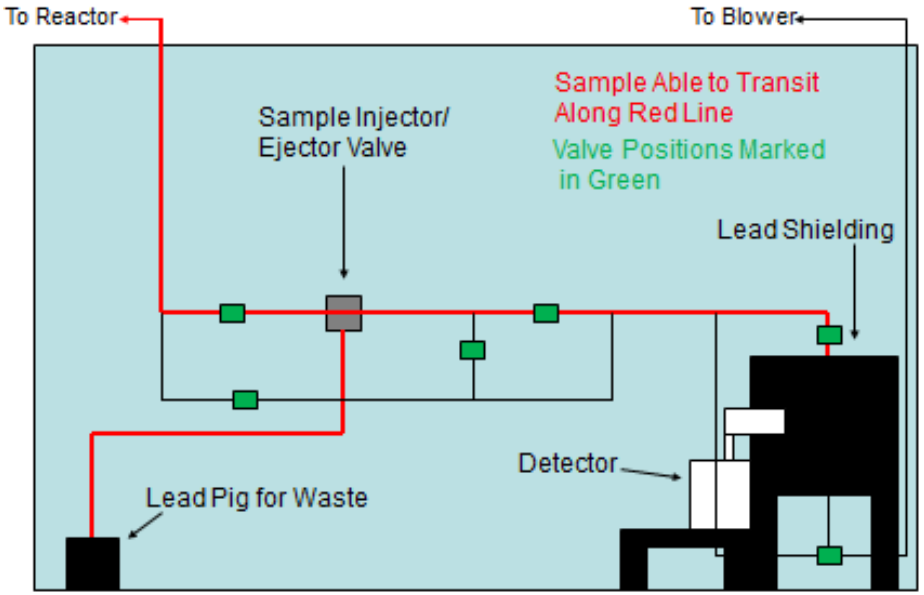


Figure 5.1: Planned Pneumatic Valve Placement.

Table 5.3: Pneumatic Valve Control Plan.

| Valve | Idle (Nothing inside) | Sample Loading | Shoot Sample Into Core | Sample Remaining in Core | Sample Ejection From Core | Counting Sample | Sample 2 Loading While Counting | Sample 2 Injection to Core While Counting | Sample 2 In Core While Counting | Sample 2 In Core Sample Ejected From Counting | Emergency Ejection While Counting(Part I) | Emergency Ejection While Counting(Part II) | Emergency Ejection Finished Counting(III) |
|---|---|---|---|---|---|---|---|---|---|---|---|---|---|
| **BV1** | Closed | Closed | Open | Open | Open | Closed | Closed | Open | Open | Open | Open | Open | Open |
| **BV2** | Closed | Closed | Open | Open | Open | Closed | Closed | Open | Open | Open | Closed | Open | Open |
| **BV3** | Open | Open | Closed | Closed | Closed | Open | Open | Closed | Closed | Closed | Closed | Closed | Closed |
| **BV4** | Closed | Closed | Closed | Closed | Closed | Closed | Closed | Closed | Closed | Closed | Open | Closed | Closed |
| **BV5** | Closed | Closed | Closed | Closed | Open | Closed | Closed | Closed | Closed | Open | Closed | Closed | Open |
| **BV6*** | Down | Down | Down | Down | Up | Down | Down | Down | Down | Up | Down | Down | Up |
| **Airflow** | Clockwise | Clockwise | Clockwise | Clockwise | Counter-Clockwise | Clockwise | Clockwise | Clockwise | Clockwise | Clockwise | Counter-Clockwise | Clockwise | Clockwise |
| **MasterValve** | Down | Up | Down | Down | Down | Down | Up | Down | Down | Up | Down | Up | Up |
| **Loader Valve** | Retracted | After Master Moves Up, Extended | Retracted | Retracted | Retracted | Retracted | After Master Moves Up, Extended | Retracted | Retracted | Retracted | Retracted | Retracted | Retracted |
| **Ejection Valve** | De-Energized | De-Energized | De-Energized | De-Energized | De-Energized | De-Energized | De-Energized | De-Energized | De-Energized | After Master Moves Down, Energized | De-Energized | After Master Moves Down, Energized | After Master Moves Down, Energized |

### 5.3.3 Pneumatic Circuit Valve Parts Selection

The first task in deciding the components required to construct the pneumatic loop was identifying valves capable of accepting a 1" O.D., ¾" I.D. polyethylene tubing while concurrently providing a smooth path through the inside of the valve for the sample to pass through. In order to connect the valves to the pneumatic tubing, fittings would have to be purchased that would properly mate and match with the tubing and valve. Like the valves, the fittings must provide a smooth inner diameter for the sample to transit along. After extensive research on two-way, hermetically sealed, on/off valves, a company by the Banjo Liquid Handling Products Corporation was selected as the choice polypropylene ball valve for the FARIST system. A photo of the valve is provided in Figure 5.2.

Figure 5.2: Banjo Two-Way Selectable Polypropylene Ball Valve [22].

There are two primary reasons for selection of the Banjo ball valves. Firstly, the system was sealed and approved for liquid use which satisfied the hermetically sealed requirements of the system. The second major contributing factor was that the female

NPT fittings on the valve were made of polypropylene. This meant that if steel NPT fittings were used to connect the tubing to the valve, then the steel fittings could be tighten down enough for the male NPT face to mate up against inside wall of the ball valve. This was done to ensure that no "lip" would form between the NPT fitting and the ball valve thus providing a seal for the system. Additional reasons for selection of the Banjo valve included low unit cost (approx. $340 per), simple design, and easy maintenance.

The steel fitting selection was incredibly important as well. In order to properly mate the polyethylene tubing to the inside of the steel fitting, *Swagelok* compression fittings were utilized with male NPT fittings. As a result 1"O.D. with ¾" I.D. Stainless Steel compression fittings with male NPT threads were selected. An image of the fittings is provided in Figure 5.3. Through the use of these fittings the pneumatic loop remained sealed and the sample was provided a smooth path to transit along.

Figure 5.3: *Swagelok* Compression Fitting with Male NPT Thread [23].

The last significant design component worth mentioning is the three-way junction observed at five locations along the loop shown earlier in Figure 5.1. Referencing Figure 5.1, four of these junctions require the sample to transit through, while the fifth is located outside of the hot sample line. Again, issues with providing a smooth sample transit line dictated the use of a 3-way fitting that could properly mate with the polyethylene tubing while simultaneously allowing the sample to pass through the 3-way port uninterrupted. To ensure a smooth transition, *Swagelok* 3-way tube fittings were utilized. Images of the 3-way fittings are provided in Figure 5.4 along with the internal sleeve. The stock *Swagelok* fittings inner diameter measure 0.88" which failed to match the 0.75" inner diameter of the polyethylene tubing. This difference in inner diameters, along with the third port, presented serious potential problems as an almost certain sample catch point. This issue was mitigated by fabricating an aluminum sleeve to be placed inside of the three-way fitting thus creating a smooth service that matched the ¾" I.D. of the circuit. Additionally the third port had to be adequately covered to allow for uninterrupted travel of the sample across it while concurrently allowing $CO_2$ to pass through the third port relatively unimpeded when required. The solution developed is the sleeve shown in Figure 5.4. Once installed, no appreciable system flow resistance, or sample interruption was noted through function testing.

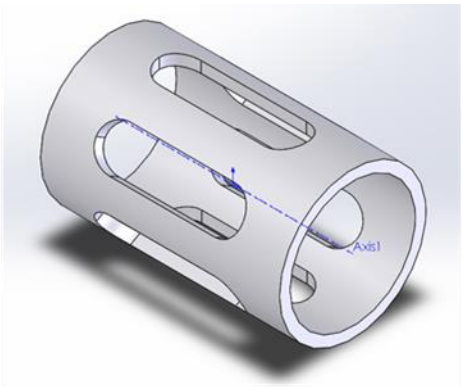


Figure 5.4: Swageloke Three-Way Tube Fitting with Feed Through Sleeve.

With valve and fitting selection complete, an overall system diagram was created to assist in the installation phase of the project. The system diagram that was created is shown in Figure 5.5 identifying the number and type of valves and fittings required across the circuit. With the plan of the overall system setup complete, the additional components of the system could now be designed.

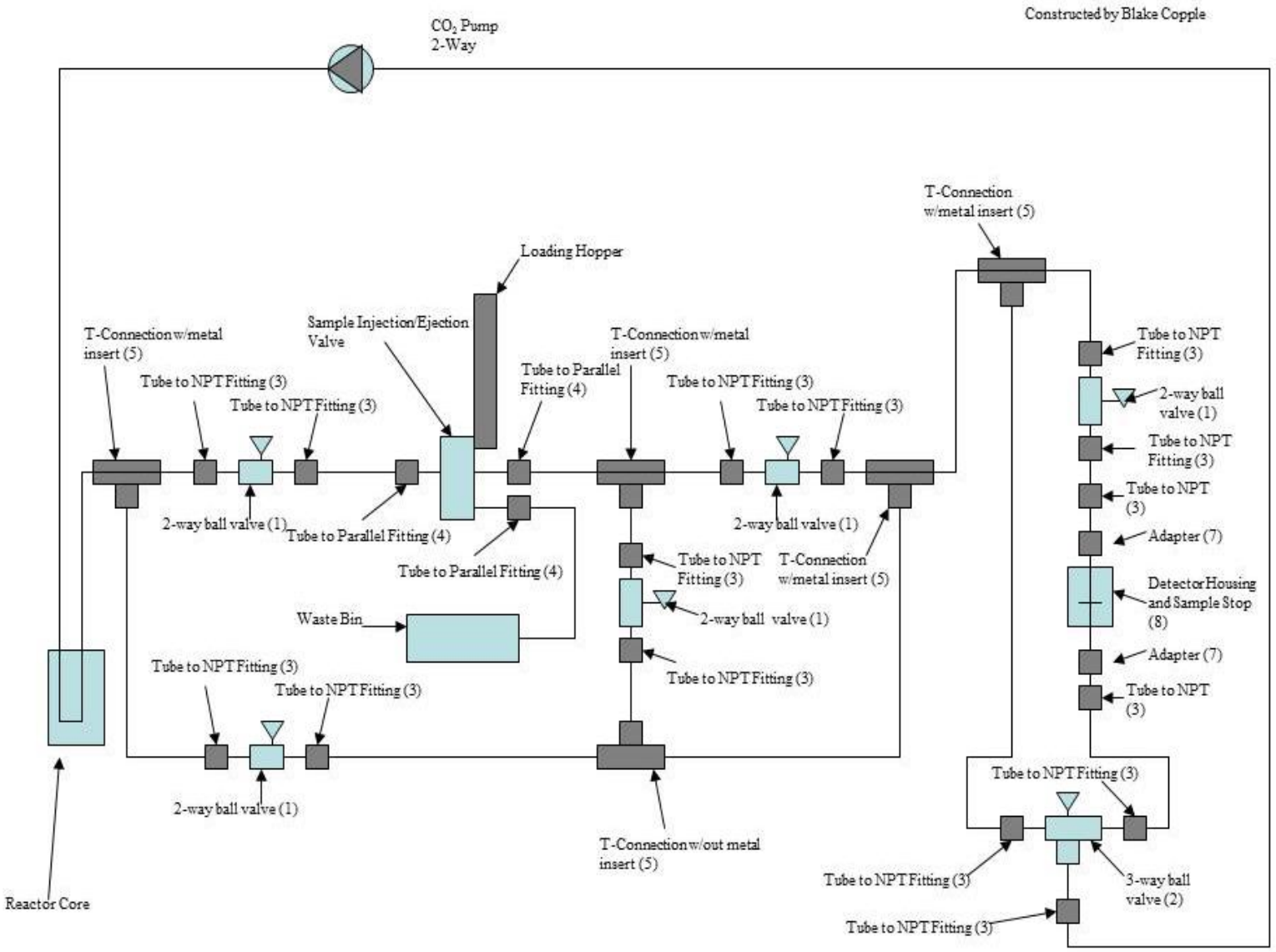


Figure 5.5 Pneumatic Circuit Setup with Applicable Fittings and Valves Identified.

## 5.4 SAMPLE INJECTION/EJECTION/TRANSFER VALVE

The sample injection/ejection valve proved to be the most difficult component of the system to design. A variety of different valve designs exist to transfer a sample as was shown in the chapter on previous DNAA facilities. Existing valve setups all had one issue in common however: the lack of automation. As a result, a completely new valve design was pursued. The valve design developed was then compared to the existing valves in the systems described in chapter FOUR utilizing a Puegh chart to determine the best available option. The following sections examine the valve design process concluding with a Peugh chart comparison of the new valve with previous systems.

### 5.4.1 Research and Design

In the brainstorming phase, a single design concept stood out. The concept involved a housing unit that utilized horizontal tubes to receive samples from the exterior and shift them into the pneumatic circuit. The same tubes were then utilized to either allow the sample to pass through unimpeded, or to catch the sample and transfer it out of the housing for waste. The conceptual design, shown in Figure 5.6, was conceptually sound and ultimately selected as the choice concept for the FARIST system's sample injection/ejection valve. The single valve shown in Figure 5.6 combined the functionality of previous DNAA sample valves into a single package. The valve shown in Figure 5.6 is a section cut of the proposed valve.

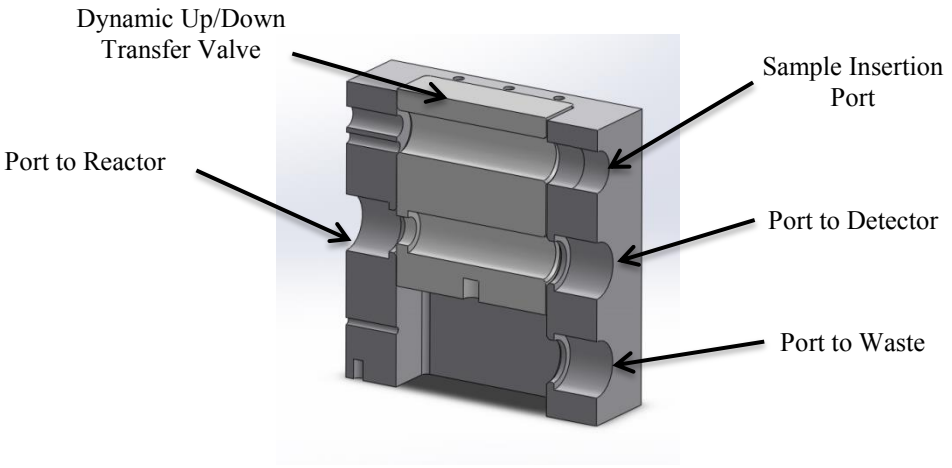


Figure 5.6: Sample Injection/Ejection Valve Computer Assisted Design Model.

To visually assist in describing the valves operation a graphic is provided in Figure 5.7. The sample is represented in green prior to entry to the reactor while an activated sample is represented in red. In the first stage of operation, a sample is inserted into the valve. Following insertion of the sample (shown in stage two) the inner valve then shifts down, exposing the sample to the pneumatic loop. Once inside the pneumatic loop, the incident pneumatic pressure would propel the sample into the reactor as represented in stage three of Figure 5.7. Once irradiation is complete the sample then transits through the sample valve to the detector for counting represented in stage four of Figure 5.7. In stage five, the valve shifts back up to receive a new sample while also exposing the lower tube containing a sample catch. The sample exits the detector and is arrested by the catch in the lower compartment of the valve while the new sample is loaded into the top tube. Finally, the valve shifts down and the new sample is sent to the reactor while the post irradiation sample is then discarded through the waste port as shown in stage six. The cycle is then repeated for X number of samples or, the valve can

be adjusted for cyclic irradiation by allowing the sample to pass through the top tube of the valve back and forth between the reactor and the detector.

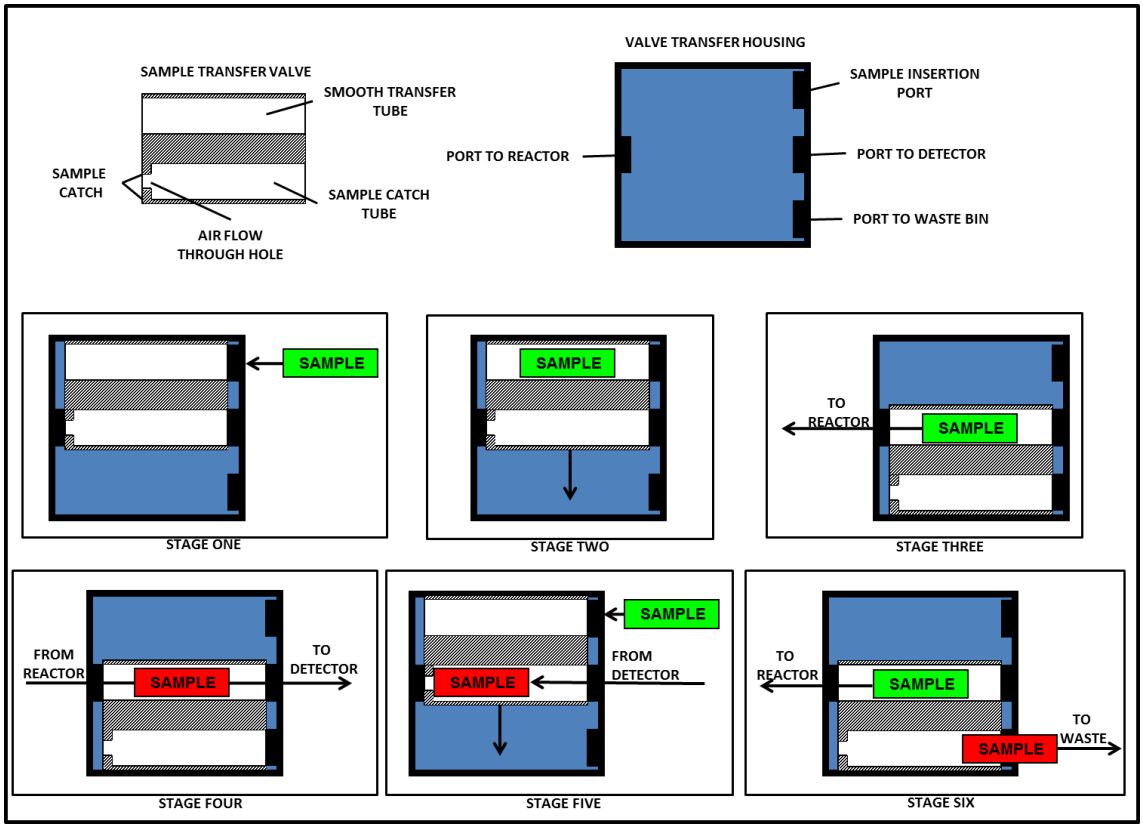


Figure 5.7: Sample Injection/Ejection Valve Position During Operation.

With the conceptual design and function flowchart complete, the valve was then modified to satisfy the requirements and constraints of the project. The first modification to the valve concept was the addition of a "magazine" capable of storing up to 30 samples. A simple sleeve type magazine was designed, shown in Figure 5.8 in order to stack the samples on top of each other. To push the sample into the sample insertion port a pneumatic piston was utilized where the piston arm would slide the sample into the

sample insertion port and then retract the arm once pneumatic airflow to the piston was terminated. The retraction would be made possible through the use of an internal spring that would act to reset the piston. A brief discussion on the piston arm systems is provided near the end of this section. In order to hold the magazine a simple receiver slot was designed along the side of the valve housing to receive and fix the sleeve into place. The addition of the slot to the original design is also shown in Figure 5.8. Through the addition of a vertical sleeve, the need for a large sample holder with multiple motors and additional complexity, like in the Finnish system, was eliminated.

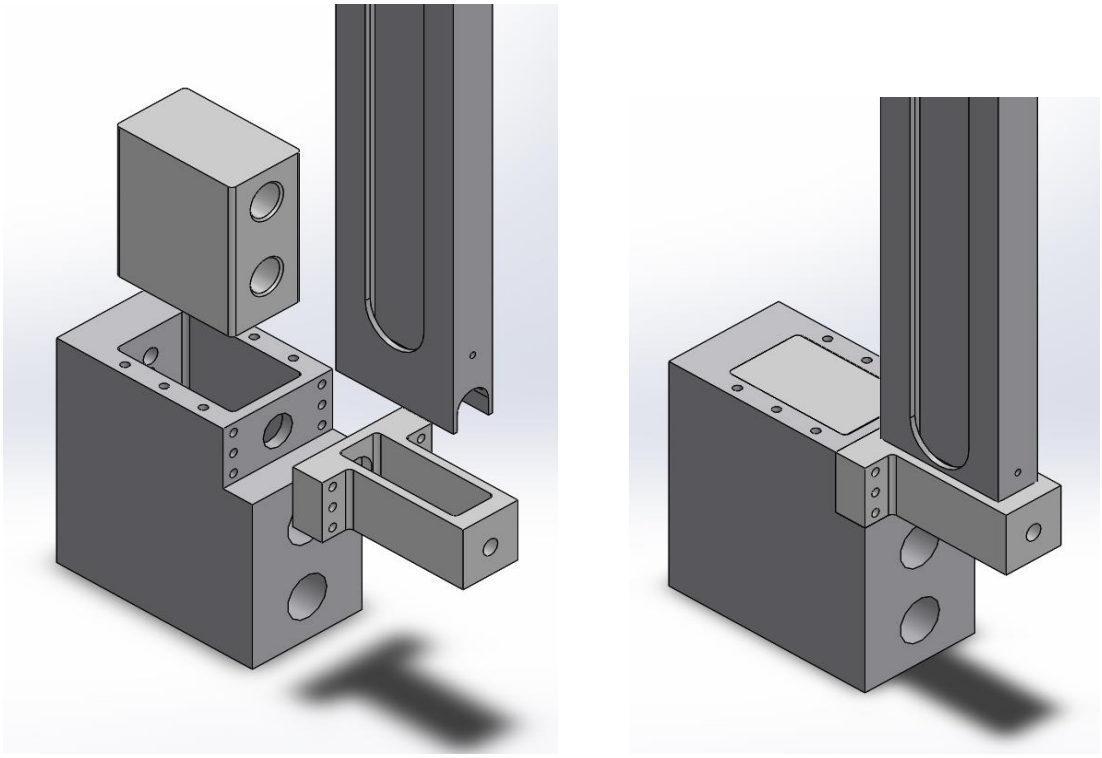

Figure 5.8: CAD Drawing of the Addition of a Sample Magazine and Magazine Receiver to Original Sample Injection/Ejection Valve (Exploded and Assembled View Provided).

The next challenge to creating a sample injection/ejection valve was ensuring that the valve retained a proper seal during operations. O-rings were employed around the sample transfer valve ports, and along the exterior of the sample transfer valve, inside of the housing. The reason for the second set of additional O-rings around the valve ensure that metal to metal rubbing was not occurring on the interior of the valves. On the valve transfer housing, *Swagelok* fittings were again used to mate the valve with polyethylene tubing. Instead of using Nation Pipe Thread (NPT) threads, as for the ball valves, straight thread fittings were used to mate the male end of the Swagelok fitting straight to the wall of the transfer housing. This was done to eliminate any gap between fittings which could potentially catch the sample as it was transferring through. With the addition of the straight threading and O-ring requirements the design was further modified with the refined product shown in Figure 5.9.

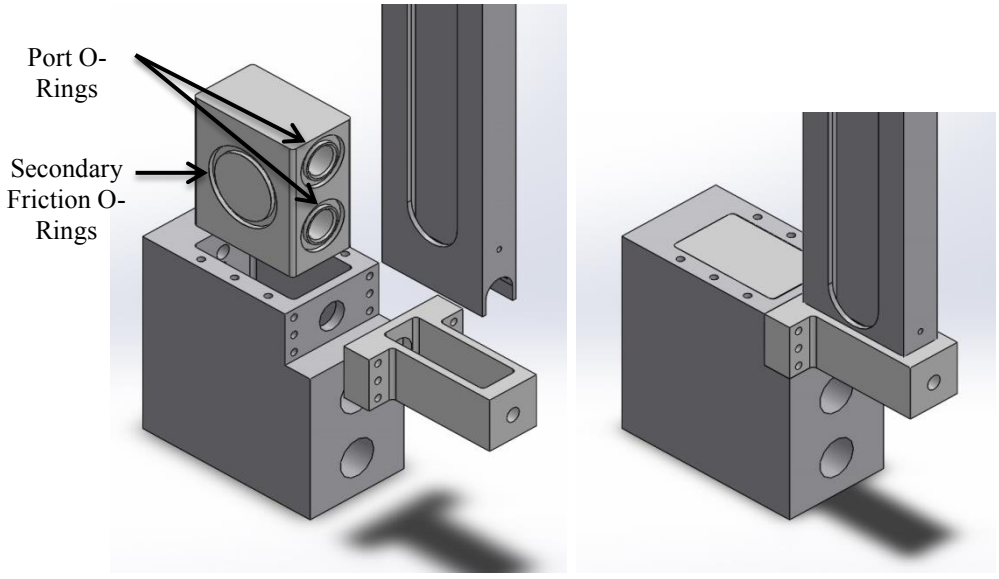


Figure 5.9 CAD Drawing of the Addition of O-Ring Slots.

With the additions to the sample transfer valve described previously, the design of the valve was almost complete. The sample transfer valve however, still had no means of actuation. To remedy the issue a two way pneumatic piston was installed on the bottom of the valve housing with an arm that connected directly to the sample transfer valve. The piston could then actuate to place the sample transfer valve to the upper or lower position. In order to accept the piston to the valve transfer housing, a threaded fitting was created on the bottom of the housing which would double to seal the bottom of the valve housing. After the creation of the bottom cap, an additional system cap was created to seal the top of the valve. With the creation of the appropriate fittings and caps, the sample injection/ejection valve design was complete. The final product design for the sample injection ejection valve is shown in Figure 5.10 with CAD drawings of exploded, sectioned, and completed assembly view.

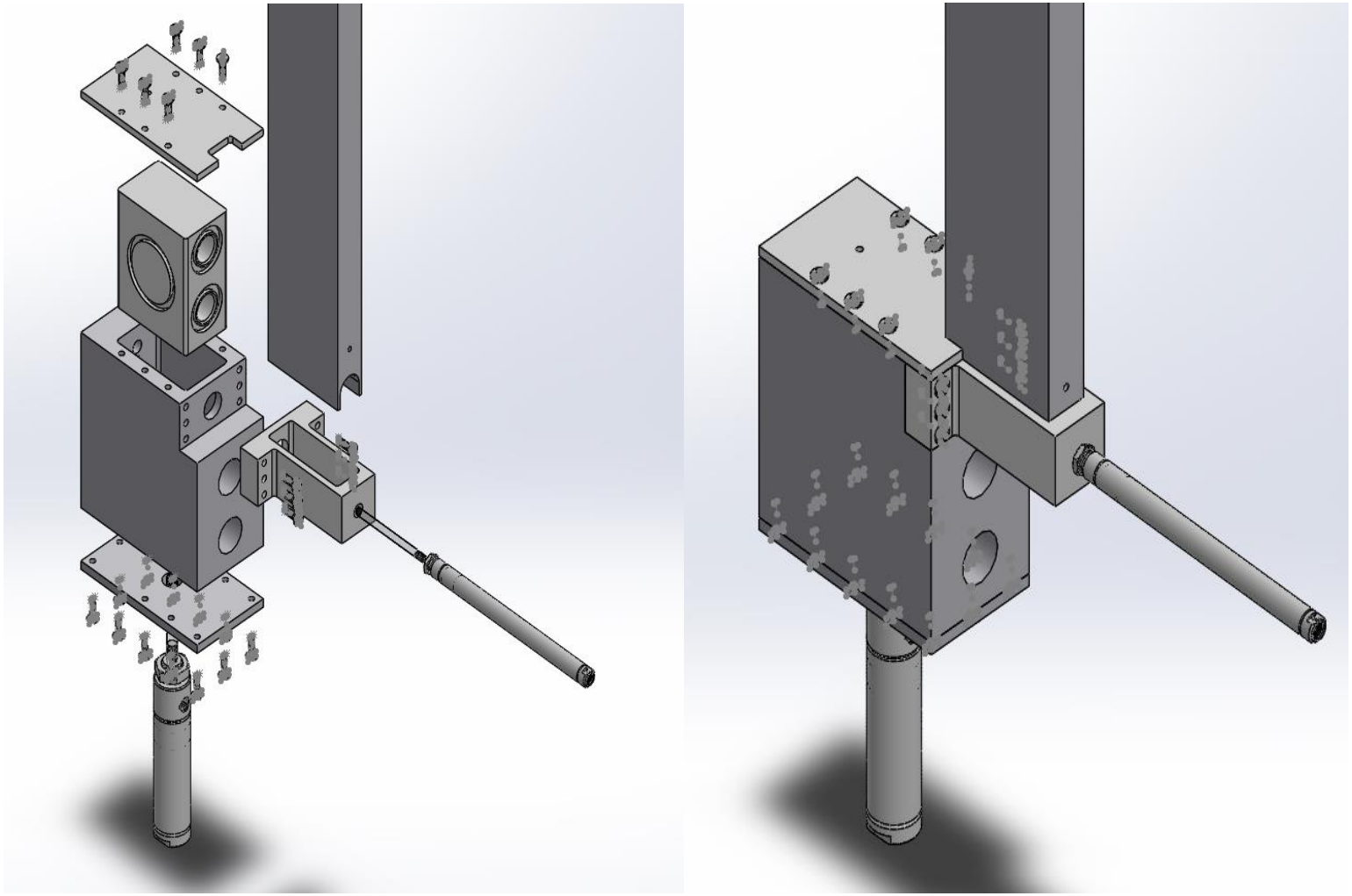

Figure 5.10: CAD Exploded and Assembled View of Sample Injection/Ejection Valve.

The pistons employed to actuate both the sample transfer valve and the sample into purchased from *McMaster-Carr*. The pistons were simple in design and cost affordable. The force output on the two cylinders was paired to match the force necessary to complete the individual tasks each was assigned. A two way pneumatic piston with a 2" stroke and 61 pounds of available force was employed at the bottom of the sample transfer housing to control the sample transfer valve. A single action pneumatic piston with a 3" stroke and 12 pounds of available force with a spring loaded return was utilized to push the sample into the top chamber of the sample transfer valve. Figure 5.11 displays the pneumatic pistons utilized in the FARIST system with the difference between the two types highlighted. With a low unit cost of approximately $30, the pistons selected proved to be a simple, off the shelf solution for sample valve actuation.

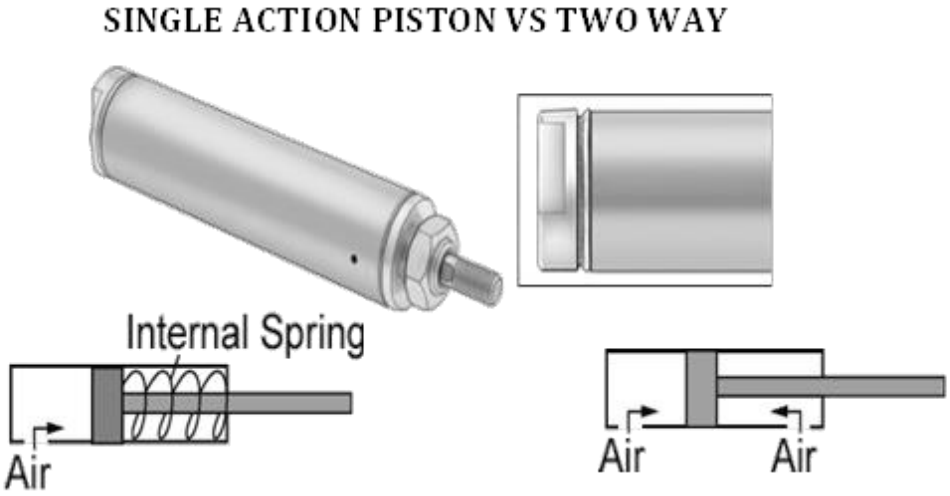


Figure 5.11: Piston Design for Sample Valve Actuation [24].

### 5.4.2 Material Selection

Due to the potential for certain system components to activate as a result of an irradiated sample, special material considerations were applied. The O-rings located inside of the sample transfer valve, originally planned to be rubber, were changed to lithium O-rings due to lithium's slower degradation qualities in a radioactive environment. The sample injection/ejection valve was also chosen to be fabricated out of aluminum for a combination of reasons including cost, machinability, low attenuation qualities, and availability. The pneumatic pistons employed for sample valve actuation utilized stainless steel bodies which posed no issues to system effectiveness. Lastly, stainless steel Swagelok fittings were selected to mate the polyethylene tubing with the sample valve. Again, no issues with system activation were posed through this material selection. Overall, by selecting relatively inert materials for the sample valve, issues with system longevity and activation were effectively eliminated.

### 5.4.3 Peugh Chart Comparison to Previous Systems

With the sample valve design complete, a comparison can be drawn between the previous system transfer valves through the use of defined metrics. As discussed in Chapter FOUR, the FARIST system's aim was to carry the advantages of previous NAA designs into the construction of the FARIST system while making up for the disadvantages of previous systems. The new FARIST system's sample transfer valve combines the advantages of both the Finnish and Austrian systems into a simple,

automated, operationally robust package. Additionally, the system adds functionality to make up for several downfalls of the previously discussed systems.

Table 5.4: Peugh Chart Comparison Between Previous System Sample Valves with the FARIST Sample Valve.

| | | 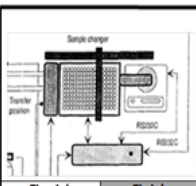 | | 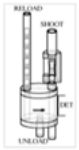 | |  | | 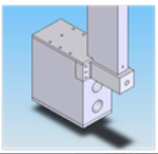 | |
|---|---|---|---|---|---|---|---|---|---|
| **Constraints :** | **Weighing Factor (1-3)** | **Finnish Sample Valve System** | **Finish Weighted Total** | **Austrian Sample Valve System** | **Austrian Weighted Total** | **Texas Sample Valve System** | **Texas Weighted Total** | **FARIST Sample Valve System** | **FARIST Weighted Total** |
| Size | 2 | 0 | 0 | 2 | 4 | 2 | 4 | 1 | 2 |
| Simplicity | 3 | 0 | 0 | 2 | 6 | 2 | 6 | 1 | 3 |
| Cost/benefit | 2 | 1 | 2 | 1 | 2 | 2 | 4 | 1 | 2 |
| Position Reproducability | 3 | 2 | 6 | 2 | 6 | 1 | 3 | 2 | 6 |
| 20+ Sample Capacity | 3 | 2 | 6 | 1 | 3 | 0 | 0 | 2 | 6 |
| Minimize $t_w$ | 2 | 2 | 4 | 1 | 2 | 0 | 0 | 1 | 2 |
| Fully Automated | 3 | 2 | 6 | 0 | 0 | 0 | 0 | 2 | 6 |
| Manufacturability | 2 | 1 | 2 | 1 | 2 | 2 | 4 | 2 | 4 |
| Detection/Irradiation Dual Functionality | 1 | 0 | 0 | 0 | 0 | 2 | 2 | 2 | 2 |
| No User Exposure | 3 | 1 | 3 | 0 | 0 | 0 | 0 | 2 | 6 |
| Hermetically Sealed | 3 | 1 | 3 | 2 | 6 | 0 | 0 | 2 | 6 |
| Detector Background Noise | 2 | 0 | 0 | 1 | 2 | 2 | 4 | 1 | 2 |
| Sample Activity w/no suppression or LFC | 3 | 0 | 0 | 0 | 0 | 2 | 6 | 1 | 3 |
| Available Space | 3 | 2 | 6 | 2 | 6 | 2 | 6 | 2 | 6 |
| TOTAL: | | | 38 | | 39 | | 39 | | 56 |

A Peugh chart with weighted metrics is applied in Table 5.4 to compare earlier systems methods of inserting samples, to the one created for the FARIST system. Each constraint has an associated weighing factor between one and three with three being of the highest importance. Each sample valve system is also assigned a performance factor between zero and two. ZERO means the valve system cannot satisfy the specific constraint and TWO means the system is exceptional at satisfying the particular constraint. The weighing factor is then multiplied to each systems performance factor to receive a corrected point total for that particular systems constraint. Each systems

corrected performance factor is then summed to find an overall system performance factor total. The system with the highest total is then deemed the best system for the purposes of the FARIST system. The previous three systems are analyzed with the results shown in Table 5.4. It is readily apparent that due to the FARIST sample changers performance factors on important constraints, the newly designed system is the best available option.

## 5.5 Detector Housing and Sample Stop

### 5.5.1 Detector and Shielding Cave Geometry

Due to space, load bearing structure availability, and lead supply considerations, a cubed shaped shielding structure was selected to house sample analysis. To ensure the sample did not move once inside the sample stop it was decided the pneumatic circuit would enter through the top of the shielding cave and the exhaust would extrude through the bottom. This setup would ensure that gravity pulled the sample to the stop once the pneumatic circuit was shut off prior to the sample reaching the sample stop. As discussed earlier the shutoff of the pneumatic flow would act to cushion the sample as it fell to the stop. As a result of the top-to-bottom pneumatic geometry, the detector system would be placed along the side of shielding cave with the detector face protruding into the cave via a hole cut through the side. The overall conceptual setup was highlighted at the beginning of the chapter in Figure 5.1 and was deemed the best choice possible to ensure low backgrounds during analysis.

### 5.5.2 Detector Shielding Cave Material Selection

As with all gamma ray detection systems, lead was selected as the primary method of shielding around the detector/sample system. Standard lead bricks were both available and relatively easy to reposition making them ideal for selection. One issue presented through the use of lead however, is the emission of the characteristic 75 and 85 keV rays [25]. In order to mitigate the $^{210}$Pb characteristic x-ray, the use of a cadmium and copper layered cave interior was chosen to drop down the emitted x-ray energies to non-appreciable levels [25]. The practice is common place in gamma ray detection systems and the availability of high purity copper and cadmium made the addition an easy and affordable way to decrease the background to the detector. As a result, high purity cadmium and copper were then purchased for use in the detector cave.

### 5.5.3 Sample Stopper

The sample stopper located inside of the detector cave represented one of the most critical components of the system. The sample stopper needed to be designed to minimally attenuate emitted gamma rays while maintaining the structural integrity to remain fixed at all times so as not to interfere with sample/detector proximity. Gamma ray attenuation through a material is defined as:

$$I(x) = I_0 \cdot e^{-\mu x} \tag{5.1}$$

Where $I_0$ is the initial intensity, $x$ is the distance from the source in cm and $\sigma$ is the gamma ray mass attenuation coefficient [26]. This equation makes it fairly apparent that the material to be used for the sample stop requires low absorption cross sections across different gamma rays energies while remaining as least dense as possible. To determine what material best suited the needs for the sample stop, Table 5.5 was referenced from *Introduction to Nuclear Engineering* by Lamarsh and Baratta [27]. Table 5.5 is broken down with the least dense material at the top of the list with increasing atomic densities going down the list. Additionally the mass attenuation coefficient is divided by the atomic density across a typically measured gamma ray energy spectrum to better identify attractive attenuation properties.

Table 5.5: Mass Attenuation Coefficients for Common Materials in $cm^2/g$ [27].

| | Gamma-ray energy, MeV | | | | | | | | | | | | | | | | | |
|---|---|---|---|---|---|---|---|---|---|---|---|---|---|---|---|---|---|---|
| Material | 0.1 | 0.15 | 0.2 | 0.3 | 0.4 | 0.5 | 0.6 | 0.8 | 1.0 | 1.25 | 1.50 | 2 | 3 | 4 | 5 | 6 | 8 | 10 |
| H | .295 | .265 | .243 | .212 | .189 | .173 | .160 | .140 | .126 | .113 | .103 | .0876 | .0691 | .0579 | .0502 | .0446 | .0371 | .0321 |
| Be | .132 | .119 | .109 | .0945 | .0847 | .0773 | .0715 | .0628 | .0565 | .0504 | .0459 | .0394 | .0313 | .0266 | .0234 | .0211 | .0181 | .0161 |
| C | .149 | .134 | .122 | .106 | .0953 | .0870 | .0805 | .0707 | .0636 | .0568 | .0518 | .0444 | .0356 | .0304 | .0270 | .0245 | .0213 | .0194 |
| N | .150 | .134 | .123 | .106 | .0955 | .0869 | .0805 | .0707 | .0636 | .0568 | .0517 | .0445 | .0357 | .0306 | .0273 | .0249 | .0218 | .0200 |
| O | .151 | .134 | .123 | .107 | .0953 | .0870 | .0806 | .0708 | .0636 | .0568 | .0518 | .0445 | .0359 | .0309 | .0276 | .0254 | .0224 | .0206 |
| Na | .151 | .130 | .118 | .102 | .0912 | .0833 | .0770 | .1676 | .0608 | .0546 | .0496 | .0427 | .0348 | .0303 | .0274 | .0254 | .0229 | .0215 |
| Mg | .160 | .135 | .122 | .106 | .0944 | .0860 | .0795 | .0699 | .0627 | .0560 | .0512 | .0442 | .0360 | .0315 | .0286 | .0266 | .0242 | .0228 |
| Al | .161 | .134 | .120 | .103 | .0922 | .0840 | .0777 | .0683 | .0614 | .0548 | .0500 | .0432 | .0353 | .0310 | .0282 | .0264 | .0241 | .0229 |
| Si | .172 | .139 | .125 | .107 | .0954 | .0869 | .0802 | .0706 | .0635 | .0567 | .0517 | .0447 | .0367 | .0323 | .0296 | .0277 | .0254 | .0243 |
| P | .174 | .137 | .122 | .104 | .0928 | .0846 | .0780 | .1685 | .0617 | .0551 | .0502 | .0436 | .0358 | .0316 | .0290 | .0273 | .0252 | .0242 |
| S | .188 | .144 | .127 | .108 | .0958 | .0874 | .0806 | .0707 | .0635 | .0568 | .0519 | .0448 | .0371 | .0328 | .0302 | .0284 | .0266 | .0255 |
| Ar | .188 | .135 | .117 | .0977 | .0867 | .0790 | .0730 | .0638 | .0573 | .0512 | .0468 | .0407 | .0338 | .0301 | .0279 | .0266 | .0248 | .0241 |
| K | .215 | .149 | .127 | .106 | .0938 | .0852 | .0786 | .0689 | .0618 | .0552 | .0505 | .0438 | .0365 | .0327 | .0305 | .0289 | .0274 | .0267 |
| Ca | .238 | .158 | .132 | .109 | .0965 | .0876 | .0809 | .0708 | .0634 | .0566 | .0518 | .0451 | .0376 | .0338 | .0316 | .0302 | .0285 | .0280 |
| Fe | .344 | .183 | .138 | .106 | .0919 | .0828 | .0762 | .0664 | .0595 | .0531 | .0485 | .0424 | .0361 | .0330 | .0313 | .0304 | .0295 | .0294 |
| Cu | .427 | .206 | .147 | .108 | .0916 | .0820 | .0751 | .0654 | .0585 | .0521 | .0476 | .0418 | .0357 | .0330 | .0316 | .0309 | .0303 | .0305 |
| Mo | 1.03 | .389 | .225 | .130 | .0998 | .0851 | .0761 | .0648 | .0575 | .0510 | .0467 | .0414 | .0365 | .0349 | .0344 | .0344 | .0349 | .0359 |
| Sn | 1.58 | .563 | .303 | .153 | .109 | .0886 | .0776 | .0647 | .0568 | .0501 | .0459 | .0408 | .0367 | .0355 | .0355 | .0358 | .0368 | .0383 |
| I | 1.83 | .648 | .339 | .165 | .114 | .0913 | .0792 | .0653 | .0571 | .0502 | .0460 | .0409 | .0370 | .0360 | .0361 | .0365 | .0377 | .0394 |
| W | 4.21 | 1.44 | .708 | .293 | .174 | .125 | .101 | .0763 | .0640 | .0544 | .0492 | .0437 | .0405 | .0402 | .0409 | .0418 | .0438 | .0465 |
| Pt | 4.75 | 1.64 | .795 | .324 | .191 | .135 | .107 | .0800 | .0659 | .0554 | .0501 | .0445 | .0414 | .0411 | .0418 | .0427 | .0448 | .0477 |
| Tl | 5.16 | 1.80 | .866 | .346 | .204 | .143 | .112 | .0824 | .0675 | .0563 | .0508 | .0452 | .0420 | .0416 | .0423 | .0433 | .0454 | .0484 |
| Pb | 5.29 | 1.84 | .896 | .356 | .208 | .145 | .114 | .0836 | .0684 | .0569 | .0512 | .0457 | .0421 | .0420 | .0426 | .0436 | .0459 | .0489 |
| U | 10.60 | 2.42 | 1.17 | .452 | .259 | .176 | .136 | .0952 | .0757 | .0615 | .0548 | .0484 | .0445 | .0440 | .0446 | .0455 | .0479 | .0511 |
| Air | .151 | .134 | .123 | .106 | .0953 | .0868 | .0804 | .0706 | .0636 | .0567 | .0517 | .0445 | .0357 | .0307 | .0274 | .0250 | .0220 | .0202 |
| NaI | 1.57 | .568 | .305 | .155 | .111 | .0901 | .0789 | .0657 | .0577 | .0508 | .0465 | .0412 | .0367 | .0351 | .0347 | .0347 | .0354 | .0366 |
| $H_2O$ | .167 | .149 | .136 | .118 | .106 | .0966 | .0896 | .0786 | .0706 | .0630 | .0575 | .0493 | .0396 | .0339 | .0301 | .0275 | .0240 | .0219 |
| Concrete | .169 | .139 | .124 | .107 | .0954 | .0870 | .0804 | .0706 | .0635 | .0567 | .0517 | .0445 | .0363 | .0317 | .0287 | .0268 | .0243 | .0229 |
| Tissue | .163 | .144 | .132 | .115 | .100 | .0936 | .0867 | .0761 | .0683 | .0600 | .0556 | .0478 | .0384 | .0329 | .0292 | .0267 | .0233 | .0212 |

Two metals with low densities and attractive attenuation coefficients are identified in Table 5.5. The two metals are beryllium and aluminum. Aluminums low cost, strength, availability, and machinability made it an ideal candidate over beryllium's high cost and poor machining characteristics. To ensure high aluminum purity for the sample stop tubing, high purity, ultra-corrosion-resistant 1100 Aluminum tube stock was utilized. The 1100 Aluminum offered a 99% purity level to researchers along with high formability and favorable machining qualities. 1" O.D. with the ½" I.D. aluminum tubing was selected from McMaster-Carr. The tubing was then bored out on both sides to leave a quarter inch stop in the center. This stop would act to stop the incoming sample. In order to further improve the intensity of the gamma rays moving through the aluminum, the tubing above the sample stop (where the sample would rest) was milled down for an aluminum wall thickness of 0.06". The sample stop shown in Figure 5.12 highlights the dimensions used to provide a thin aluminum window for the sample. Also shown in the figure is the sample stop located near the center. The ½" hole that remained in the center proved to have a minimal impact to overall pneumatic system airflow.

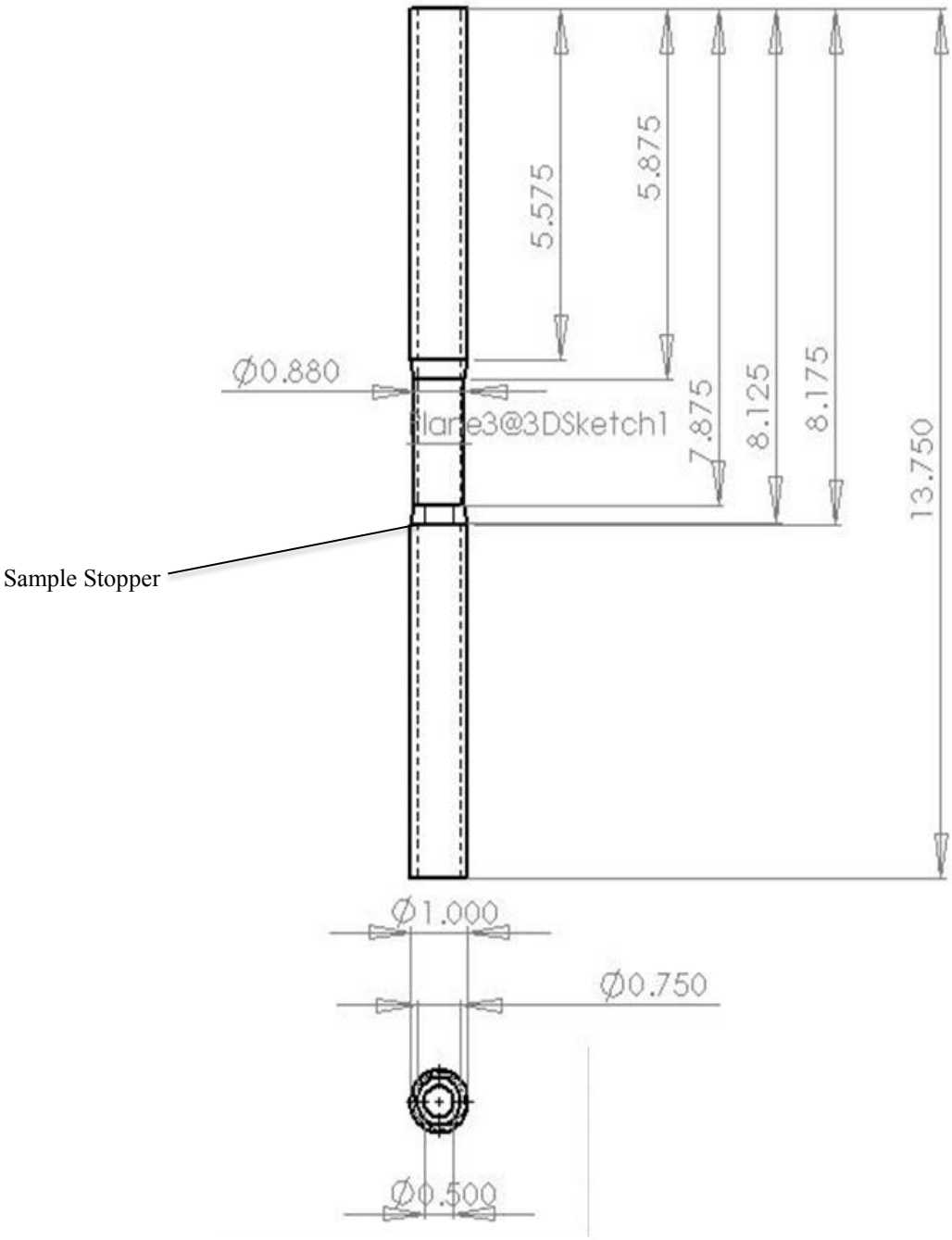


Figure 5.12 Mechanical Drawing of Al 1100 Sample Stopper

### 5.6 SENSOR SELECTION AND EMPLACEMENT

In order for the system to execute on assigned irradiation and counting times, the installation of sensors was required along key points of the pneumatic circuit. As a result, four critical areas were identified as locations requiring sensor emplacement. The first location was at the top of the reactor pool. With the emplacement of a sensor at that location, the system could begin the irradiation timer as soon as the sample passed into the reactor. With the ability to start irradiation time, the next step was employment of a sensor that could register the arrival of the sample at the detector thus triggering the analysis process. As a result, the second sensor would be placed on top of the detector housing. The third location identified for sensor emplacement was at the half-way point between the reactor and the detector along the pneumatic line. The purpose of this location was that in the event of a system jam or malfunction, the location of this sensor would help to narrow down the unknown position of the sample along the pneumatic loop to either between the reactor bay or NAA facility.

The final location requiring sensor emplacement would be along the sample injection/ejection valve. In order for the system to run correctly, a sensor would be required to confirm that a sample had indeed been loaded through the sample insertion port. As a result, a sensor would be placed along the housing to register that a sample had been inserted successfully and the system can move to the next step of sample insertion into the pneumatic circuit. Additionally, in order to ensure that the sample injection/ejection valve was working correctly it was deemed prudent to install sensors that confirmed the valves “up” or “down” position. This would be done with the

insertion of a sensor along the top and bottom of the sample valve housing. Figure 5.13 is provided to highlight the proposed location of the sensors across the FARIST system.

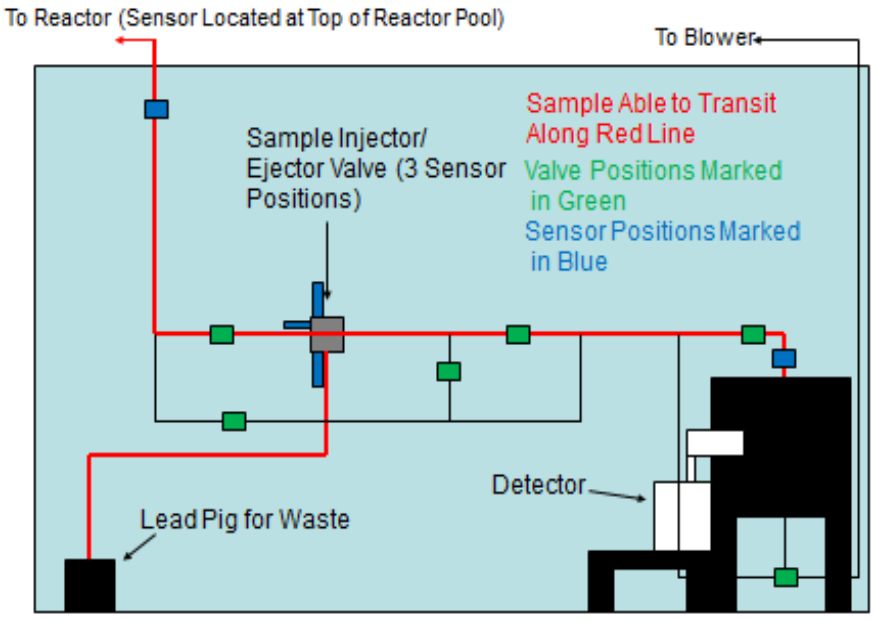


Figure 5.13: Planned Sensor Locations Across the FARIST System

The next step was deciding what type of sensor would be utilized and how they would be fixated to the system. For the sensors required to detect the sample passing through the circuit, diffuse photo sensors were selected. Fixating the sensors to the pneumatic tubing presented challenges however as there was no way to thread the sensors to the polyethylene tubing. A solution was formulated with the creation of a specialized clamp, shown in Figure 5.14, which would grasp the poly tubing. Drilled into the center of the clamp would be threading to allow the sensor to be screwed in and thus remain fixed along the tubing. Additionally, shown in Figure 5.15, an image is provided of the diffuse photo sensor that was selected for use.

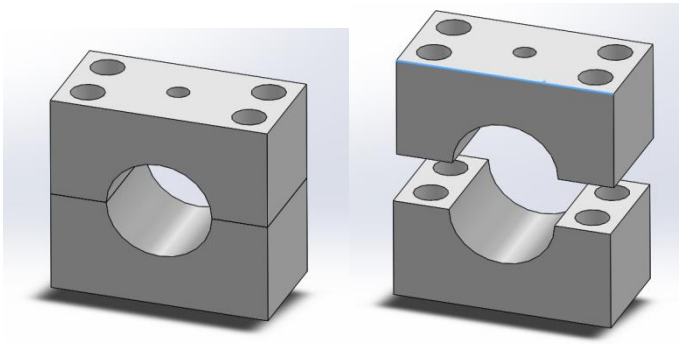

Figure 5.14: Sensor Clamp Utilized to Fix Sensor to Polyethylene Tubing.

Figure 5.15: Diffuse Photo Sensor [28].

To determine what position the sample valve was in, two inductive sensors with an exterior design matching the diffuse photo sensor were chosen based on their ability to detect the proximity of the metal from the internal sample valve. The sensors were fixed into place by drilling and tapping holes onto both the top and bottom of the sample valve housing. In conjunction with the inductive sensors, an additional diffuse photo sensor was utilized to detect the successful insertion of the sample into the sample insertion port. Like the sample proximity sensors, this sensor could be fixed to the sample housing through drilling and tapping at a location near the sample insertion port to detect when

the sample was located inside of the inner sample valve. A CAD graphic is shown in Figure 5.16 identifying the locations of the sensors along the sample injection and ejection valve.

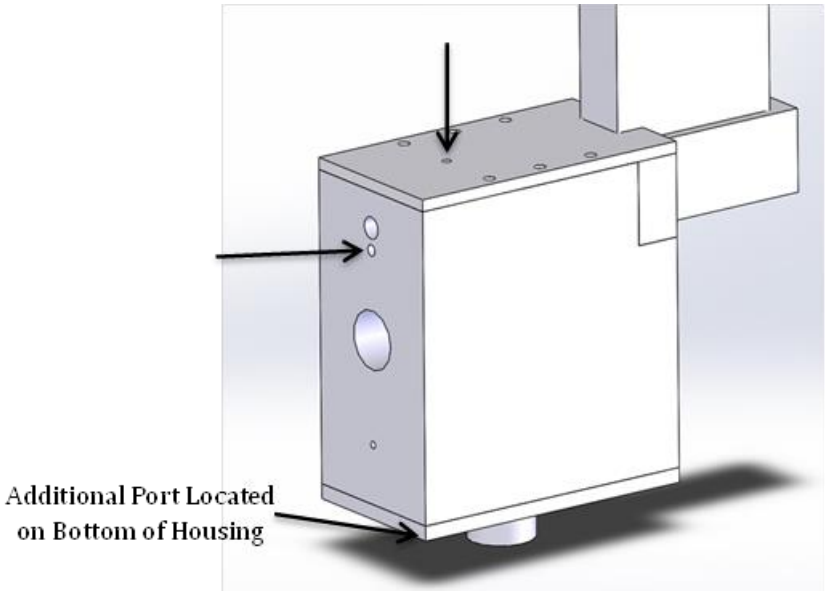


Figure 5.16: Sensor Emplacement Port Locations Along Sample Injection/Ejection Valve.

### 5.7 PROGRAMMABLE CONTROL SYSTEM/SENSOR UTILIZATION

The entire system was designed to be controlled from a desktop computer. A single touch screen display would be employed to display overall system status so the researcher could maintain awareness on setup. Inputs and subsequent counting would be completed on a desktop system. Inputs gathered by the desktop would be the number of samples to be irradiated, duration of irradiation, duration of counting, and the number of cycles each sample would complete in the event of cyclic irradiation. With the system inputs, the computer could then interact with both the PLC and the MCA to operate the

system. The PLC utilizes a ladder logic system to control valve movement around the system while the MCA would interact with the detection system and provide the analysis to the researcher. With the number of pneumatic valves in the system, a Direct Logic (DL)205 Series PLC was selected. With the DL205 unit a DL240 CPU, D2-16ND3-2, D2-16TD1-2, and D2-DCM were provided to provide reliable control across the system. A 6" touch LCD screen was selected from AutomationDirect.com to be utilized as a system status screen. In Chapter SIX, images are provided of the installed system with the corresponding wiring, routing, and physical system setup.

## 5.8 CONCLUSION/SUMMARY

Each component of the FARIST system was designed to maximize performance throughout the system. Previous systems advantages we carried into the design while solutions to previous system downfalls were resolved. With a modern approach to the design and programming, a more efficient system overall was designed. With the mechanical drawings and system components selected, fabrication, purchase, and installation could begin. Inevitably problems would arise from the transition between the planned design and the real world product. The following chapter bridges the gap between the decisions and designs made in this chapter, to the *real world* final product.

# Chapter 6: FARIST System Installation

## 6.1 Pneumatic Circuit

During the installation phase of the pneumatic circuit, a potential improvement was identified. The change involved the relocation of one of the 3-way junctions along the pneumatic loop. The change removed one of the 3-way junctions from along the sample transfer loop and relocated the junction to another position along a bypass loop. The change offered no impact to system functionality and improved system efficiency by removing a potential sample catch point along the circuit. The change is displayed in Figure 6.1 with a side by side comparison of the planned design and the *real world* setup.

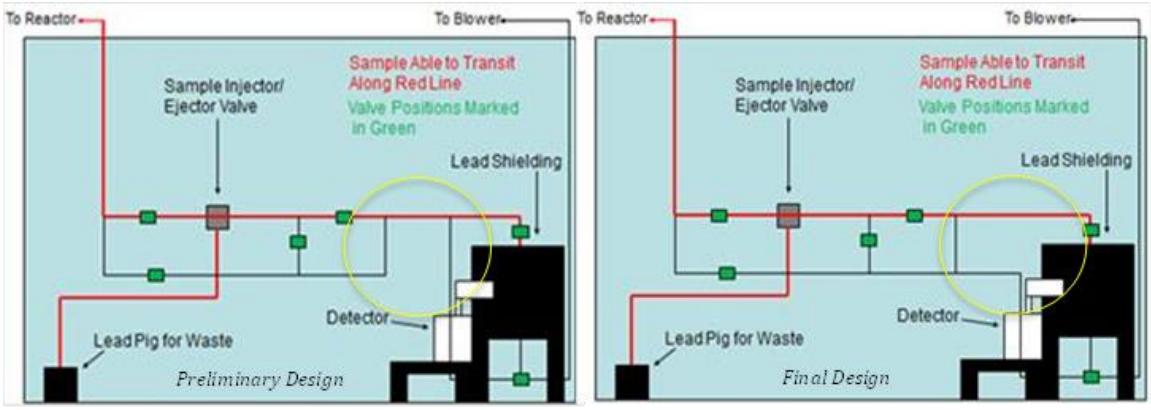


Figure 6.1: Pneumatic System Modification Comparison to Preliminary Design.

Tubing was then installed through pre-existing aluminum guides inside of the reactor bay and routed to the NAA lab. To identify tubing and component placement a *blueprint* was created along the NAA facility wall shown in Figure 6.2. With the outline

complete, tubing was then fixed to the wall using aluminum struts and guides. It was found that the polyethylene tubing was required to bend at no more than a three foot radius otherwise the length of the sample would cause jamming along the bend. As a result, additional care was given to the tubing angles resulting in modifications to the pneumatic circuit's entry geometry into the detector housing. The final product is shown in Figure 6.3.

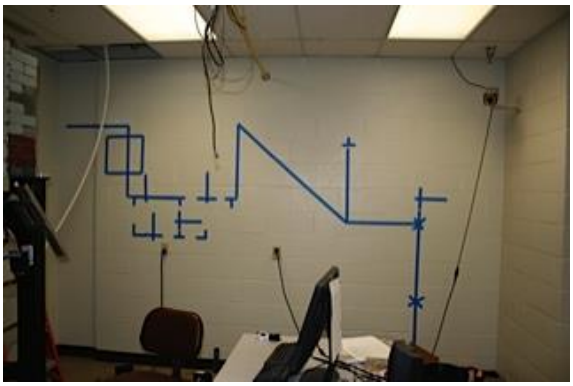

Figure 6.2: Pneumatic Tubing Outline Along NAA Lab Wall.


Figure 6.3: Completed Pneumatic Circuit.

Another issue was presented with the Banjo ball valves. After requisition of the valves a small lip on the anterior of the valve ball and the interior of the housing was observed causing concern as a potential sample catch point. The valves were function tested and the observed lip was indeed causing the sample to catch and jam inside of the valve. To alleviate the problem, all the polyethylene ball ports were grinded and polished down to remove the lip. After successive iterations of polishing and re-testing, the problem was corrected and the pneumatic circuit was in place and ready to receive the additional components of the FARIST system.

### 6.2 SAMPLE INJECTION/EJECTION VALVE

The sample injection/ejection valve construction and installation went as planned with the only issue being with the use of straight threads to mate the Swagelok fittings to the valve housing. The straight threads were unable to maintain a hermetic seal along the junction. NPT self-sealing fittings were not an option as the steel would have destroyed the aluminum housing in the attempt to tighten and mate the male end of the *Swagelok* to the wall of the housing. Instead, the *Swagelok* straight threads were heavily wrapped in Teflon® tape which proved to solve the sealing issues. Once installed on the wall, the valve was repeatedly function tested to ensure all components were operating effectively. After a multitude of tests, no issues were presented with the functionality of the valve.

The pneumatic pistons utilized to control the injection/ejection valve can be observed in Figure 6.4 along the side of the magazine rack and at the bottom of the valve housing. The pistons required an air supply which was provided through the use of

several pneumatic actuation valves. The pneumatic tubes extruding from the pistons can be observed to flow to the pneumatic control box. Inside of the control box four solenoid valves were installed with the feed line provided by tapping into pre-existing air lines. *Swagelok* compression fittings were utilized throughout the pneumatic air circuit. Figure 6.5 provides a view of the interior of the pneumatic control box, highlighting the circuit setup and solenoid valve placement. It should be noted that in order to remove the sample from the injection/ejection valve, a pneumatic feed line was attached to "blow" the sample out of the tubing toward a waste receptacle. To better visualize the placement of the line, the sample removal line is identified in Figure 6.4.

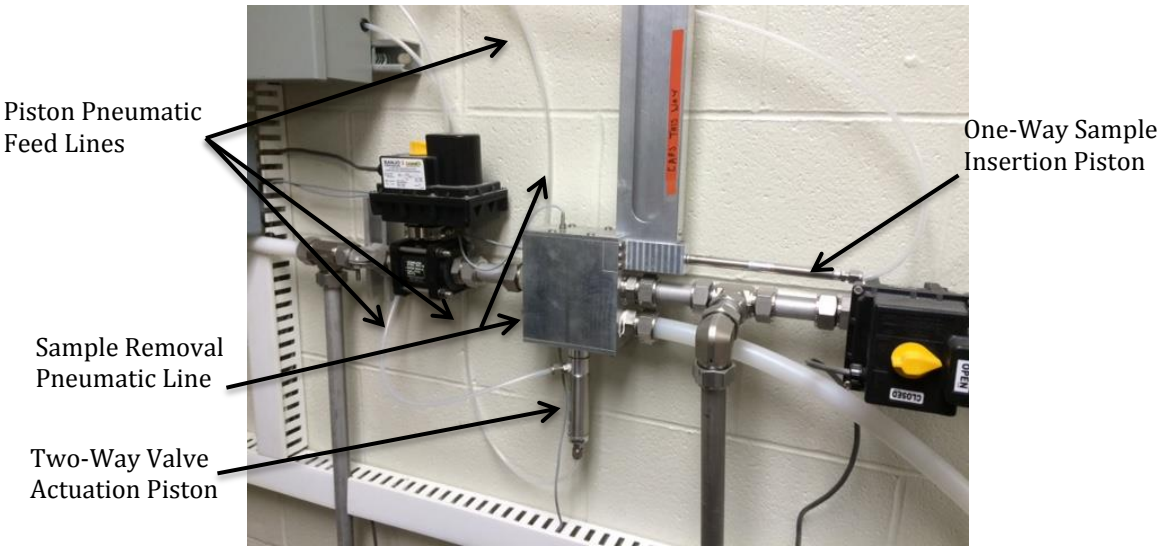


Figure 6.4: Piston Placement along Sample Injection/Ejection Valve.

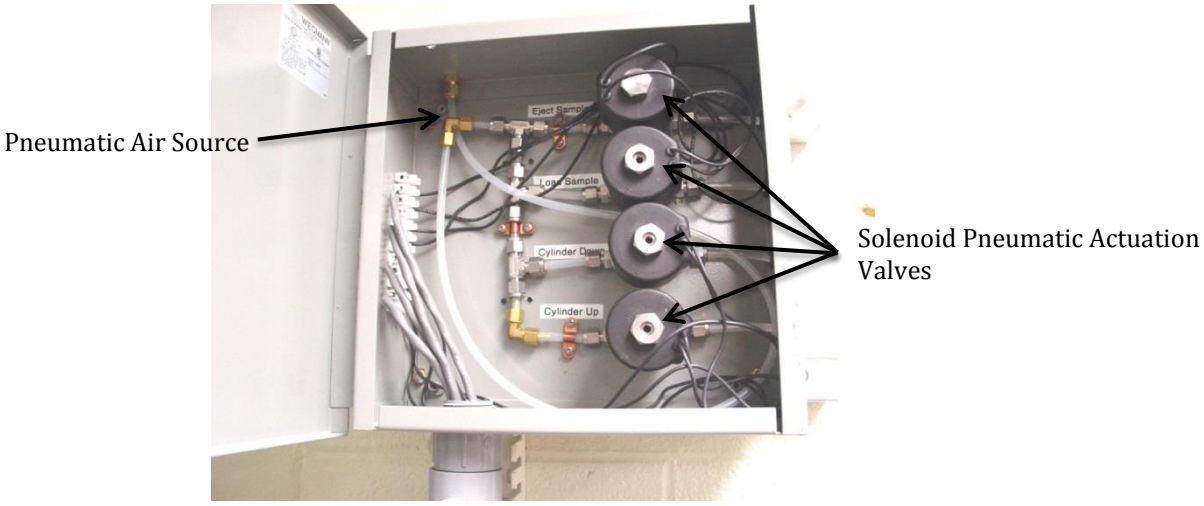


Figure 6.5: Pneumatic Actuation Control Box.

### 6.3 Detector Housing and Sample Stop

No issues were presented during the construction of the detector housing. Lead was lined on the top of a load bearing table with openings provided for the detector and the pneumatic circuit to pass through. Once the lead housing was built, tin was formed to the interior of the cave and lined around. Following the installation of the cadmium, copper was inserted to further drop the energy of the emitted lead x-rays. Images of the shielding layers are shown in Figure 6.6.

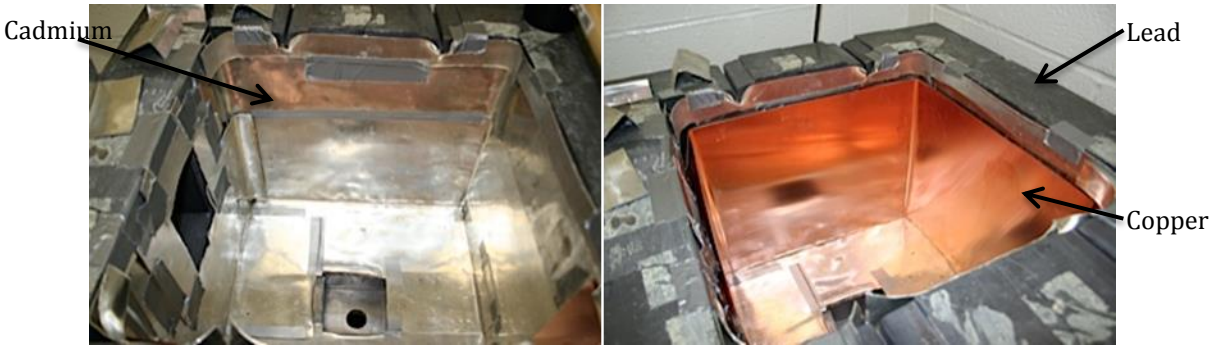


Figure 6.6: Cadmium and Copper Lining Utilized in FARIST System Detector Housing.

Following installation of the shielding layers, the pneumatic circuit, along with the sample stop was installed. The sample stopper tubing utilized *Swagelok* tube fittings to connect the polyethylene tubing to the Aluminum 1100 sample stop tube. To fixate the sample tube inside of the detector a 1" hole was drilled through the ¼" thick steel table used to support the shielding cave. The tube was inserted into the top of the table with compression Swagelok fittings. Two compression nuts were threaded on the tube, one below the steel table, the other above. The nuts were tightened to the table and the result was a rigid sample stop. Images of the installed sample stop are shown in Figure 6.7.

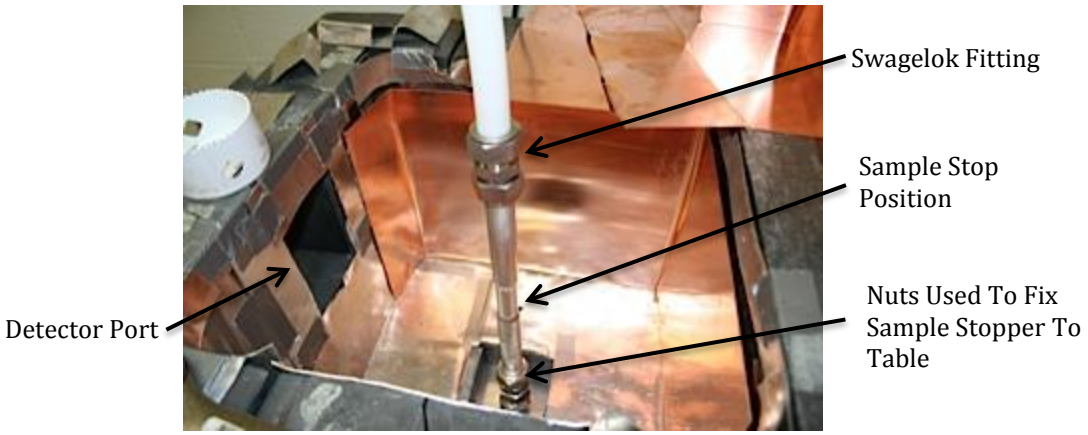


Figure 6.7: Sample Stop Construction Located Inside Detector Cave.

## 6.4 Sensor Emplacement

Sensor selection and emplacement proved effective upon requisition and testing of both the sensors and the polyethylene clamps. One issue was presented however with the diffuse photo sensors ability to detect a sample passing through along the pneumatic

line. The problem was caused as a result of the polyethylene tubing being too thick for the sensor to register the sample. To eliminate the issue, a small ¼" hole was drilled into the side of the tubing for the sensor to be placed. The clamps were then placed to allow the sensor to be bored into the drilled polyethylene guide hole. With subsequent testing, no issues with this modification were presented. An image of the final sensors placement on the tubing is presented in Figure 6.8. Additionally, provided in Figure 6.9 are images of the sensor locations on the finished sample injection/ejection valve.

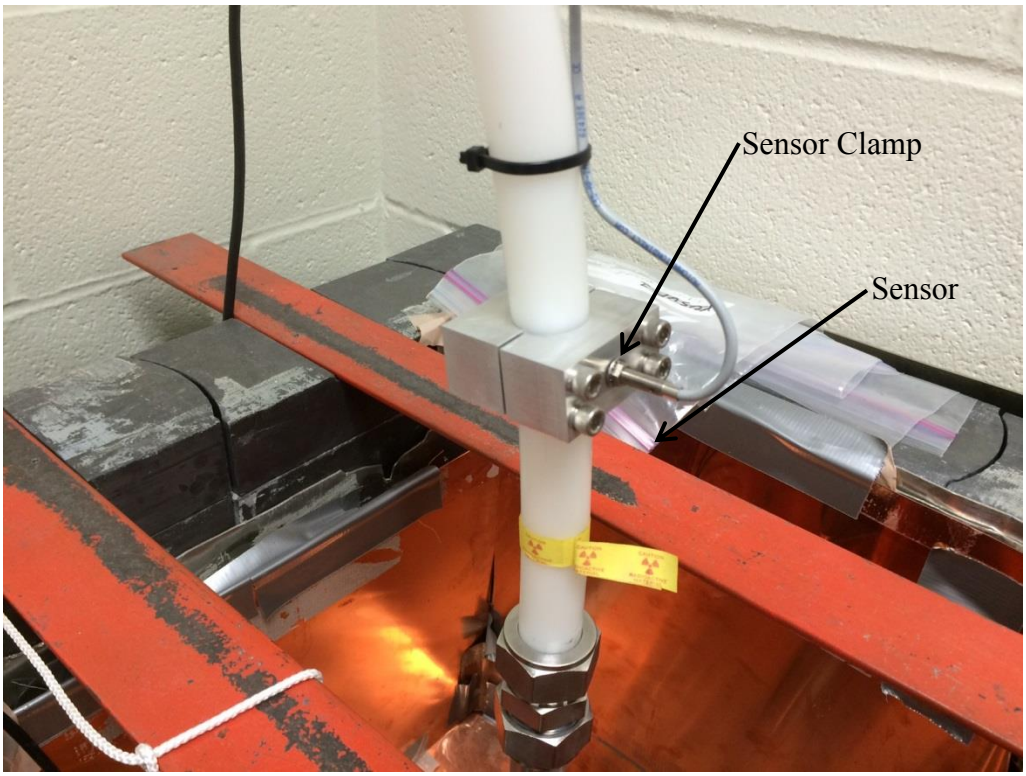


Figure 6.8: Sensor Clamp Located Along Pneumatic Tubing.

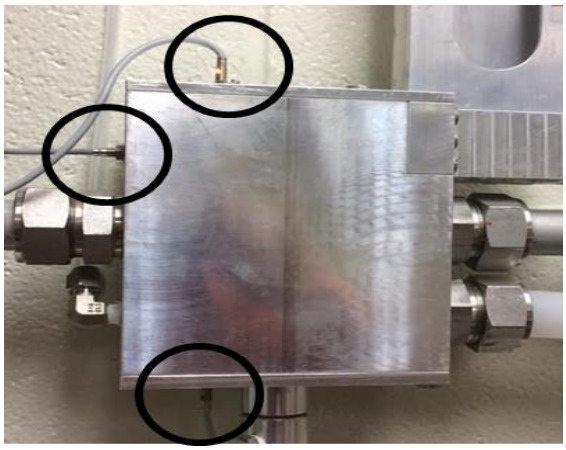

Figure 6.9: Sensor Locations Along Sample Injection/Ejection Valve.

## 6.5 ELECTRONIC CONTROL/USER INTERFACE

Planning of the electronic control's physical setup was delayed until all other systems were installed due to the flexibility of where the system could be placed. The DLC systems were installed inside a breaker box along with the additional electrical components shown in Figure 6.10. From the control box, wiring was routed along the wall through electrical guides to each individual valve.

Figure 6.10: FARIST Electronic Control Box.

The next step in the installation process was the creation of a graphical user interface that would gather the user inputs and control the FARIST system accordingly. The goal of the design was to be ergonomic, flexible, and informative. Based on these goals, a user input program was created on a desktop PC with the final image of the user input screen shown in Figure 6.11. This program would gather irradiation times, counting times, number of cycles per sample, and decay times from the user. Once all inputs had been entered, the system would then standby until the user pressed the "start" button. From that point, user interaction was no longer required.

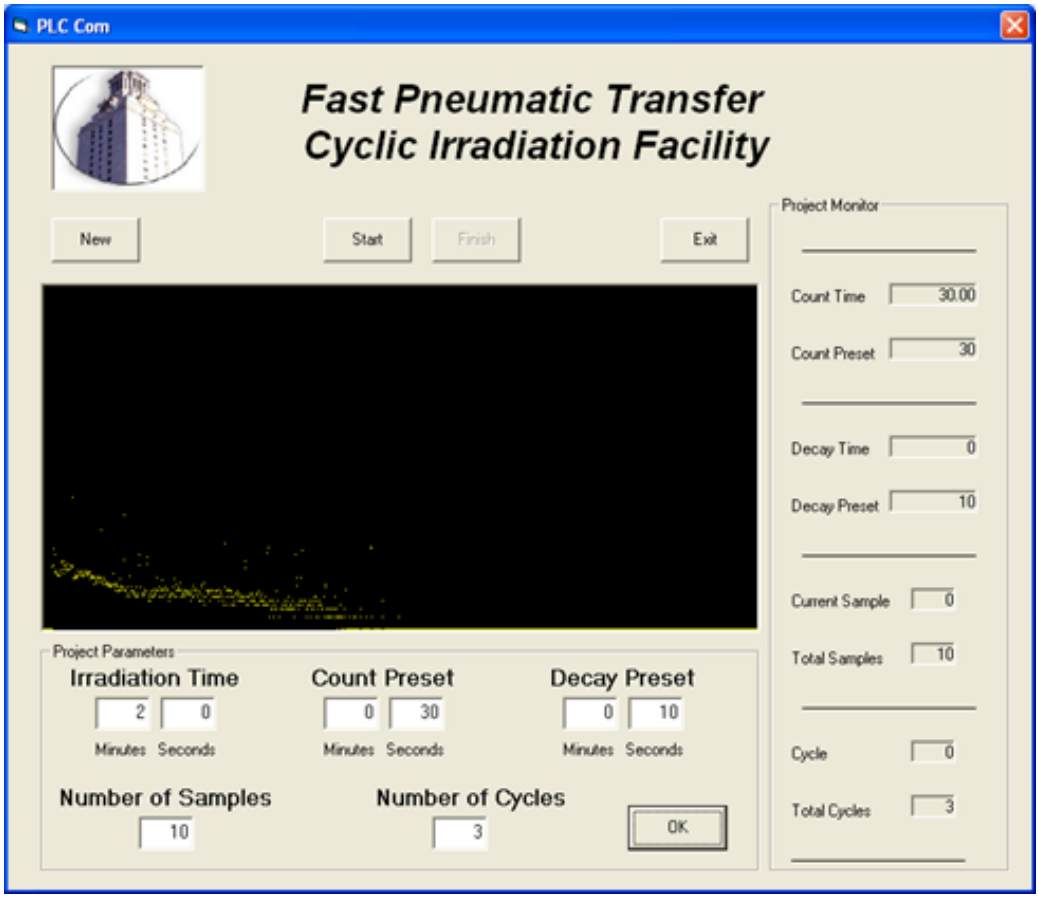


Figure 6.11: FARIST NAA User Constraints Input Program.

In addition to the program created on the computer, the system was complemented with the addition of a 6" touch screen. The goal of the touch screen was to provide three basic displays that would serve to assist the user with information on system status. The first screen designed was a system status screen that would highlight applicable details to the researcher like what cycle the sample was on, the current counting time, etc. The second screen created included a graphic of the overall system status with figures identifying where the samples were located throughout the system. The third and final screen was designed to display the pneumatic valve positions throughout the entire circuit. The third screen was created for technicians to identify valve problems in the event of a system malfunction. Images of the three display screens are shown in Figure 6.12. It should be noted that master control of the FARIST system would be retained inside of the reactor control room. Purpose of the "big brother" control was so the reactor operator could maintain awareness of what was going in and out of the core. Additionally, in the event of an emergency, the reactor operator would also retain the control to eject the sample from the reactor.

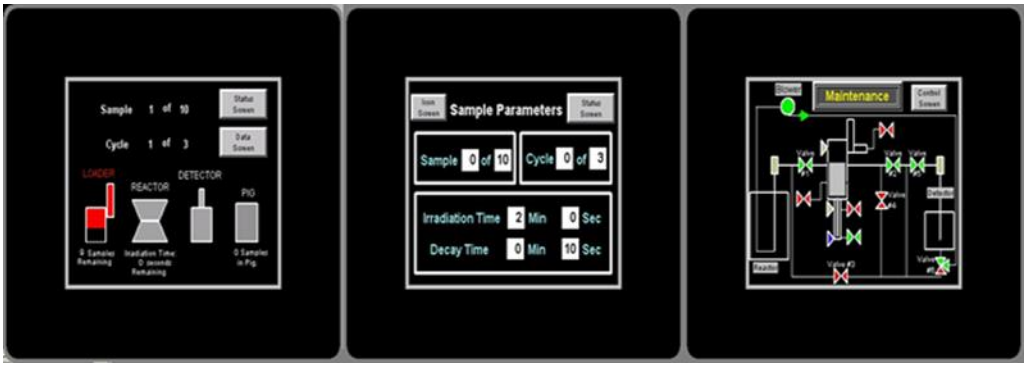


Figure 6.12: FARIST Touch Screen Display Options.

## 6.6 FARIST System Final Product

With all the individual components and programming installed and functionally running, they system could now begin initial testing. An image of the completed system is shown in Figure 6.13. Upon completion of the system, a look at the component and net cost is appropriate to determine if the $10,000 budget limit was attained. At a cursory look, the most expensive component of the system was the electronics coming in at around $4500. The second most expensive component was materials required to construct the pneumatic circuit throughout the FARIST system. The total cost for the pneumatic circuit came out to around $3500. The construction costs required to fabricate the sample injection/ejection and sample stop, plus purchase the pneumatic pistons, totaled out to be around $1500. A total of all the different components brought the total system cost to just under $9500; $500 below the original planned budget.

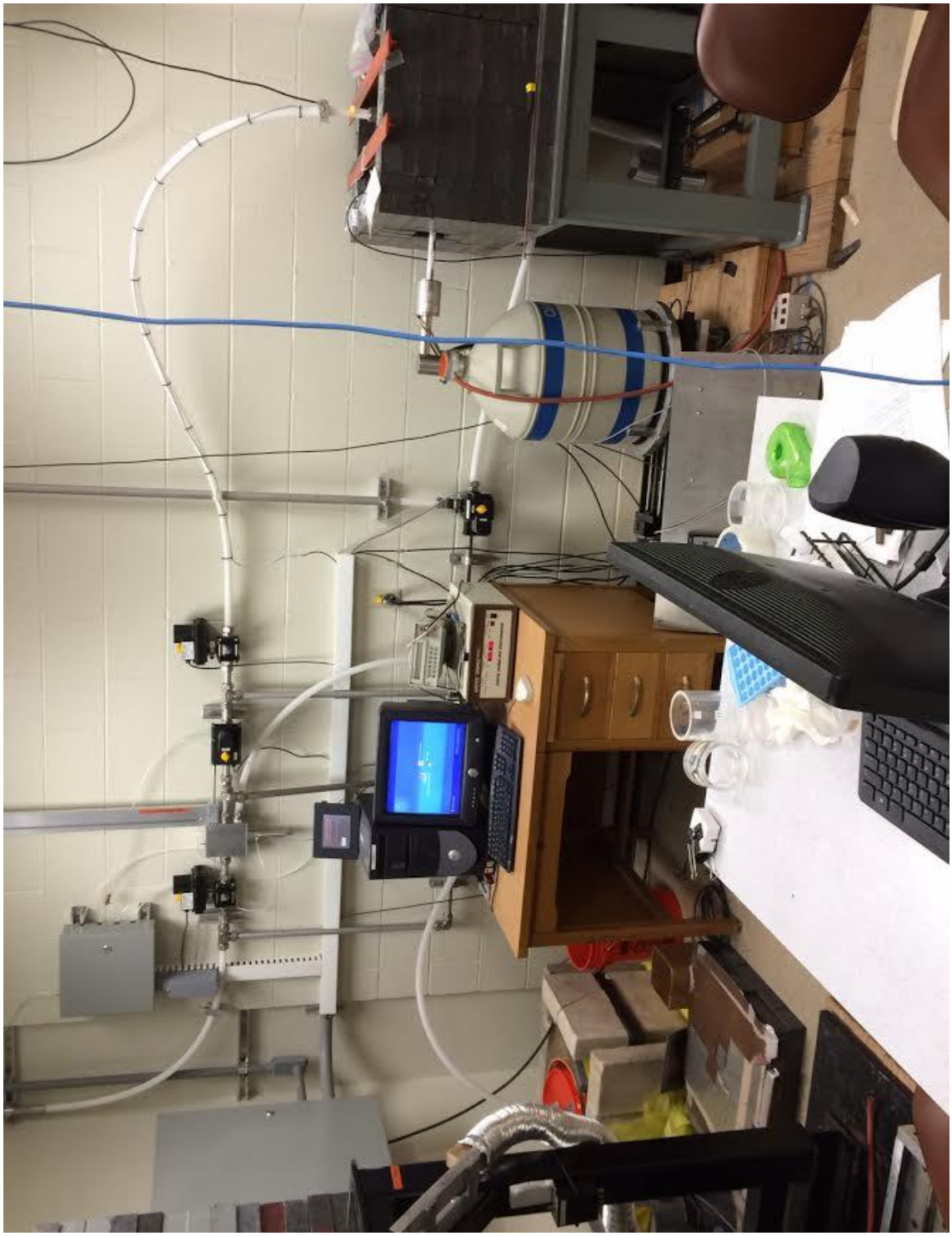

Figure 6.13: Fully Installed FARIST System.

# Chapter 7: FARIST System Experimental Validation

With the installation of the FARIST system complete, initial validation testing commenced. Due to FARIST systems relatively small infrastructure footprint, the existing NAA system was able to remain in place and operational utilizing the existing Compton suppressed detection system. This chapter highlights the improvements in sample reactor-to-detector time, analytical results, and experimenter exposure afforded by the FARIST system over the older NAA counterpart.

## 7.1 FARIST Detector Capability Characterization

### 7.1.1 Detector Efficiency/Resolution/Expected FWHM Values

In order to characterize the FARIST detector's efficiency, resolution, and FWHM values as a function of energy, a mixed gamma source was counted over the course of 48 hours. The mixed gamma source contained $^{210}$Pb, $^{241}$Am, $^{109}$Cd, $^{57}$Co, $^{139}$Cs, $^{203}$Hg, $^{113}$Sn, $^{137}$Cs, $^{88}$Y, and $^{60}$Co. From these elements associated gamma peaks were analyzed with the results shown in Figure 7.1, 7.2, and 7.3. Figure 7.1 displays the detector efficiency curve across the gamma ray spectrum that was analyzed. Figure 7.2 provides the % resolution curve across the gamma spectrum while Figure 7.3 provides the FWHM values across the spectrum as well.

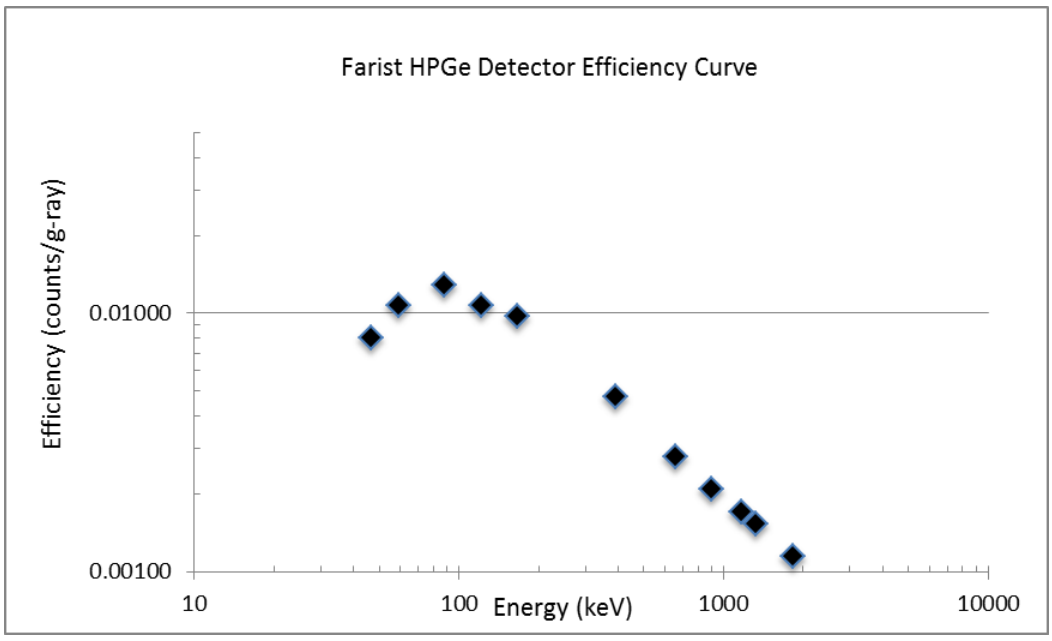


Figure 7.1: FARIST HPGe Detector Efficiency Curve across Gamma Ray Spectrum.

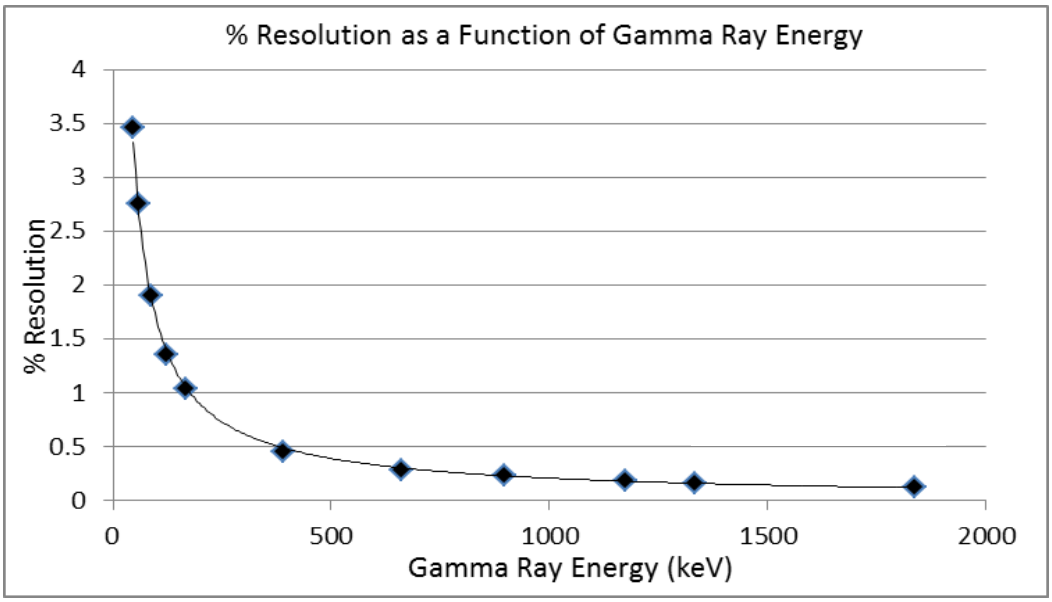


Figure 7.2: FARIST HPGe Detector % Resolution Curve Across Gamma Spectrum.

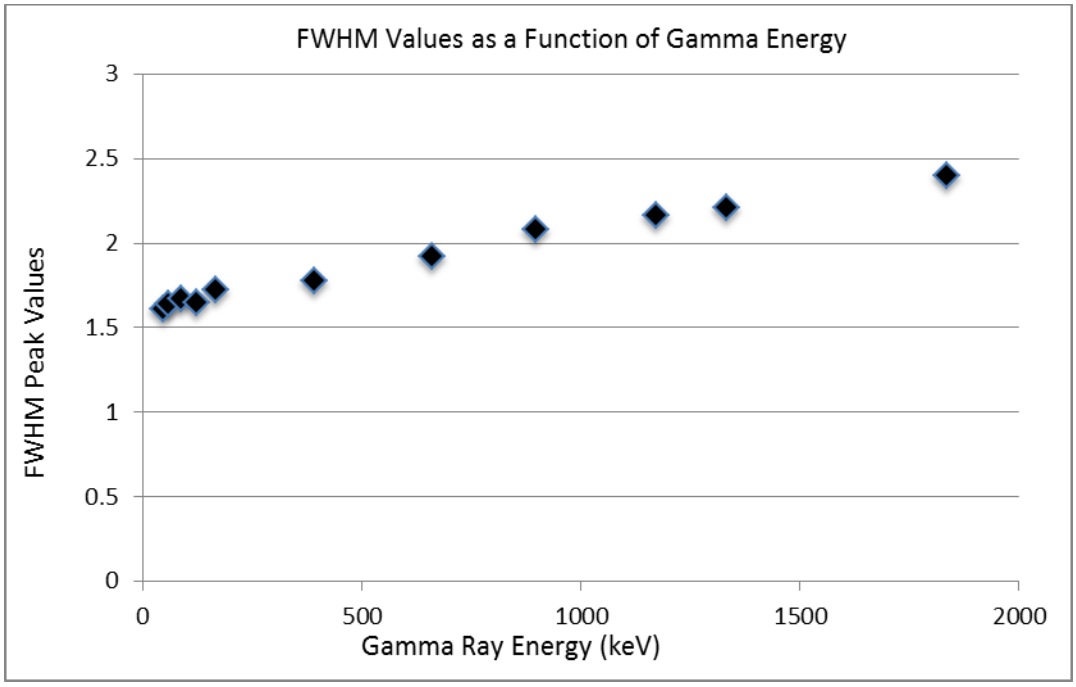


Figure 7.3: FARIST Detector FWHM Values across Gamma Spectrum.

From a cursory look at Figure 7.1, we obtain a data point curve matching what we would expect to observe referencing the Europium-152 source sample observed previously in Figure 2.5. With a look at the detector's % resolution across the gamma ray spectrum, depicted in Figure 7.2, we observe an exponential decay with the data points matching extremely well to the trend line shown. The data points set provided in Figure 7.3 display a relatively smooth increase in FWHM values as the incident gamma ray energy increases. This behavior is expected with an HPGe detector. With the results of this analysis indicating normal detector behavior, it is clear the detector utilized for the FARIST system is operating normally.

### 7.1.2 Peak-to-Compton Ratio

A $^{60}$Co sample was utilized to determine the peak-to-Compton Ratio for the FARIST detector system. A sample was placed at the location of the sample stop to ensure the gamma ray geometry to the detector mimicked that of a sample located inside the sample stop. The sample was counted for 45 minutes and found to have 2952 counts under the $^{60}$Co 1332 keV photopeak. Subtracting 256 keV from the Cobalt peak to determine the energy to the measured Compton background of 77 counts. As a result the peak-to-Compton ratio for the FARIST system was found to be R=38.3. Typical HPGe detection systems typically yield around 40-60 so in summary, the current setup is on the lower end of the optimum operating parameters.

## 7.2 Sample Reactor to Detector Transit Time Improvements

The FARIST system was repeatedly function tested to determine the average transit time required for the sample to exit the reactor core and arrive at the sample stop. In order to assign performance parameters, the system was cycled for a total of 10 iterations and performance data was gathered. The testing yielded the fastest time transit time at 6.43 seconds and the slowest at 7.21 seconds, with the average duration being 6.78 seconds with a standard deviation of 1.58 seconds. As a result, a mandatory 10 second delay time was programmed into the FARIST programming software. This meant that as soon as irradiation was complete, the detection would start counting no earlier than 10 seconds later. This ensured with an extremely high degree of confidence that the sample would be at the sample stopper within 10 seconds of irradiation.

As a result of this 10 second programmed delay time, a variety of radionuclides could now be detected that would have otherwise decayed away prior to detection on the old system. As a general rule of thumb, with a 10 second transit time, it would now be reasonable to detect radionuclides with half-lives on the order of eight seconds or longer. It should be noted that this is just a general rule of thumb and that other factors such as sample activity, composition, irradiation time, etc. can affect overall analytical quality.

### 7.3 FARIST System Cyclic Analytical Comparison to Previous NAA Setup

In order to highlight the analytical improvement from the old to the new system, organic samples containing silver underwent *single shot* and cyclic irradiation. Ore samples containing $^{110}$Ag were chosen due to its relatively short half-life (24.6 seconds) and difficulty to detect in most NAA systems. Through single shot irradiation, the 657 keV photopeak is almost unnoticeable and the spectrum attained is shown in blue on Figure 7.4. The same sample then underwent five iterations of irradiation for 10 seconds and counting for 60 seconds. The results of the cyclic analysis are shown in red on Figure 7.4.

From a cursory look at the data results, it is fairly obvious that cyclic irradiation improves the statistical accuracy of the results for this experiment. This example provides a basic proof of concept that the system functions as planned for cyclic NAA.

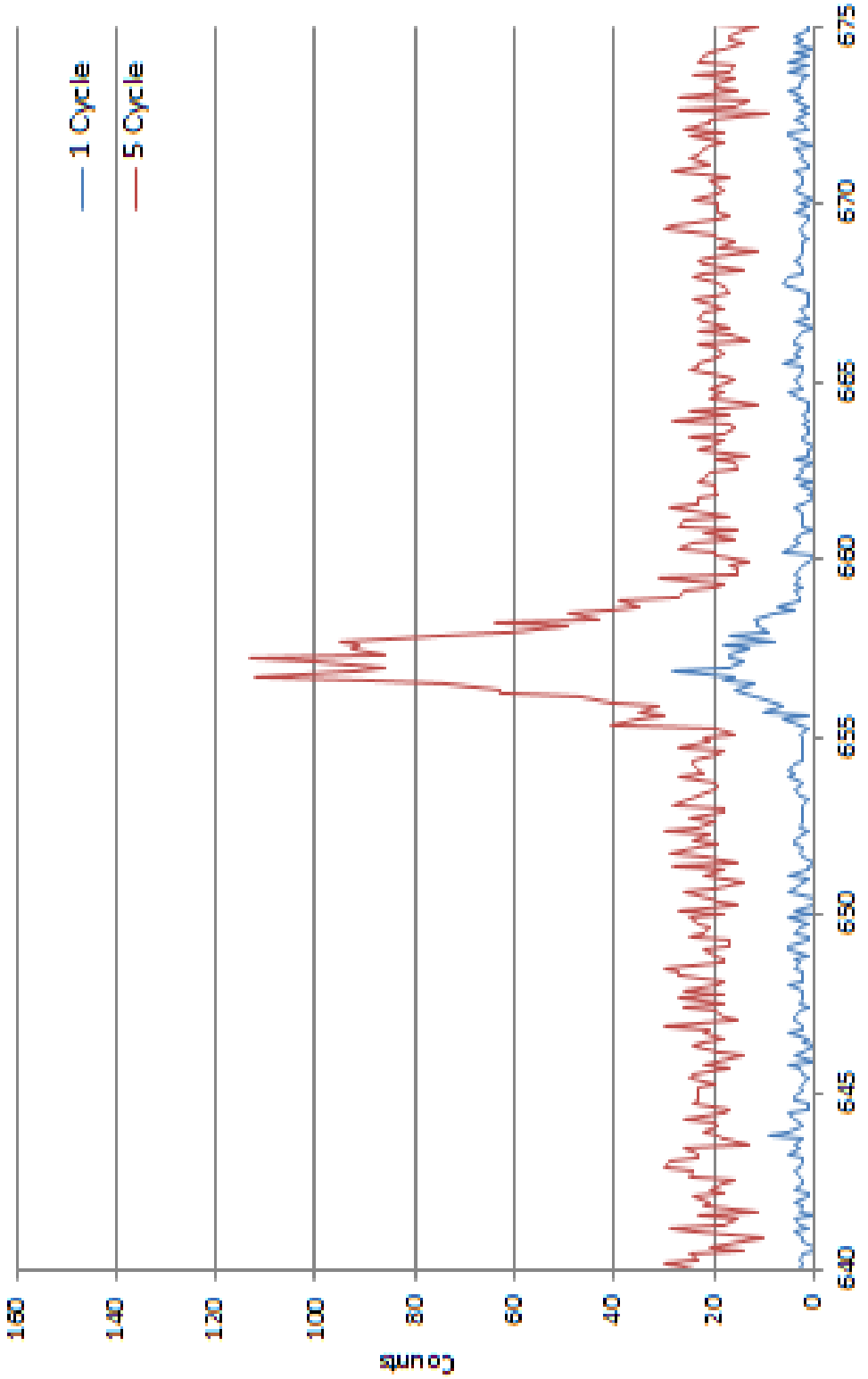


Figure 7.4: Gamma Ray Acquisition Spectrum for Ore Samples Containing Silver.

## 7.4 FARIST System NAA User Exposure Improvements

The purpose of the FARIST system, as discussed earlier, was to remove all human interaction to the NAA process in order to reduce exposure to the user. Quantifying the exposure improvements proved to be difficult as there is not much work in the field of measuring exposure to the NAA researcher. Through extensive research, a paper by Belandi and Landsberger concerning beta-exposure during NAA was found [29]. A qualitative look at the average exposure an NAA researcher receives when conducting NAA experiments when user interaction is required to transport the sample to a detector. The purpose of the research was to not only investigate the beta exposure to the researcher, but the gamma exposure as well. Belandi utilized four samples (aluminum foil, soil sediment, marine tissue, and coal fly ash) in his research that were irradiated in a TRIGA reactor between 10 and 60 seconds [29]. The samples were then immediately placed in front of a detector at one and three foot distances. The one foot distance represented the average distance a sample would be from the researcher's torso while the three foot measurement represented the distance between the torso and the sample when transporting the sample to a detector with arms outstretched [29]. The three feet also represented the distance between the sample and the eyes of the researcher. This process was completed with the sample having a clear line of sight to the detector. The process was then repeated however, in the following iterations the detector was placed on the outside of a fume hood with the sample internal. The purpose was to simulate the use of the fume hood to reduce exposure, a common practice in NAA. By conducting experiments with both setups, accurate exposure rates could be calculated for when the

sample arrived inside of the fume hood and then removed for physical transport to a detector.

The results of Belandi's research are summarized in Figures 7.5 and 7.6. Figure 7.6 presents the exposure rates incident on the researcher after the aluminum foil standard was irradiated. From the two graphs, it is important to note that when the fume hood was not present, the researcher is subject to almost nine times the exposure rate as when the fume hood was down. With the aluminum sample, exposure rates as high as 15mR/h was observed. With the hood down, exposure rates were reduced to 2mR/h upon initial handling of the sample. While the exposure levels for the aluminum foil were not extremely dangerous, the same could not be said for the marine sediment that was irradiated, shown in Figure 7.6. Exposure levels as high as 440mR/h was observed without the fume hood and 50mR/h with the fume hood constituting a legitimate hazard to the researcher.

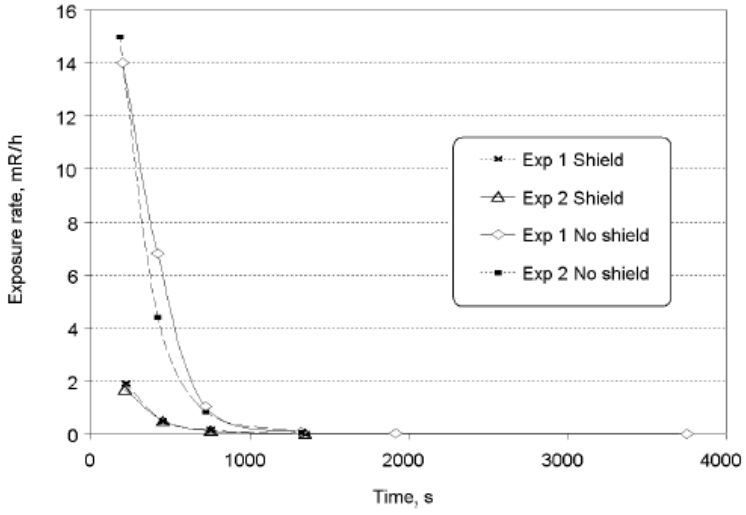


Figure 7.5: Aluminum Foil Exposure Rates During NAA [29].

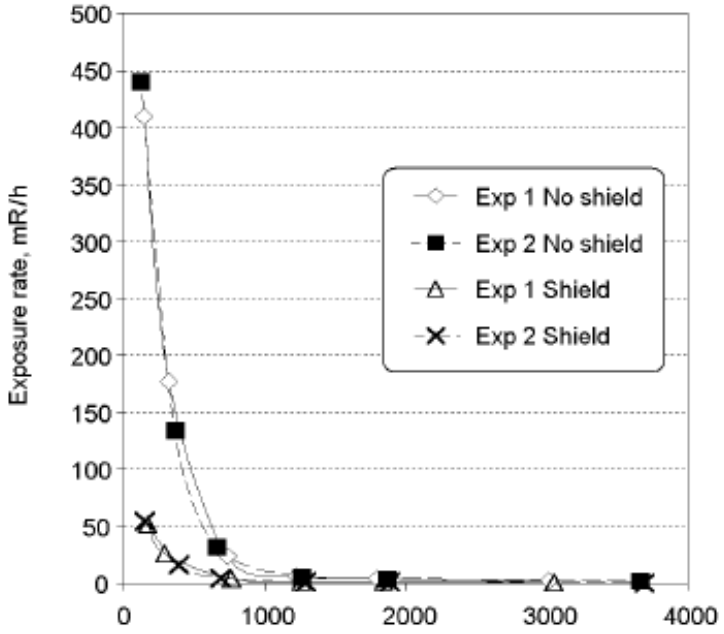


Figure 7.6: Organic Sample Exposure Rates During NAA [29].

With the background provided by Belandi's work, it is obvious to see the significant exposure improvements provided by the FARIST. With the implementation of the FARIST system for NAA, the exposure to the researcher caused by the activated sample, regardless of composition, is reduced to near zero; a major improvement in safety.

# Chapter 8: Conclusion

The FARIST system affords The University of Texas Nuclear Engineering Teaching Labs capability and safety in the NAA environment that has never been offered before. Through the use of this system, more reliable analytical results are attained with less user involvement. Four years have passed between the installation of the FARIST system and the completion of this paper. Over this time, the FARIST system has been employed successfully on a multitude of separate experiments. This can be translated to a multitude of experiments where: researchers no longer were required to expose themselves to unnecessary doses of radiation, overall experimentation time was reduced, and experiments where cyclic capability was present and often utilized.

As with any good athlete, team, or engineer, the desire to improve on the status quo will always be prevalent. This system is no different in that it has room for improvement and it will continue to improve with changes over time. A few ideas presented on how to improve the system include:

- Transition Detection System to a Compton Suppressed System.
- Introduce dead-time correction techniques to account for different dead-times during cyclic analysis.
- Introduce LFC techniques to the detection system.
- With the addition of the two aforementioned improvements, place the detection system on top of the reactor pool to allow for very short transit times.

- Introduce Lead/Cadmium/Copper shielding to the roof of detector housing.

With these additions, the FARIST system could continue to make headway in operator safety and automated NAA. The system has performed exceptionally over the past four years. With that, the system will require constant refinement and improvement to remain an asset to the ever emerging field of nuclear science. If continuous refinement and improvement is repeatedly accomplished, the FARIST system will continue to operate for years to come.

# Appendix A: FARIST System Mechanical Drawings

The following mechanical drawings were created during the design phase of the FARIST system by Blake Copple.

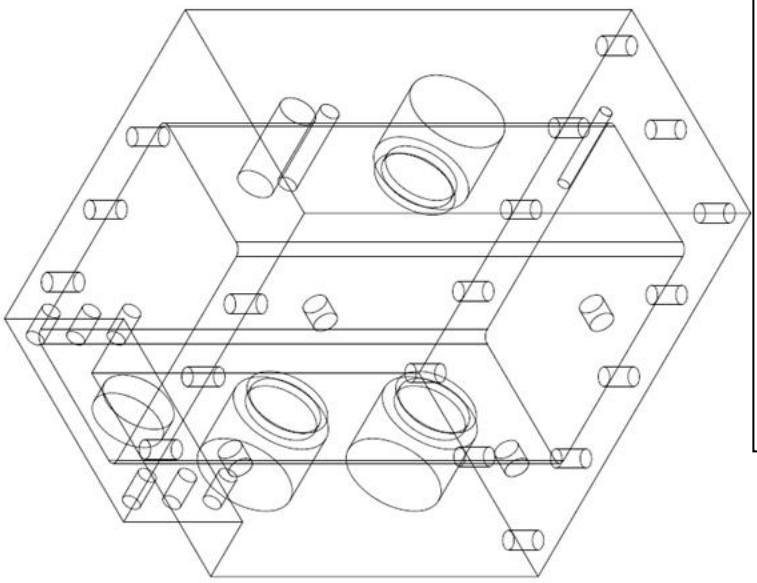

Item: Sample Transfer Housing
Material: 6061-T6 Aluminum
Image: 1 of 2

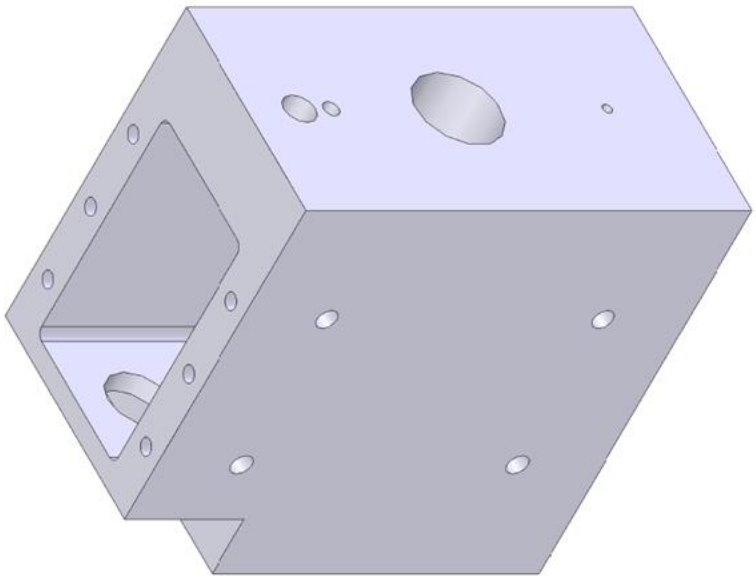

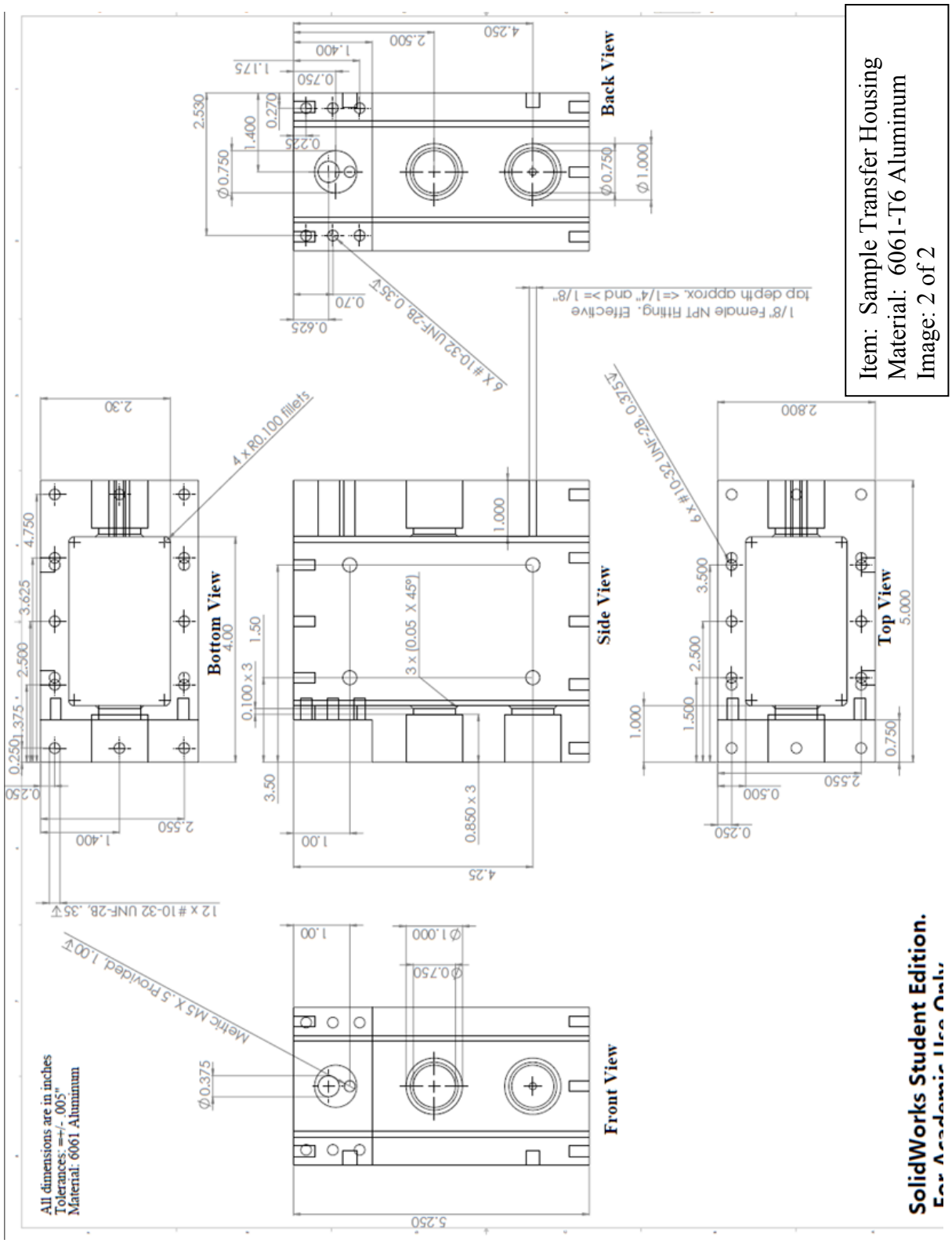
Item: Sample Transfer Housing
Material: 6061-T6 Aluminum
Image: 2 of 2
All dimensions are in inches
Tolerances: =+/- .005"
Material: 6061 Aluminum
Back View
Bottom View
Side View
Top View
Front View
SolidWorks Student Edition.

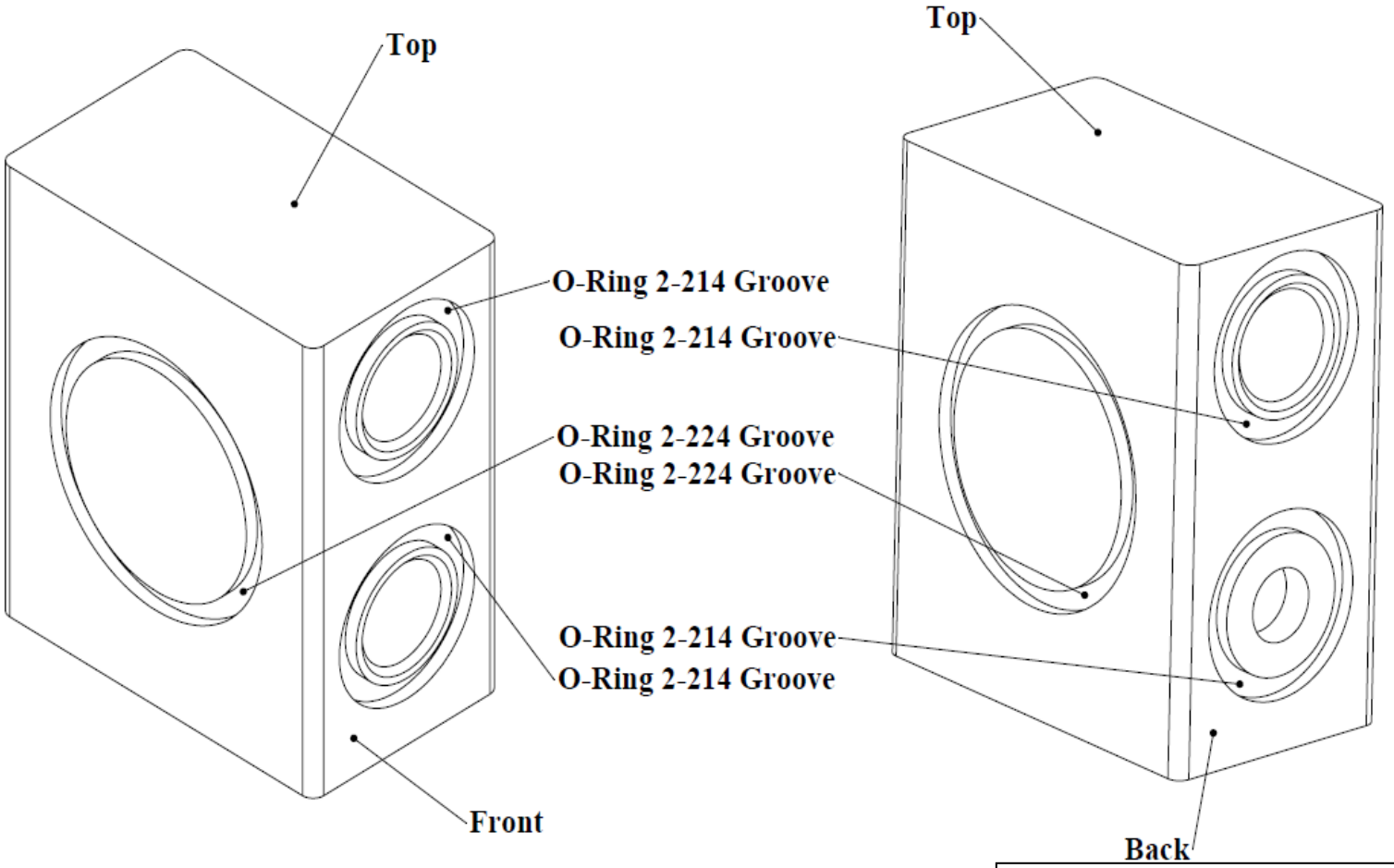


Item: Sample Transfer Inner Valve
Material: 6061-T6 Aluminum
Image: 2 of 3

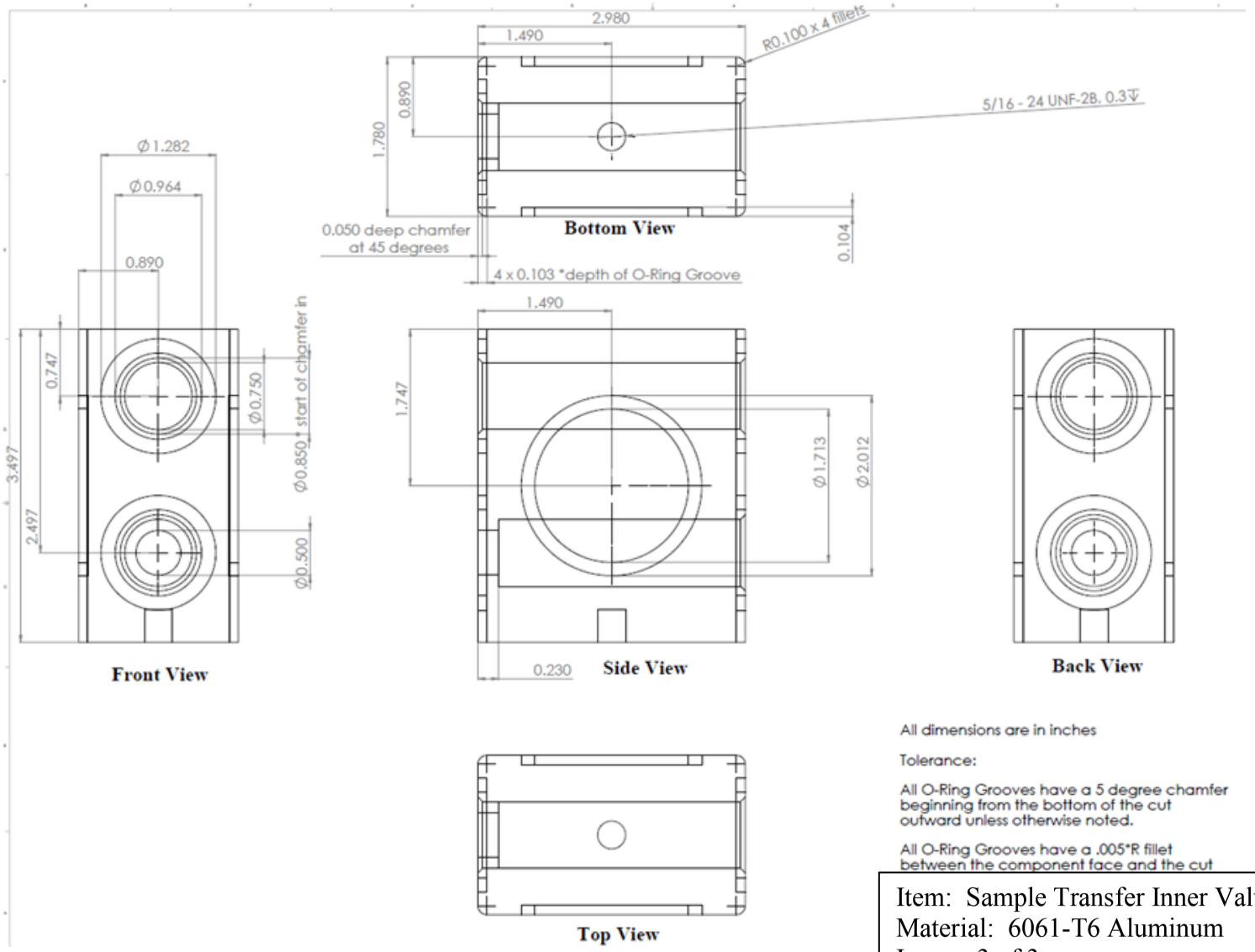


Item: Sample Transfer Inner Valve
Material: 6061-T6 Aluminum
Image: 3 of 3

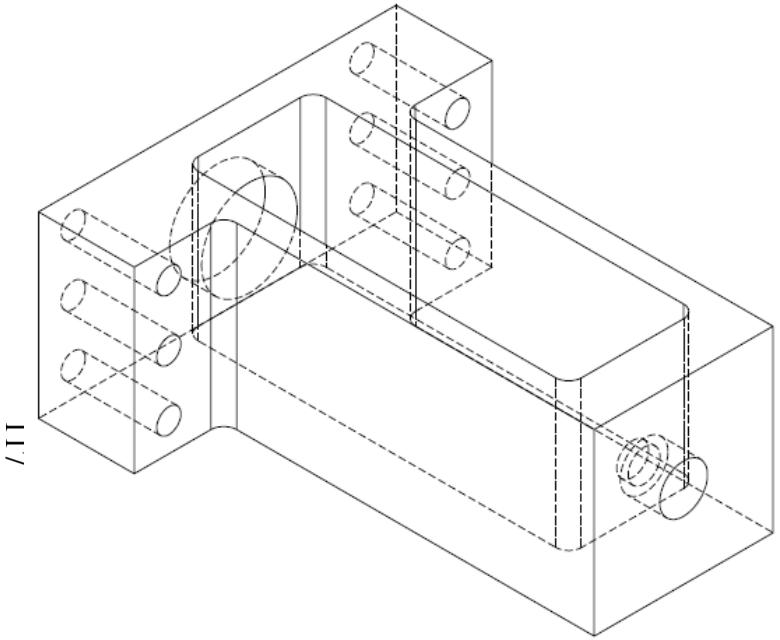

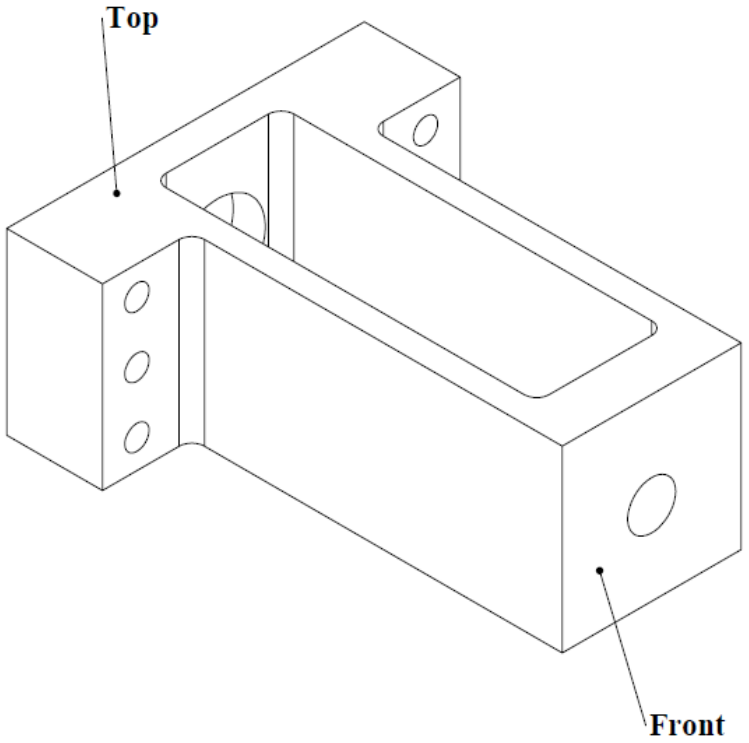


Item: Sample Transfer Housing
Magazine Retainer
Material: 6061-T6 Aluminum
Image: 1 of 2

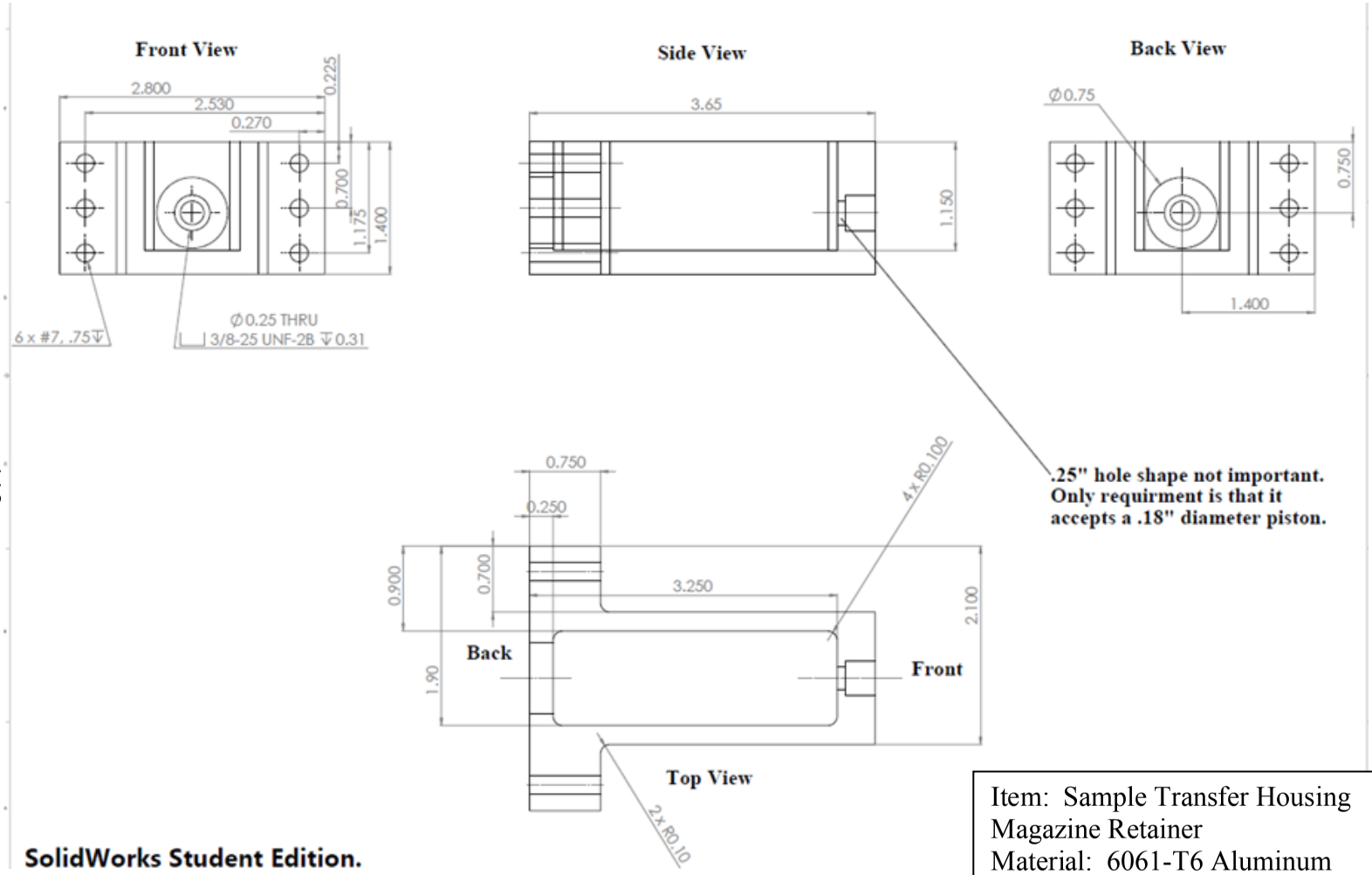


Item: Sample Transfer Housing Magazine Retainer
Material: 6061-T6 Aluminum
Image: 2 of 2

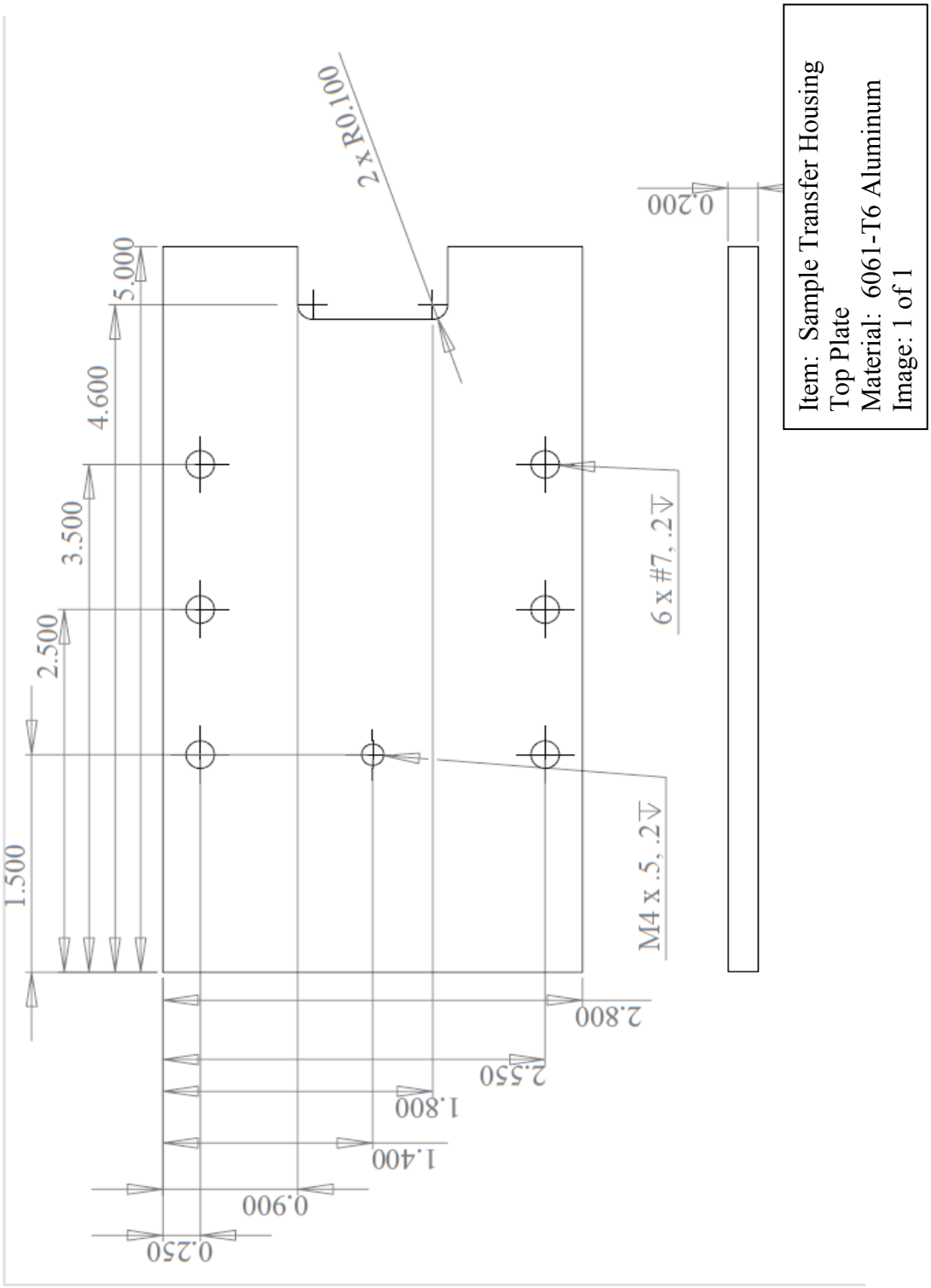
Item: Sample Transfer Housing
Top Plate
Material: 6061-T6 Aluminum
Image: 1 of 1
0.200
2 x R0.100
5.000
4.600
3.500
2.500
1.500
6 x #7, .2↧
M4 x .5, .2↧
2.800
2.550
1.800
1.400
0.900
0.250

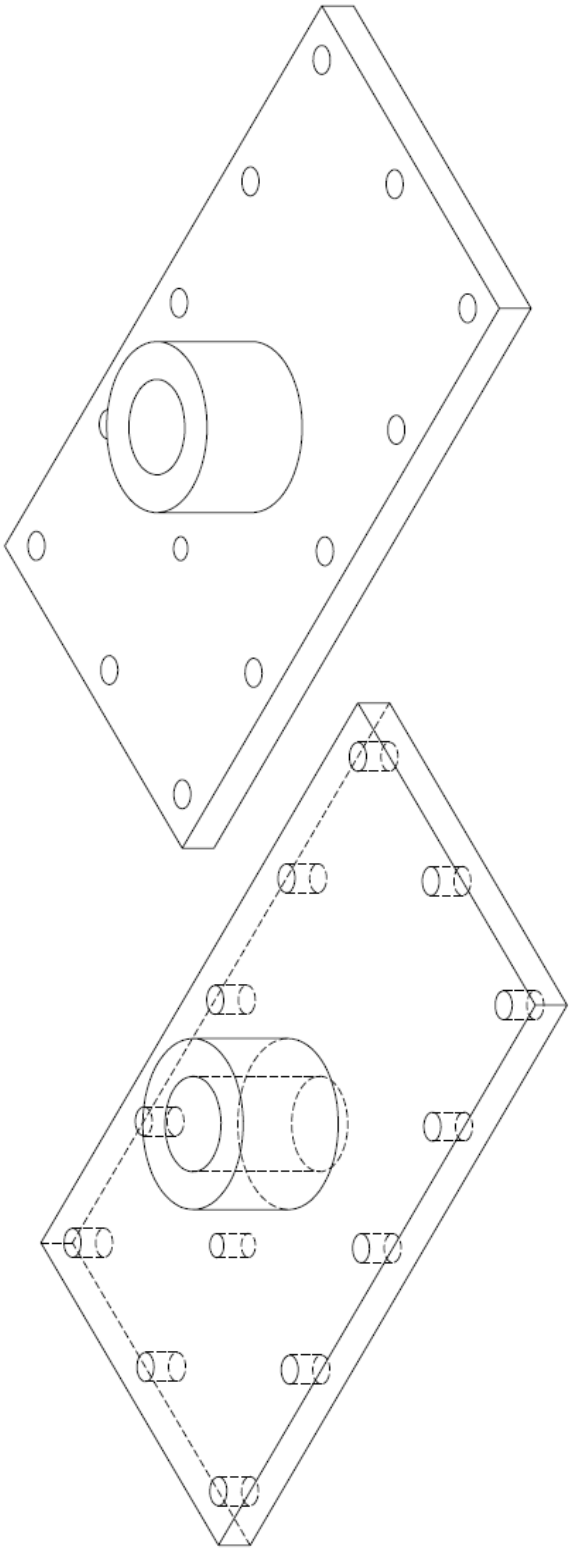

Item: Sample Transfer Housing
Bottom Plate
Material: 6061-T6 Aluminum
Image: 1 of 2

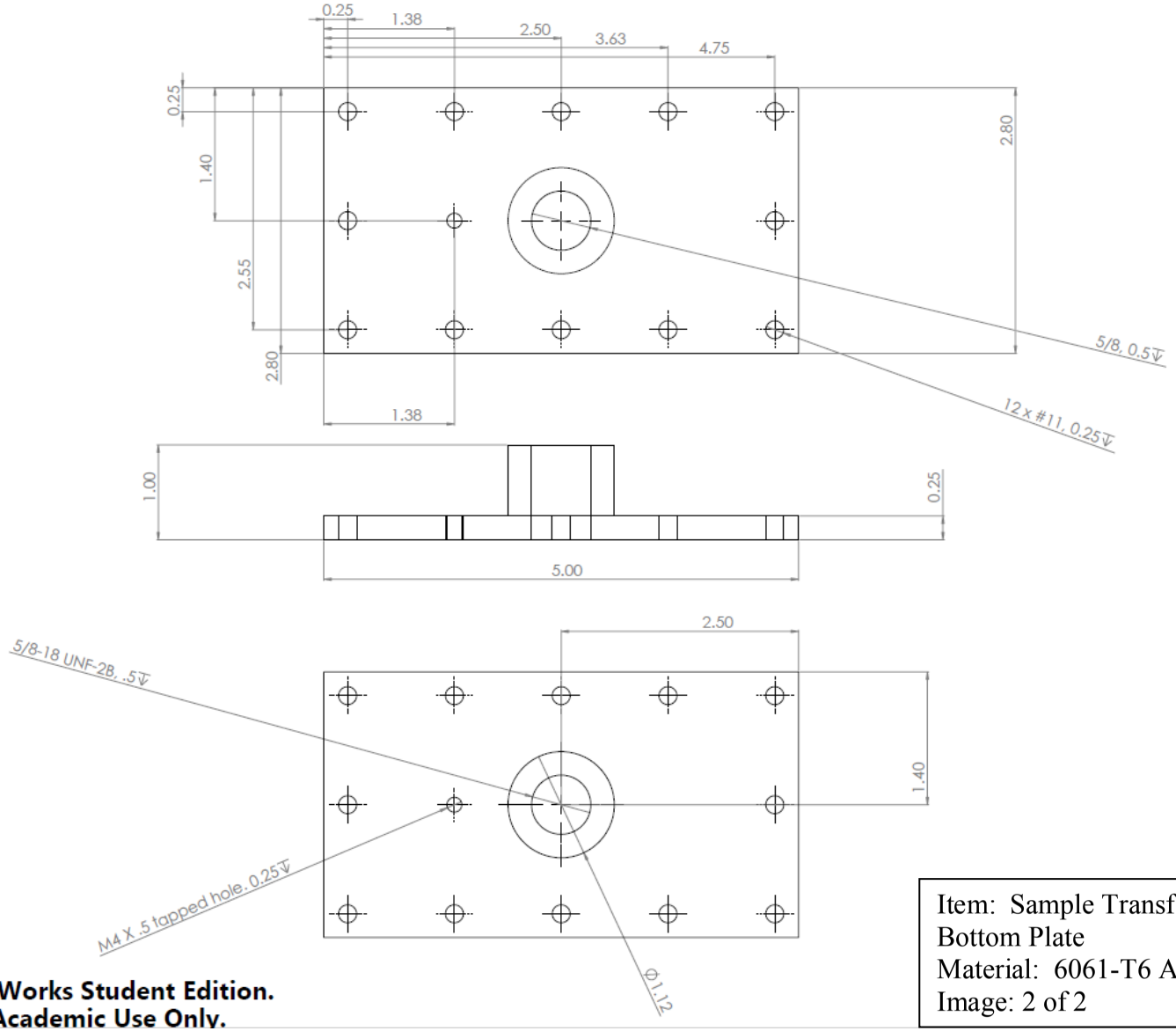


olidWorks Student Edition.
or Academic Use Only.

Item: Sample Transfer Housing Bottom Plate
Material: 6061-T6 Aluminum
Image: 2 of 2

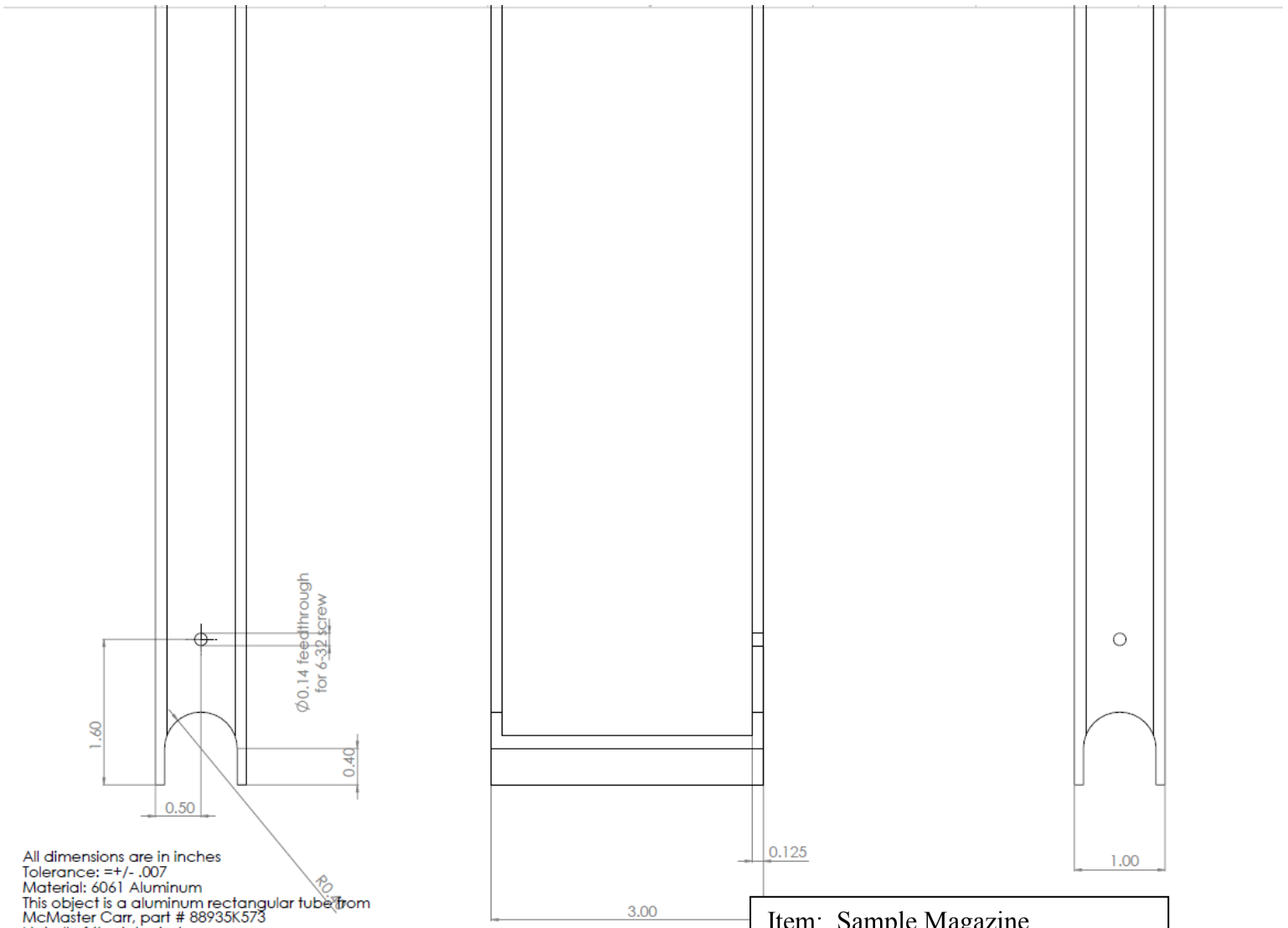


All dimensions are in inches
Tolerance: =+/- .007
Material: 6061 Aluminum
This object is a aluminum rectangular tube from McMaster Carr, part # 88935K573
Not all of the tube is shown

Item: Sample Magazine
Material: 6061-T6 Aluminum
Image: 1 of 1

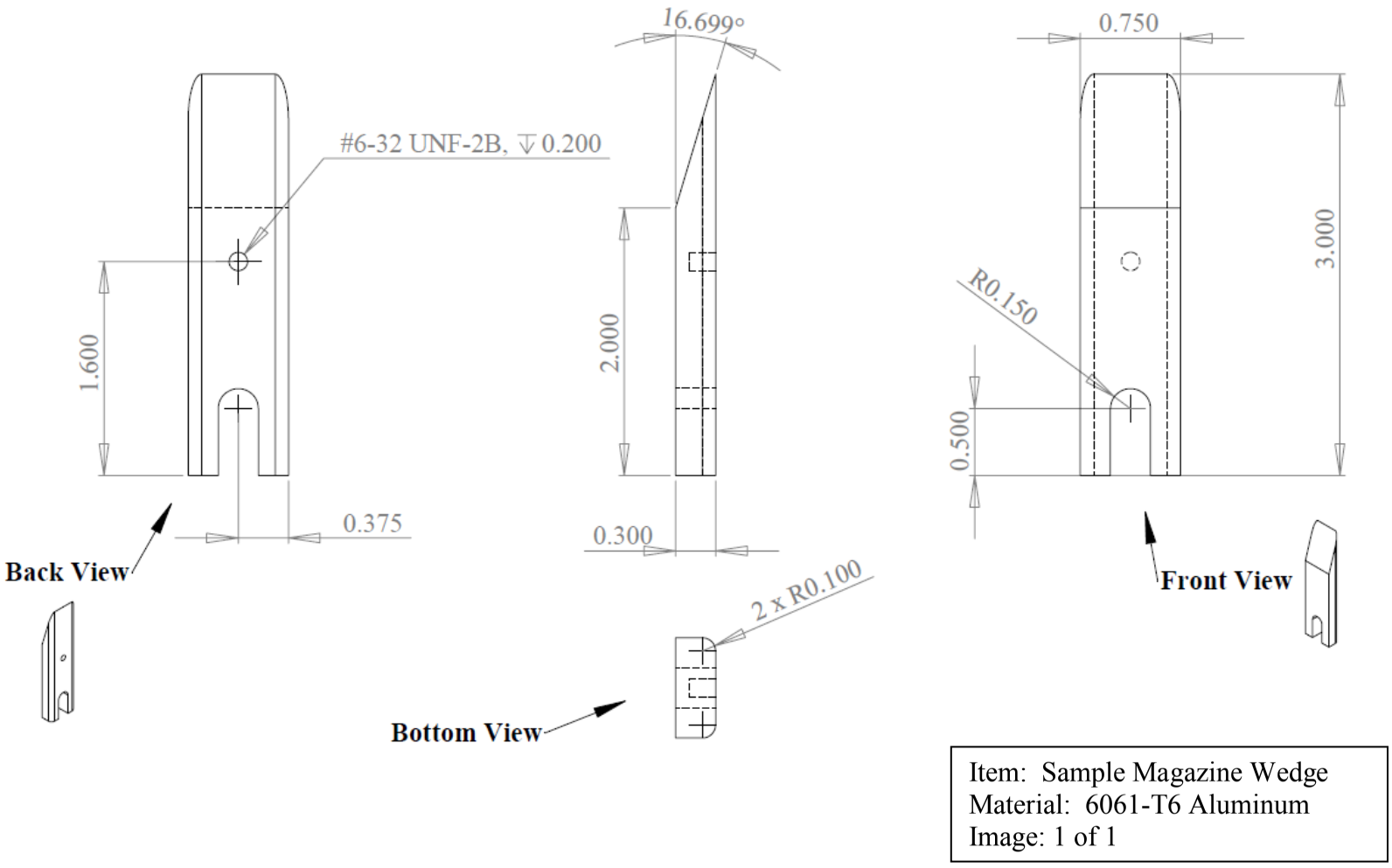


Item: Sample Magazine Wedge
Material: 6061-T6 Aluminum
Image: 1 of 1

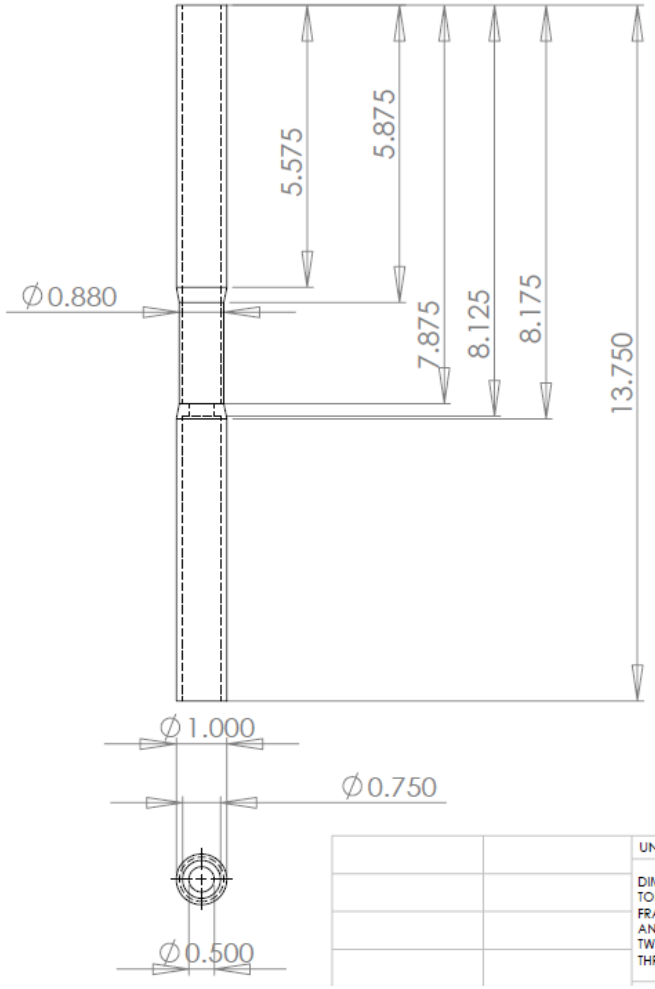


All Dimensions in Inches
+/- .003 inches
Material: 6061-T6 Aluminum

| | | | |
|---|---|---|---|
| UNLESS OTHERWISE SPECIFIED: | | NAME | DATE |
| DIMENSIONS ARE IN INCHES<br>TOLERANCES:<br>FRACTIONAL ±<br>ANGULAR: MACH ± BEND ±<br>TWO PLACE DECIMAL ±<br>THREE PLACE DECIMAL ± | DRAWN | | |
| | CHECKED | | |
| | ENG APPR. | | |
| | MFG APPR. | | |

Item: Sample Stop
Material: 1100 Aluminum
Image: 1 of 1

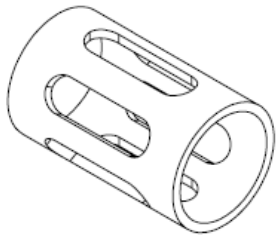

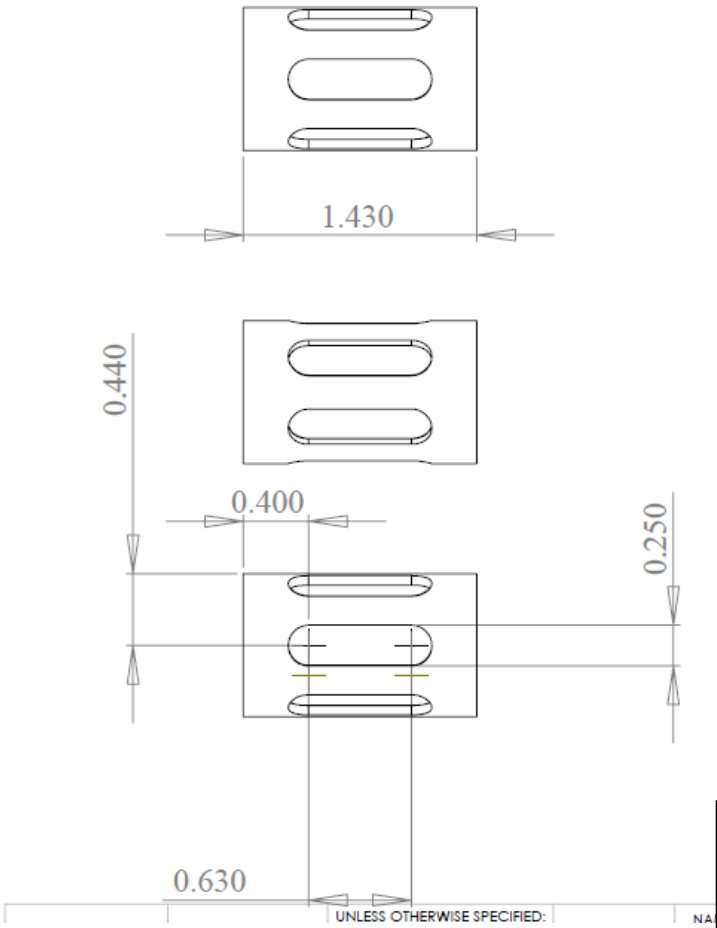


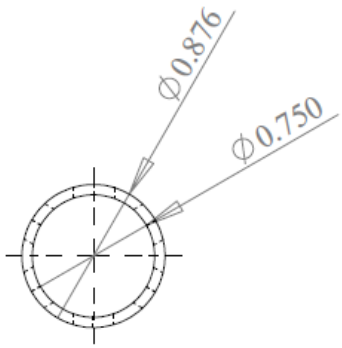


Item: Three-Way Feed Through Fitting
Material: 6061-T6 Aluminum
Image: 1 of 1

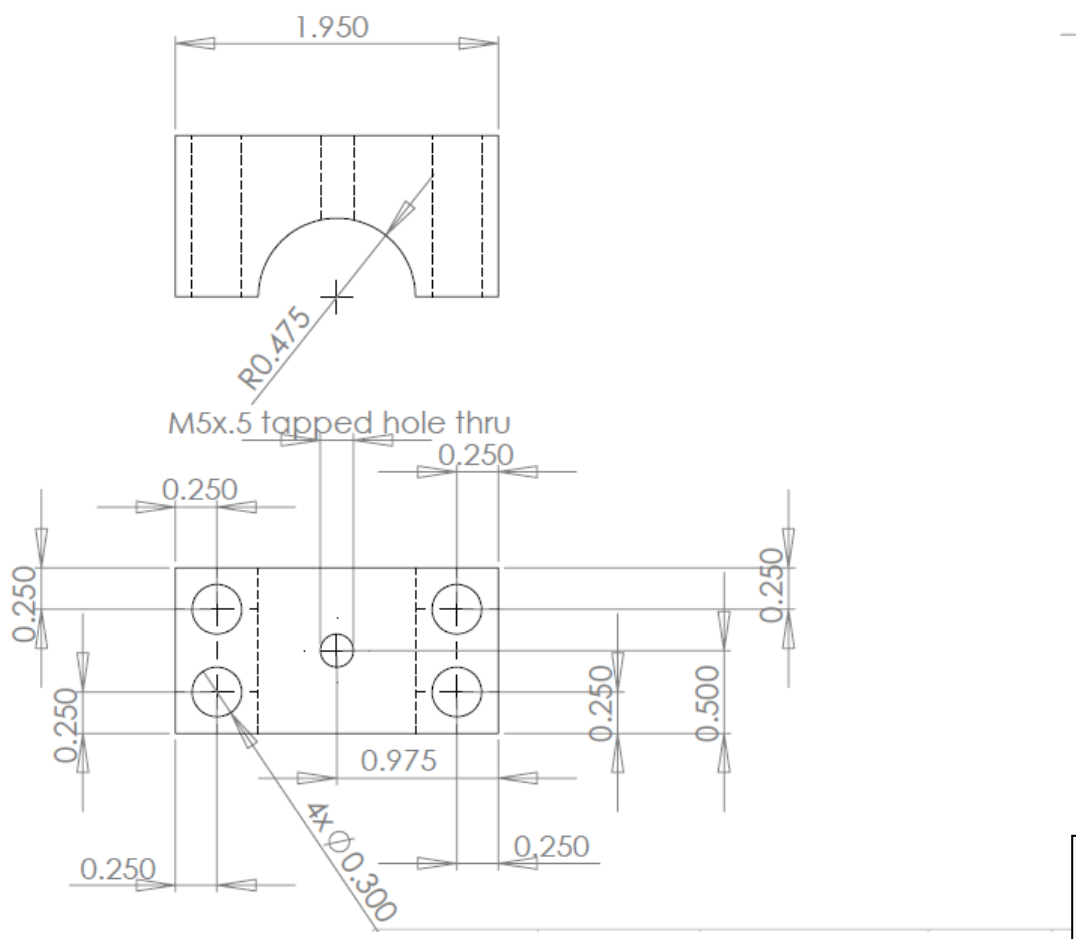


Item: Sensor Clamp (Top)
Material: 6061-T6 Aluminum
Image: 1 of 1

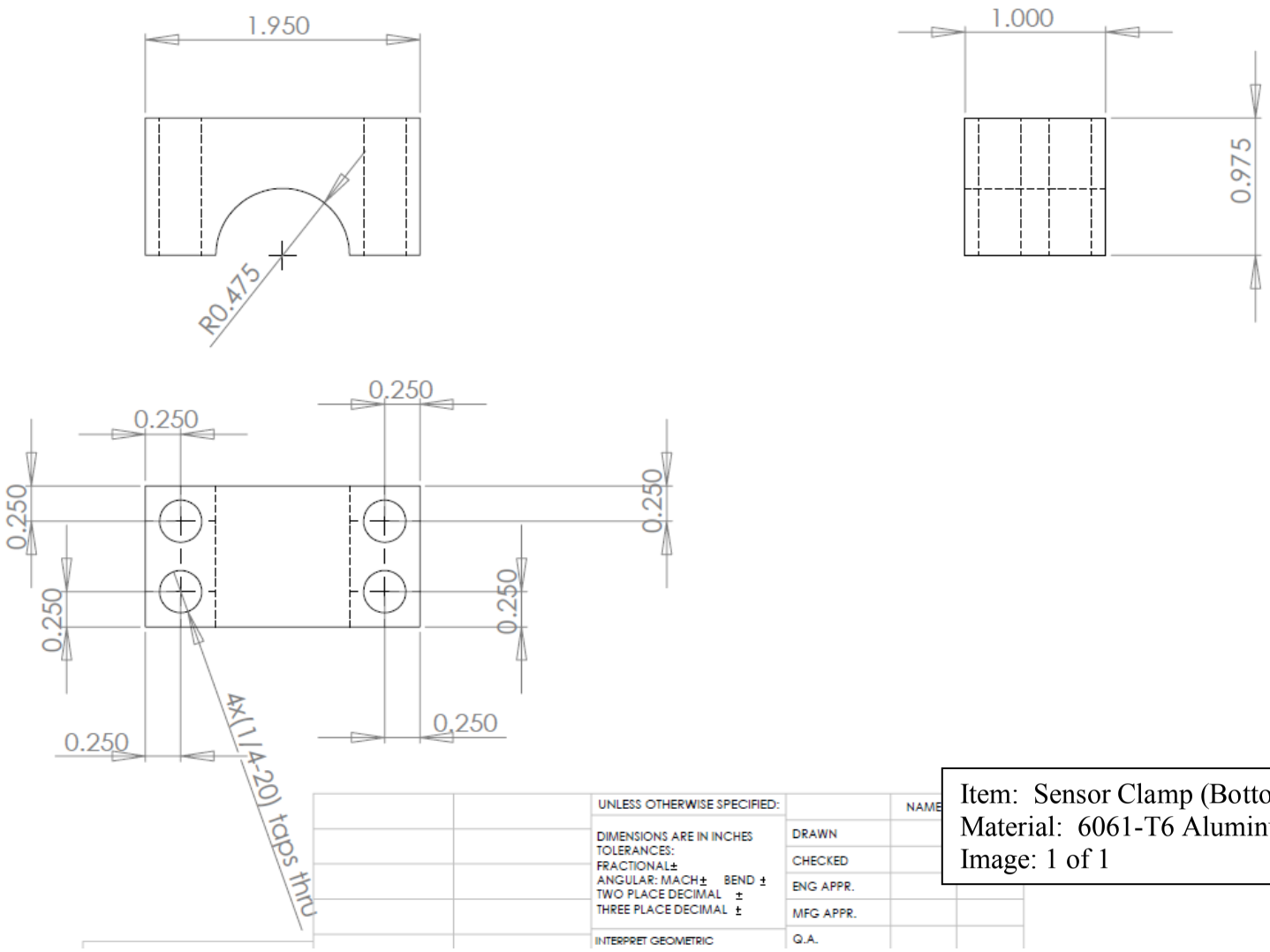


Item: Sensor Clamp (Bottom)
Material: 6061-T6 Aluminum
Image: 1 of 1

# Appendix B: Operational Testing Procedure

1. Ensure reactor operators have adjusted pneumatic lines to receive FARIST system samples.
2. Load samples into sample rack with caps facing to the right.
3. Open File Name: “Cyclic-RT” from FARIST computer system desktop.
4. Input screen will appear. Enter values for: irradiation time, counting time, decay time (≥10 seconds), number of samples to be tested, number of cycles each sample will undergo.
5. Select from the options for counting to either counting time to be “live time” or “corrected for dead time.”
6. Press “OK.” System is now ready.
7. Contact control room and confirm they are ready for FARIST system operation, wait for verbal confirmation.
8. Once verbal confirmation is given, press “Start.” System will standby as the pneumatic loop begins purging. Purging takes approx. two minutes to complete. Once ready, the system will engage automatically and analysis will begin.
9. Return once all analysis is complete. Spectrums can be referenced in the “C:user” file.
10. Spent samples can be recovered inside of the waste bin.

# References


[1] "World GDP, 20 Countries and Regional Totals, 0 – 1998 A.D." Hosted Online by The World Economy. Last Accessed October 31, 2014. < http://www.theworldeconomy.org/MaddisonTables/MaddisontableB-18.pdf>

[2] "Overview of Neutron Activation Analysis" Hosted Online by The University of Missouri Research Reactor. Last Accessed October 3 , 2014. < http://archaeometry.missouri.edu/naa_overview.html>

[3] Alfassi, Z.B. "Activation Analysis, Volumes I and II." CRC Press: Boca Raton, FL. 1990.

[4] De Soete, D., R. Gijbels, and J. Hoste. "Neutron Activation Analysis." John Wiley and Sons: New York, NY. 1972.

[5] "UNLV: Introduction to Radiochemistry." Hosted Online by University of Nevada Las Vegas. Last Accessed Novemeber 25, 2012. < http://radchem.nevada.edu/classes/chem312/lect%208%20fission.html>

[6] Biegalski, Steven "Prompt Gamma Activation Analysis Part 1" Nuclear Engineering. The University of Texas. 2008.

[7] "Table of Nuclides." Hosted Online by Korea Atomic Energy Research Institute. Last Accessed November 11, 2014. < http://atom.kaeri.re.kr/>

[8] "Chart of Nuclides." Hosted Online by NNDC. Last Accessed October 29, 2014. < http://www.nndc.bnl.gov/chart/reCenter.jsp?z=63&n=89>

[9] Biegalski, Steven. Lecture #5. Introduction to Nuclear Power Systems. The University of Texas, Austin, TX. October 2006.

[10] Landsberger, Sheldon. "Gamma-Ray Spectroscopy with Hyper-pure Germanium Semiconductors and Neutron Activation Analysis" Nuclear and Radiochemistry. The University of Texas. June 2007.

[11] "Canberra: Genie 2000 Software Family." Hosted Online by the Canberra Corporation. Last Accessed September 24, 2014. <http://www.canberra.com/products/radiochemistry_lab/genie-2000-software.asp>

[12] Landsberger, Sheldon. "Detection Limit Determination with Hyper Pure Germanium Semiconductors and Neutron Activation Analysis" Nuclear and Radiochemistry. The University of Texas. June 2007.

[13] Spyrou, N.M. "Cyclic Activation Analysis – A Review." Journal of Radioanalytical Chemistry, Vol 61. No. 1 – 2. 1981.

[14] Hou, X. "Cyclic Activation Analysis" Encyclopedia of Analytical Chemistry. John Wiley and Sons Ltd. Denmark, 2006.

[15] Biegalski, Steven. Lecture #6. Introduction to Nuclear Power Systems. The University of Texas, Austin, TX. October 2006.

[16] Currie, L.A. "Limits for Qualitative Detection and Quantitative Determination." Analytical Chemistry Division, National Bureau of Standards, Washington D.C., 1968.

[17] Spyrou, N.M., Matthews, I.P. "A Cylic Neutron Activation System Using an Isotropic Neutron Source for the Measurement of Short-Lived Isotopes." Journal of Radioanalytical and Nuclear Chemistry, Vol. 61, No. 1 – 2, 1981.

[18] Westphal, G.P., Grass, F., Lemmel, H., Niedermaier, H., Jostl, K., Schroder, P., Bock, H., Schachner, H., Klapfer, E. "Low-cost Activation Analysis at Small Research Reactors." Journal of Radioanalytical and Nuclear Chemistry, Vol. 257, No. 1, 2003.

[19] Ismail, S.S., Grass, F., Westphal, G.P. "A New Highly Efficient Setup for Cyclic and Pseudocyclic Short Time Activation Analysis with High Count Rates." Journal of Radioanalytical and Nuclear Chemistry, Vol. 233, No. 1 – 2, 1998.

[20] Niskala, P., Pitkanene, V., Rosenberg, R.J., Vanska, L. "An Automatic NAA Analyzer for Short Lived Nuclides." Journal of Radioanalytical and Nuclear Chemistry, Vol. 160, No. 2, 1992.

[21] Westphal, G.P. "Real-Time Correction of Counting Losses in Nuclear Pulse Spectroscopy." Journal of Radioanalytical Chemistry, Vol. 70, No. 1 – 2, 1982.

[22] "1" PP THRD ON/OFF ELECTRIC VALVE-3/4 SEC RESPONSE TIME." Image Provided by ALSCO Banjo Valves and Fittings. Last Accessed 05 November 2014.<http://www.banjovalves.com/1ppthrdonoffelectricvalve-34secresponsetime.aspx>

[23] "Swagelok Straight Tube Fittings." Image Provided by Swagelok. Last Accessed 25 November 2013.<http://www.swagelok.com>

[24] "McMaster-Carr Stainelss Steel Air Cylinders." Image Provided by McMaster-Carr. Last Accessed 14 November 2014. <http://www.mcmaster.com/#=ukbcyx>

[25] "How to Calculate Required Material Thickness For Making Graded Shielding." Provided by AnotherWally. 11 December 2013.

[26] Shultis, J.K., Faw, R.E. "Radiation Shielding." American Nuclear Society, La Grange Park, IL. 2000.

[27] Lamarsh, J.R., Baratta, A.J. "Introduction to Nuclear Engineering: Third Edition." Prentice Hall, Upper Saddle River, New Jersey. 2001.

[28] "Diffuse Photo 5mm PNP 50mm RNG 3-Wire DC Sensor" Image Provided by Automation Direct. Last Accessed 05 November 2014. <http://www.automationdirect.com/adc/Shopping/Catalog/Sensors_-z-_Encoders/Photoelectric_Sensors/5mm_Round__Stainless_(C5_Series)/Diffuse_(C5D_Series)/C5D-AP-1A>

[29] Belandi, T.J., Landsberger, S. "Beta-exposure in a Neutron Activation Laboratory" Journal of Radioanalytical and Nuclear Chemistry, Vol. 269, No. 2, 2006.